Understanding Amyloid Inhibition:

Toward a Residue-Resolution Map of the Interactions between the Alzheimer's Aβ-Peptide and Human Serum Albumin

ACKNOWLEDGEMENTS

First, I would like to acknowledge Dr. Melacini for his continuous support. I have learned a lot form him on the personal and professional level. I am so happy with what I have accomplished in his research group and I believe that this will be the stepping-stone for my future career as a scientist and I will always find his instructions and research methodology very useful. I also would like to thank my committee members Dr. Ortega and Dr. Britz-McKibbin for their advices and encouragements.

Second, I would like to thank all the lab members(Stephen, Kody, Melanie, Brayan Madoka, Julijana, and Rajeevan, and Naiemeh) for their support. Special thanks to Madoka for her supportive advices, Julijana for all what I learned from her, Rajeevan for being a close friend , and Naiemeh for being my sister. I have learned a lot from them too.

Finally, I would like to thank my family for their support at all levels, and specially my family in Vanada; Mahmoud (best friend, training partner, and twin), his wife (Alyssa) and her parents. You gave me a great support throughout the program.

Table of Contents

Table of Figures

Chapter 1

Chapter 2

Chapter 3

Chapter 4

List of Tables

List of Abbreviations

AD: Alzheimer's Disease

AGP: α1-acid glycoprotein

APP: Amyloid Precursor Protein

ATTR: Amyloidogenic Transthyretin ATTR

BBB: Blood Brain Barrier

CCD: Charge-Coupled Device

CNS: Central Nervous System

CSF: Cerebrospinal Fluid

DEST: Dark-state Exchange Saturation Transfer

DLS: Dynamic Light Scattering (DLS)

EM: Electron Microscopy

FA: Fatty Acid

FAP: Familial Amyloid Polyneuropathy

HSA: Human Serum Albumin

HSQC: Heteronuclear Single Quantum Coherence

ICP: Inductively Coupled Plasma

MA: Myristic Acid

NMR: Nuclear Magnetic Resonance

NSB: non-specific binding

SL: Spin-Lock

RC: Random Coil

SAP: Serum Amyloid P component

SSA: Senile Systematic Amyloidoses

STD: Saturation Transfer Difference

STR: Saturation Transfer Reference

Tf: Transferrin

ThT: Thioflavin T

TTR: Transthyretin

WG: Watergate water-suppression NMR technique

Thesis Summary

Amyloidogenesis refers to a process of protein misfolding and aggregation that leads to the formation of highly stable amyloid fibers. Amyloidogenesis may lead to loss of physiological protein function and/or formation of toxic intermediates, which are linked to mutliple human diseases. Amyloidogenesis is inhibited by plasma proteins, which function as extracellular chaperones by binding to stressed and misfolded proteins, including amyloidogenic peptides, and preventing their aggregation. This thesis focuses on the ability of human serum albumin (HSA), the main protein in human plasma, to inhibit amyloidogenesis, with emphasis on the molecular nature of the interactions between HSA and the amyloid β peptide (Aβ) associated with Alzhemier's disease. HSA is as a key amyloidogenic regulator, a novel function for this protein that goes beyond the traditional HSA roles as plasma osmotic pressure regulator and as binder and carrier of endogenous and exogenous low molecular weight ligands. As a first step towards understanding the detailed molecular nature of these interactions, this thesis will focus on defining the key binding determinants in the interaction between HSA and Aβ peptides. Primarily, we will try to answer two main questions. First, which HSA residues are critical for the recognition of Aβ peptides and the prevention of Aβ aggregation? Second, which Aβ residues are mostly affected by HSA binding? Starting form our knowledge about the stoichiometry and affinity of the Aβ interactions at the level of HSA domains, Chapter 2 addresses the first question through successful applications of a reductionist

approach, based on a combination of mutational comparative analyses and fatty acid (FA) competition. This strategy allowed us to identify a short HSA derived peptide that specifically recognizes Aβ and prevents its aggregation. In Chapter 3, we examine the effect of HSA on the pseudo-equilibrium state between Aβ monomers and protofibrils. Using Dark state Exchange Saturation Transfer (DEST), Saturation Transfer Difference (STD) and ^{15}N T_2 relaxation experiments, we show that Aβ peptides interact with HSA via a dual mechanism. First, selected residues in Aβ (1-40) monomers bind specifically but weakly to HSA (K_d = 0.1 - 1 mM). Second, HSA competes with Aβ monomers for the binding to the protofibrils, as indicated by an HSA-dependent decrease in the direct vs. tethered probabilities for contacts between Aβ monomer residues and the protofibril surface. The effect of HSA mimics that of dilution for the majority of the Aβ (1-40) residues involved in the cross-beta strands of amyloid fibrils. Finally, Chapter 4 will outline future investigations to address currently open questions about HSA dynamics, HSA-Aβ and HSA-FA interactions, for which we acquired preliminary data.

Introduction

Chapter 1

Introduction

Abstract

Amyloidogenesis refers to a process of protein misfolding and aggregation that leads to the formation of highly stable structures called amyloid fibers. Amyloidogenesis may lead to loss of physiological protein function and/or formation of toxic intermediates, which can be a causative factor in various human diseases. Plasma proteins may function as extracellular chaperones; that is they bind to stressed and misfolded proteins, including amyloidogenic proteins, and prevent their misfolding. This thesis focuses on the ability of human serum albumin (HSA), the main protein in human plasma, to inhibit amyloidogenesis, with emphasis on the molecular nature of the interactions between HSA and the amyloid b peptide (Aβ) associated with Alzhemier's disease. HSA emerges as a key amyloidogenic regulator, a novel function for this protein that goes beyond the traditional HSA roles as plasma osmotic pressure regulator and as binder and carrier of endogenous and exogenous low molecular weight ligands.

Introduction

Amyloidosis

Several proteins assemble into well-structured aggregates called amyloid fibers, which have been associated with various human diseases (1–3). Amyloid fibers are broadly defined by the biophysical community as fibers with a diffraction pattern reflective of a cross β structure (Figure 1)(2). On the other hand, the medical definition of amyloid fibers is significantly narrower and is confined to proteins that are part of tissue deposits, and bind the Congo Red dye resulting in green birefringence in polarized light. Moreover, a diagnosis of familial amyloidosis requires DNA sequencing to characterize the sequence of proteins in amyloid fibers (1). According to the latter definition, there are 30 amyloidogenic proteins (Table 1) (4), in addition to 6 inclusion bodies resembling amyloid fibers (Table2) (4).

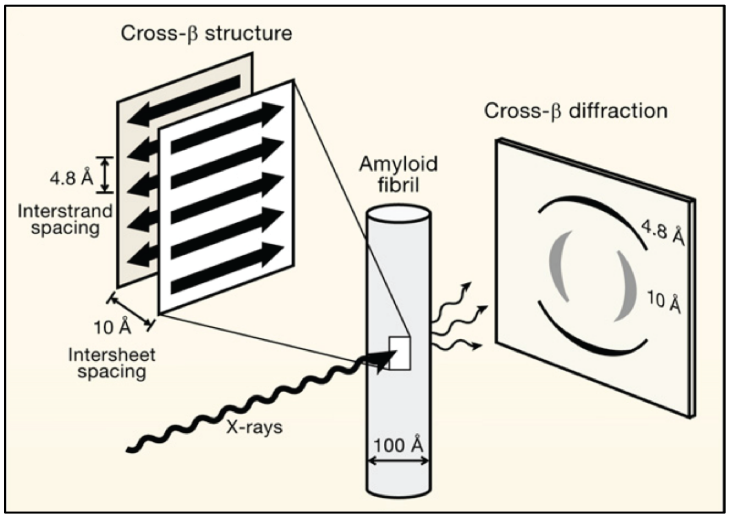

Figure 1. Typical cross-β diffraction pattern of amyloid fibers. Adapted from Eisenberg et, al.(2)

Table 1: Amyloid fibril proteins in humans.

Fibril protein (4)	Precursor protein(4)	Systemic and/or localizedi(4)	Acquired or hereditary(4)	Target organs(4)	Main clinical settings(4–9)
AL	Immunoglobulin light chain	S,L	A	All organs except CNS	Plasma cell disorders
AH	Immunoglobulin heavy chain	S, L	A	All organs except CNS	Systemic Amylodosis
Aβ2M	β2-microglobulin, wild type	L	A	Musculoskeletal system	Dialysis-associated amyloidosis
	β2-microglobulin, variant	S	H	ANS	Hereditary systemic amyloidosis
ATTR	Transthyretin, wild type	S, L	A	Heart mainly in males, Tenosynovium	Senile cardiac amyloidosis (SCA)
	Transthyretin, variants	S	H	PNS, ANS, heart, eye, leptomen.	Familial amyloid polyneuropathy (FAP), familial amyloid cardiomyopathy (FAC)
AA	(Apo) serum amyloid A	S	A	All organs except CNS	Inflammation-associated amyloidosis
AApoAI	Apolipoprotein A I, variants	S	H	Heart, liver, kidney, PNS, testis, larynx (C terminal variants), skin (C terminal variants)	Familial systemic amyloidosis
AApoAII	Apolipoprotein A II, variants	S	H	Kidney	Familial systemic amyloidosis
AApoAIV	Apolipoprotein A IV, wild type	S	A	Kidney medulla and systemic	Senile systemic (ATTR) amyloidosis
AGel	Gelsolin, variants	S	H	PNS, cornea	Familial amyloidosis (Finnish)
ALys	Lysozyme, variants	S	H	Kidney	Familial systemic amyloidosis
ALect2	Leukocyte chemotactic factor-2	S	A	Kidney, primarily	Renal amyloidosis
AFib	Fibrinogen α, variants	S	H	Kidney, primarily	Familial systemic amyloidosis
ACys	Cystatin C, variants	S	H	PNS, skin	Hereditary cerebral hemorrhage with amyloidosis (Icelandic)
ABri	ABriPP, variants	S	H	CNS	Familial dementia (British)
ADan[a]	ADanPP,	L	H	CNS	Familial dementia (Danish)

	variants				
Aβ	Aβ protein precursor, wild type	L	A	CNS	Alzheimer syndrome, Down syndrome
	Aβ protein precursor, variant	L	H	CNS	Hereditary cerebral hemorrhage with amyloidosis (Dutch)
APrP	Prion protein, wild type	L	A	CNS	Creutzfeldt-Jakob disease, fatal insomnia
	Prion protein variants	L	H	CNS	Creutzfeldt-Jakob disease, Gerstmann-Sträussler-Scheinker disease, fatal familial insomnia, Kuru
ACal	(Pro)calcitonin	L	A	C-cell thyroid tumors	Medullary thyroid carcinoma
AIAPP	Islet amyloid polypeptideb	L	A	Islets of langerhans	Insulinomas, type 2 diabetes
AANF	Atrial natriuretic factor	L	A	Cardiac atria	Isolated atrial Amyloidosis
APro	Prolactin	L	A	Pituitary prolactinomas, aging pituitary	Pituitary amyloid
AIns	Insulin	L	A	Local injection	Iatrogenesis
ASPC	Lung surfactant protein	L	A	Lung	Interstitial lung disease
AGal7	Galectin 7	L	A	Skin	Localized cutaneous amyloidosis
ACor	Corneodesmin	L	A	Cornified epithelia, hair follicles	Hypotrichosis simplex of the scalp (HSS)
AMed	Lactadherin	L	A	Senile aortic, media	Aortic amyloidosis in elderly people
AKer	Kerato-epithelin	L	A	Cornea, hereditary	Familial corneal dystrophies
ALac	Lactoferrin	L	A	Cornea	Familial corneal amyloidosis
AOaap	Odontogenic ameloblast-associated protein	L	A	Odontogenic tumors	Odontogenic tumors
ASem1	Semenogelin 1	L	A	Vesicula seminalis	Senile seminal vesicle amyloid

[a]ADan is the product of the same gene as ABrib, also called amylin.
Adapted from Sipe et al, 2012 (4)

Table 2 (4)**: Inclusion bodies having some of the amyloid characteristics.**

Inclusion name	Site	Protein nature	Examples of a ssociated disease
Lewy bodies	Neurons, intracytoplasmic	α-synuclein[a]	Parkinson's disease
Huntington bodies	Neurons, intranuclear	PolyQ expanded, huntingtin	Huntington's disease
Hirano bodies	Neurons	Actin	Neurodegenerative disorders
Collins bodies	Neurons	Neuroserpin	Forms of familial presenile dementia
Not specified	Neurons, many different cells	Ferritin	Form of familial neurodegenerative disorder
Neurofibrillary tangles	Neurons, intracytoplasmic	tau	Alzheimer disease, fronto-temporal, dementia, aging, other cerebral conditions

[a]Simplified: additional components may exist

Common Aggregation Pathway

Amyloidogenic proteins share a common aggregation pathway that can be divided into three main events (3); (1) destabilization of the monomeric protein or peptide and formation of thermodynamically unstable early oligomerization intermediates; (2) growth of the early oligomers to form a nucleus with critical size that permits formation of thermodynamically stable protofibrils; (3) protofiber elongation by the addition of monomers to the nucleus and subsequently to the ends of the growing protofibrils. Formation of the nucleus ('lag phase') is the rate-limiting step in the aggregation process; once a critical nucleus size is reached, fiber formation and elongation proceed rapidly ('growth phase') owing to the thermodynamic stability of the fibers (3). The energetics of the aggregation pathway are shown in Figure 2.

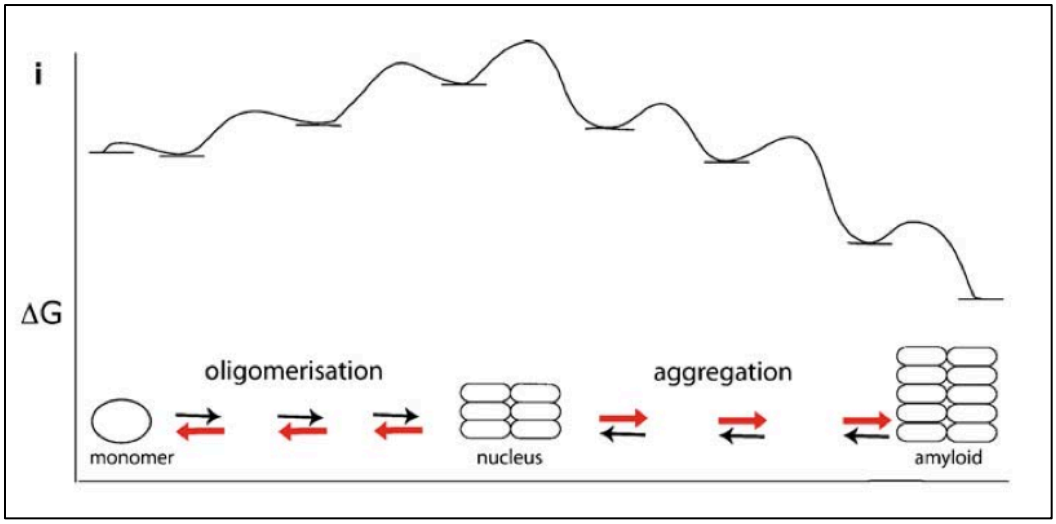

Figure 2. Free Energy diagram of the pathway of amyloid fiber formation according to a nucleation-dependent polymerisation model. Higher energy oligomerization intermediates are formed before the critical formation of the nucleus. Once the nucleus is formed, monomers will be added to it in a thermodynamically favored elongation process. (Adapted from Hurshman et al. 2004) (3)

Structural similarities among different amyloid proteins

As discussed above, the most common feature among amyloid fibers is the presence of β-sheets that are parallel to the fiber axis, resulting in a unique X-ray diffraction pattern (Figure 1)(10),(11, 12). In addition, the side chains of two layers of β-sheets interdigitate to create a water free interface named "steric-zipper"(13). Based on the crystal structures of short peptides from various disease related proteins, Eisenberg et al observed three possible structural arrangements of the β-sheets which can be combined to give eight theoretically possible types of steric zippers(13). The three structural arrangements are based on (1) whether the strands in their sheets are parallel or antiparallel, (2) whether sheets pack in a face-to-face or face-to-back surfaces arrangement, and (3) whether the sheets are oriented parallel or antiparallel with respect to one another(14). These atomic structural differences may be helpful in explaining amyloid polymorphism(14). However, the formation of these dry steric zippers by the majority of amyloid proteins suggests that the similarities are not only at the fiber level, but also at the molecular level(14). Structural similarities are also present among soluble oligomers, as suggested by the observation that a conformation dependent antibody was able to bind different oligomers formed by polypeptides of different primary amino acid sequence and prevented their toxicity(15). This finding indicates that the antibody recognizes a specific conformation of the backbone atoms, which is conserved and largely independent of the amino acid side chains in this region(15).

Amyloid Pathology

Amyloid proteins are associated with at least 25 human diseases collectively known as "amyloidoses". Early histo-pathological investigations found large deposits of amyloid fibers in the organs of the affected patients, so it has been thought that fibrils by themselves are the principal toxic moieties in amyloid diseases (16), (17), (18). However, recent data suggest that soluble aggregation intermediates (oligomers) are likely to be responsible for the toxicity and pathogenesis of the amyloid proteins (16). Furthermore, a growing body of evidence indicates that oligomers do share a common primary mechanism of pathogenesis (19). As shown in Figure 3, oligomers cause membrane permeabilization, which is followed by downstream pathogenic effects, such as increasing cytosolic calcium (20), release of reactive oxygen species (21), altered signaling pathways (22), and mitochondrial dysfunction (23). These pathways ultimately lead to cellular dysfunction and cell death.

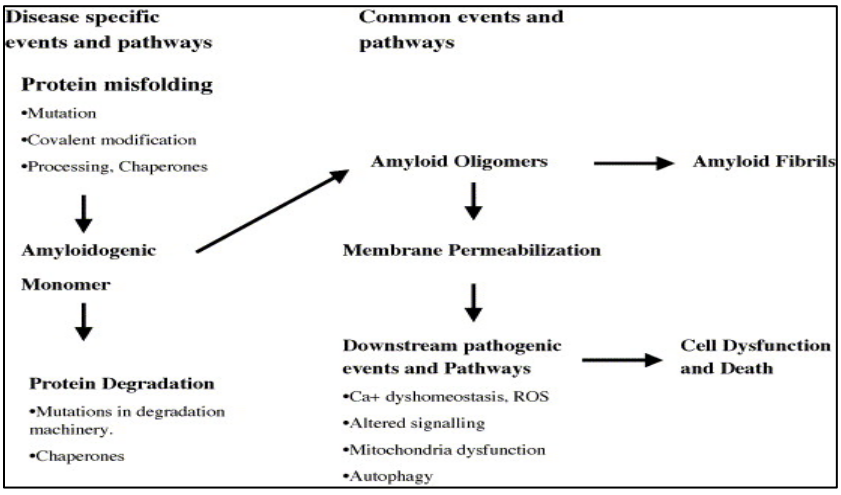

Figure 3. Common and disease-specific pathways in degenerative disorders. Scheme is adapted from Glabe et al, 2005 (19).

Human Serum Albumin

Human Serum Albumin (HSA) is one of the most abundant proteins in human plasma. The major physiological functions of albumin include: (1) binding and transport of endogenous and exogenous ligands, (2) regulating the plasma colloid oncotic pressure, (3) antioxidant activity, (4) platelet function inhibition and antithrombotic effects, and (5) regulation of vascular permeability (24). Moreover, recent investigations by Finn et al. have observed a molecular chaperone activity for bovine serum albumin (25), whereby albumin selectively binds stressed over unstressed proteins, forming soluble high molecular weight (MW) complexes and preventing their aggregation. Therapeutically, HSA is administered as a plasma expander or surrogate in cases of hypovolemia, large-volume paracentesis in cirrhotic patients, acute nephrotic syndromes with diuretic resistance, organ transplantation, and plasmapheresis (26). In addition, new promising therapeutic applications of HSA are emerging in the treatment of Alzheimer's disease (27, 28), ischemic stroke (29) and liver cirrhosis (30). This chapter will summarize recent findings concerning the HSA anti-amyloidogenic potential. Specifically, interactions of HSA with other amyloidogenic proteins circulating in the plasma such as, Transthyretin (TTR), Serum amyloid P component (SAP), Insulin, and Amyloid Beta peptides (Aβ) will be reviewed, with more emphasis on the latter peptide, which is the main focus of this thesis.

Transthyretin (TTR)

Transthyretin (TTR) is a tetrameric plasma protein synthesized predominantly in the liver. The primary established function of TTR is to transport the holoretinol-binding protein and thyroxin through plasma (31). TTR can form amyloid aggregates, and it has been linked to human diseases such as senile systematic amyloidoses (SSA) (32) and familial amyloid polyneuropathy (FAP) (33). SSA is a sporadic disease caused by the accumulation of wild type TTR, whereas FAP is a familial neurodegenerative disease caused by a mutation in the TTR gene. The most common FAP mutation is a valine to methionine point mutation at position 30 (TTR V30M), which destabilizes the wild type protein and accelerates the formation of amyloidogenic intermediates (34). TTR aggregation starts with tetramer dissociation to folded monomers followed by monomer misfolding, nucleation, oligomer and amyloid fibril formation (35).

HSA Inhibits TTR Aggregation

An interesting study by Kugimiya et al(36) monitored HSA levels in familial amyloid polyneuropathy (FAP) patients. Interestingly, HSA levels in FAP patients were lower compared to healthy individuals, and they further decreased as the disease progressed (36). The decrease in albumin level was attributed to malnutrition and/or renal dysfunction due to amyloid deposits in the gastrointestinal tract and the kidney (36). These clinical findings suggest that there is a relation between functional albumin and TTR amyloidosis. On a molecular level, Biacore analysis showed that HSA is able to bind TTR and TTR amyloids in vitro with higher affinity towards the latter (36).

Furthermore, the efficiency in the inhibition of TTR aggregation was measured for albumins with different antioxidant activities using ELISA with anti-TTR (115-124) antibody. HSA was able to inhibit TTR aggregation in a dose dependant manner as shown in Figure 4. Moreover, HSA with stronger antioxidant activity (i.e. fatty acid bound) was a more potent inhibitor (36). Finn et al. used thioflavin T fluorescence to study the interaction of bovine serum albumin (BSA) with TTR and achieved similar conclusions: BSA was able to inhibit in a dose dependent manner the aggregation and amyloid formation of TTR and a highly aggregation-prone mutant, L55P-TTR (25). Finally, in vivo studies showed that analbumineric rats with the amyloidogenic TTR V30M gene developed more severe TTR deposits and at earlier ages compared to amyloidogenic TTR V30M rats expressing functional albumin (36).

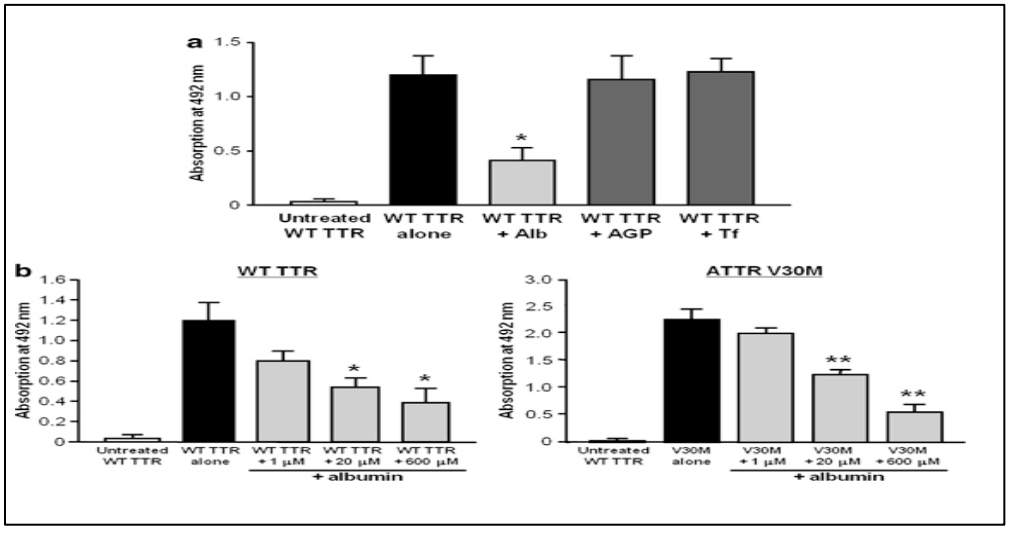

Figure 4. Effect of albumin on the formation of transthyretin (TTRs) amyloid fibers and preamyloid deposits. (a) Samples of wild-type (WT) TTR were incubated at 37 °C for 5 days in the presence and absence of physiological concentrations of serum proteins; albumin (Alb), α1-acid glycoprotein (AGP), or transferrin (Tf) . TTR amyloid formation was monitored using sandwich ELISA with an anti-TTR (115-124) antibody that is

specific for amyloid fibers and preamyloid deposits. Significant decrease in aggregation was only observed for the sample containing physiological HSA concentration. Each bar represents the mean±s.d. (n=5). *P < 0.05 vs WT TTR alone (b) HSA inhibits amyloid formation of WT TTR (left panel) and amyloidogenic transthyretin (ATTR) V30M (right panel) in a dose dependant manner as detected by ELISA. Each bar represents the mean±s.d. (n.5). *P<0.01 vs WT alone. **P<0.01 vs ATTR V30M alone. Adapted from Kugimiya et al. (36)

Serum amyloid P component (SAP)

Serum amyloid P component (SAP) is a plasma protein universally found in all amyloid deposits, including plaques, amorphous amyloid β protein deposits and neurofibrillary tangles linked to Alzheimer's disease (37),(38, 39). SAP binds the amyloid deposits and prevents their dissociation in vivo, consequently the pathogenesis of amyloid deposits is augmented due to stabilization (40). That is why interference with SAP binding to amyloid aggregates represents a promising therapeutic strategy (40). Pepys et al. designed a small molecule (R-1-[6-[R-2-carboxy-pyrrolidin-1-yl]-6-oxo-hexanoyl]pyrrolidine-2-carboxylic acid) that competes with SAP binding to amyloid fibrils (40). This small molecule promotes cross-linking and dimerization of SAP, leading to an enhancement in the SAP clearance by the liver and a decrease in the SAP circulating plasma levels (40).

HSA Prevents SAP Aggregation

SAP is known to aggregate quickly in the presence of calcium (41, 42). However, Hutchinson et al. showed that HSA was able to prevent SAP aggregation in a dose dependent manner, with full inhibition achieved at physiological HSA concentrations (Figure 5) (43). In another study, it was shown that SAP binds to fully reduced HSA

forming a complex. Addition of ApoE to this complex resulted in the displacement of SAP, suggesting that ApoE and SAP bind competitively to fully reduced HSA. It was suggested SAP and ApoE oligomeric states contributed to that competition (44).

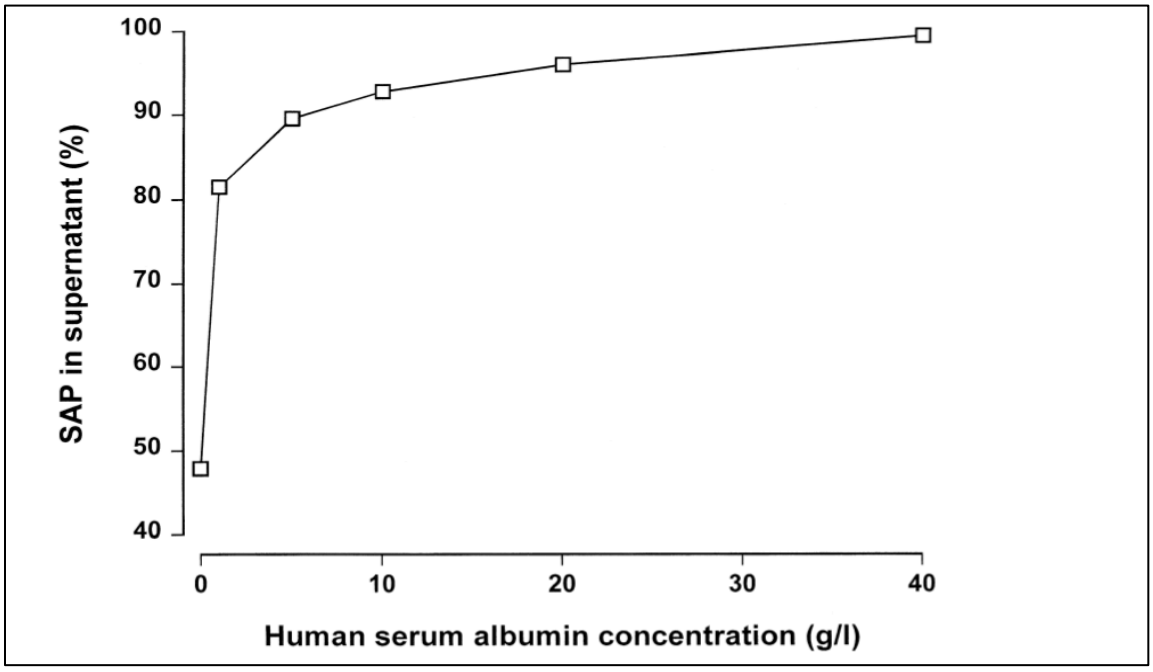

Figure 5. Pure SAP molecules at a 30 mg/l were incubated with incrementally increased albumin concentrations in the presence of 2 mM calcium, in order to promote SAP auto-aggregation. Aggregated SAP molecules were sedimented by centrifugation at 10000 g for 10 min and quantified using SAP specific electroimmuneassay. (43)

Insulin

Insulin is a polypeptide hormone secreted by pancreatic beta cells and is essential for regulating blood sugar levels (45). Structurally, insulin is a dimer of two polypeptide chains (A & B) connected with two disulfide bonds (46). Insulin fibrillization can cause a rare condition named "injection amyloidosis". In patients affected by injection amyloidosis, insulin forms amyloid fibers at its frequent site of injection (47), (48). Moreover, Insulin can form amyloid fibers in vitro if incubated at high concentrations, low pH and high temperature (49), (50, 51). . It should be noted that amylin, a peptide hormone co-secreted with insulin, is another amyloid protein that has been associated with loss of islets of Langerhans in type 2 diabetes (52). However, insulin aggregation has not been linked to a serious disease state, but it still represents a biomedical and a biotechnological problem due to loss of effective insulin in pharmaceutical preparations (53). Human serum albumin was tested for its efficiency in inhibiting insulin amyloid formation. Interestingly, HSA was able to stabilize insulin and prevent its aggregation, as compared to HSA-free preparations (54) (Figure 6).

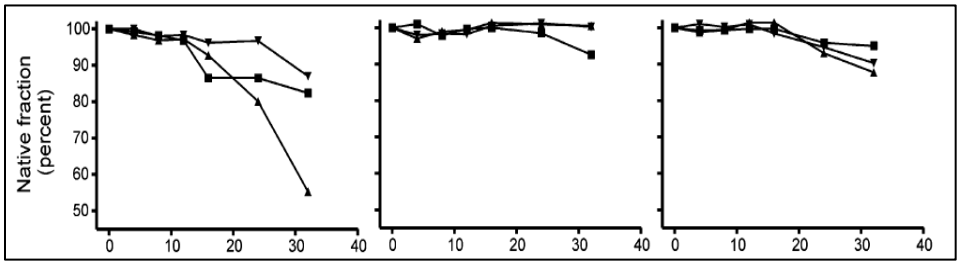

Figure 6. Effect of HSA on Insulin self-association. 0.58 mg ml^{-1} of Insulin were stirred in glass vials at 25°C in the absence of stabilizer, and in the presence of 0.2 mg ml^{-1} α-crystallin or 2.5 mg ml^{-} HSA. The percentage recovered of native insulin was measured at different time points using high performance size-exclusion chromatography (54).

Amyloid Beta Peptides (Aβ)

Aβ peptides are believed to be key players in the pathogenesis of Alzheimer's disease. The peptides are generated by the stepwise cleavage of the trans-membrane amyloid precursor protein (APP) (55). APP processing is divided into two main pathways, amyloidogenic and non-amyloidogenic (56). In the amyloidogenic pathway, APP is first cleaved by the -secretase enzyme, which releases a soluble fragment called sAPP and leaves a 99 a.a. C-terminal polypeptide in the membrane, which is further cleaved by the γ-secretase to release the insoluble Aβ peptides (56). The majority of released Aβ peptides are 40 a.a. long with only 10 % 42 a.a. long. Aβ aggregation follows a nucleation dependent mechanism, in which the released peptides slowly assemble into oligomers. Once the oligomers reach their critical size (nuclei), they further self associate into protofibrils that are elongated rapidly by monomer addition to form mature fibers (3).

HSA Prevents Aβ Aggregation

Clinical studies have shown that low HSA levels are associated with cognitive impairment in elderly populations (57). Moreover, plasmapheresis with therapeutic albumin is being assessed in clinical trials as a potential treatment for mild to moderate Alzheimer's disease (27). Current clinical data indicate that plasmapheresis therapy is safe and tolerable (58), mobilizes the Aβ peptide (28, 59, 60) and results in detectable improvements in the neuropsychological evaluations (58, 61). At a molecular level, numerous studies have shown that HSA is able to bind Aβ with high affinity (59, 62, 63),

yet, there is a disagreement about the underlying mechanism of interaction. Rózga et al. studied the mechanism of albumin Aβ interactions using CD spectroscopy and suggested that albumin binds Aβ monomers with a K_D of 10 μM(60). In agreement with Rózga, Stanyon et al. monitored the HSA/Aβ interaction using thioflavin T fluorescence experiments, noticing that HSA was able to prolong the lag phase and decrease the total amount of fibers formed. Based on these findings, they suggested that HSA binds to Aβ monomers or low molecular weight oligomers (64). However, monitoring the interaction using thioflavin T dye is not straightforward. HSA binds thioflavin T dye with relatively high affinity (K_D of 10 μM) (65), complicating the data analysis due to the competition between HSA and the fibers for the dye binding. On the other hand, Milojevic et al. have performed a series of NMR experiments that rule out the possibility of interaction with Aβ monomers in the μM range (62) and suggest that HSA binds to oligomers or higher molecular weight aggregates more tightly than to Aβ monomers (59, 63, 66).

Structurally, HSA is a single polypeptide chain composed of three homologous domains, which can be further divided into six helical subdomains. Milojevic was able to determine the stoichiometry and affinity of the HSA/Aβ complex. As shown in Figure 7, each HSA domain is able to bind to Aβ oligomers with affinities in the nM- sub μM range. These findings are consistent with Bohrmann et al., who, based on surface plasma resonance, suggested that albumin selectively recognizes Aβ fibers over monomers (67). Similar conclusions were observed by Barcelo et al. using bovine serum albumin (68).

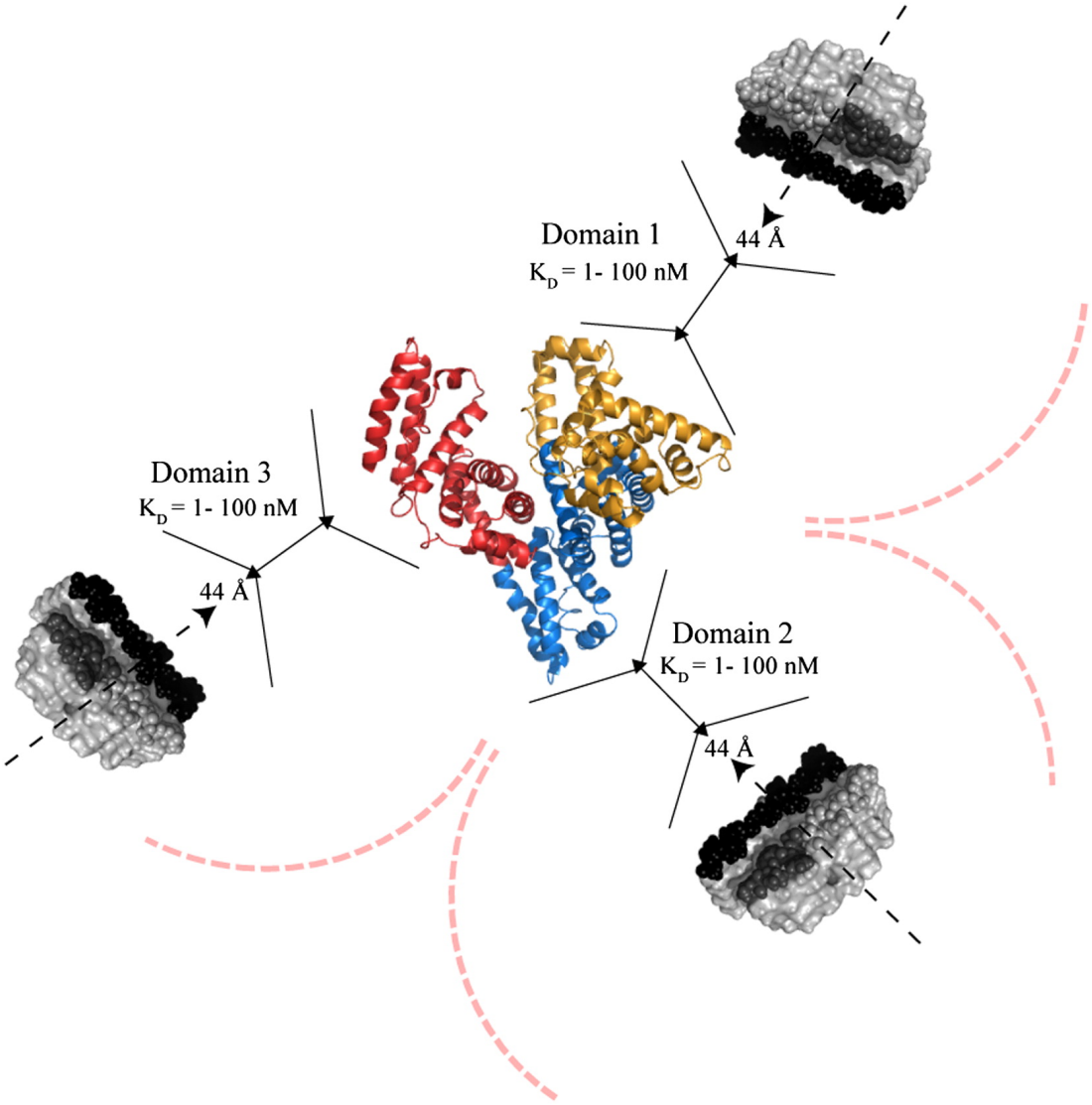

Figure 7. Schematic model summarizing the stoichiometry and affinity of the interaction between HSA and Aβ protofibrils. HSA domains 1, 2, and 3 are colored in yellow, blue, and red, while the Aβ protofibrils central hydrophobic core residues and C-terminus residues are colored in dark gray and black, respectively. Possible Steric hindrance due to binding of Aβ protofibrils to different domains are indicated by red dashed lines, while the black solid lines are aids in the size comparison of HSA domains and Aβ protofibril. The direction of protofibril growth is depicted by dashed lines, while 44 Å indicate the width of a protofibril. Structures of apo HSA and Aβ protofibrils were illustrated using the PDB files 1A06 and 2BEG, respectively. (59)

Summary and Thesis Outlook

Anti-amyloidogenic activity is a new potential function for HSA that pertains to its interaction with various amyloidogenic peptides and proteins endogenously present in human plasma (*e.g.* TTR, SAP, insulin and Aβ peptides). In the majority of these cases, HSA was suggested to bind preferentially to the oligomeric forms rather than to the monomers (36, 44, 66). In addition, HSA also has the ability to bind stressed over non-stressed proteins (25). Studying these interactions at the molecular level will help us to gain insight about the physiological roles of HSA, providing also a valuable tool in designing new inhibitors for amyloidogenesis.

As a first step towards understanding the detailed molecular nature of these interactions, this thesis will focus on defining the key binding determinants in the interaction between HSA and Aβ peptides. Primarily, we will try to answer two main questions. First, which HSA residues are essential for the recognition of Aβ peptides and the prevention of Aβ aggregation? Second, which Aβ residues are mostly affected by HSA binding? Starting form our knowledge about the stoichiometry and affinity of the Aβ interactions at the level of HSA domains, Chapter 2 addresses the first question through successful applications of a reductionist approach, based on a combination of mutational comparative analyses and fatty acid (FA) competition. This strategy allowed us to identify a short HSA derived peptide that prevents Aβ aggregation. In Chapter 3, we examine the effect of HSA on the pseudo-equilibrium state between Aβ monomers and protofibrils. Using a novel NMR experiment, *i.e.*

Dark state Exchange Saturation Transfer (DEST) and ^{15}N T_2 relaxation experiments, we show that Aβ peptides interact with HSA in a dual binding mode. In the first mode, Aβ monomers bind specifically but weakly to HSA (K_d = 0.2-1mM). Despite the weakness of this interaction, it is still physiologically relevant owing to the high concentration of HSA in the plasma (~0.6 mM). In the second binding mode, HSA competes with Aβ monomers for the binding to the protofibrils, as indicated by an HSA-dependent decrease in the contact probabilities between monomer residues and the protofibril surface. Moreover, we also show that this effect is more pronounced for the central hydrophobic core Aβ residues and for part of the C-terminal Aβ residues, highlighting the importance of these regions in the aggregation pathway and in anti-amyloid treatment strategies. Finally, Chapter 4 will map an outline for future investigations to address currently open questions about HSA dynamics, HSA-Aβ and HSA-FA interactions, for which we acquired preliminary data.

References

1. Sipe, J.D., M.D. Benson, J.N. Buxbaum, S.-I. Ikeda, G. Merlini, et al. 2010. Amyloid fibril protein nomenclature: 2010 recommendations from the nomenclature committee of the International Society of Amyloidosis. *Amyloid Int. J. Exp. Clin. Investig. Off. J. Int. Soc. Amyloidosis*. 17: 101–104.
2. Eisenberg, D., and M. Jucker. 2012. The Amyloid State of Proteins in Human Diseases. *Cell*. 148: 1188–1203.
3. Harrison, R.S., P.C. Sharpe, Y. Singh, and D.P. Fairlie. 2007. Amyloid peptides and proteins in review. *Rev. Physiol. Biochem. Pharmacol*. 159: 1–77.
4. Sipe, J.D., M.D. Benson, J.N. Buxbaum, S. Ikeda, G. Merlini, et al. 2012. Amyloid fibril protein nomenclature: 2012 recommendations from the Nomenclature Committee of the International Society of Amyloidosis. *Amyloid*. 19: 167–70.
5. Bergström, J., C. Murphy, M. Eulitz, D.T. Weiss, G.T. Westermark, et al. 2001. Codeposition of apolipoprotein A-IV and transthyretin in senile systemic (ATTR) amyloidosis. Biochem. *Biophys. Res. Commun*. 285: 903–8.
6. Caubet, C., L. Bousset, O. Clemmensen, Y. Sourigues, A. Bygum, et al. 2010. A new amyloidosis caused by fibrillar aggregates of mutated corneodesmosin. *FASEB J*. 24: 3416–26.
7. Miura, Y., S. Harumiya, K. Ono, E. Fujimoto, M. Akiyama, et al. 2013. Galectin-7 and actin are components of amyloid deposit of localized cutaneous amyloidosis. *Exp. Dermatol*. 22: 36–40.
8. Baethge, Bruce A and Jacobson, D.R. *Amyloidosis*, Overview. .
9. Willander, H., G. Askarieh, M. Landreh, P. Westermark, K. Nordling, et al. 2012. High-resolution structure of a BRICHOS domain and its implications for anti-amyloid chaperone activity on lung surfactant protein C. *Proc. Natl. Acad. Sci. U. S. A*. 109: 2325–9.
10. Makin, O.S., and L.C. Serpell. 2004. X-Ray Diffraction Studies of Amyloid Structure. *Methods Mol. Biol*. 299: 67–80.
11. Kirschner, D.A., C. Abraham, and D.J. Selkoe. 1986. X-ray diffraction from intraneuronal paired helical filaments and extraneuronal amyloid fibers in Alzheimer disease indicates cross-beta conformation. *Proc. Natl. Acad. Sci. U. S. A*. 83: 503–507.
12. Kirschner, D.A., H. Inouye, L.K. Duffy, A. Sinclair, M. Lind, et al. 1987. Synthetic peptide homologous to beta protein from Alzheimer disease forms amyloid-like fibrils in vitro. *Proc. Natl. Acad. Sci. U. S. A*. 84: 6953–6957.
13. Colletier, J., A. Laganowsky, M. Landau, M. Zhao, and A.B. Soriaga. 2011. Molecular basis for amyloid-β polymorphism. *Proc. Natl. Acad. Sci. U. S. A*. 108: 1–6.
14. Sawaya, M.R., S. Sambashivan, R. Nelson, M.I. Ivanova, S. a Sievers, et al. 2007. Atomic structures of amyloid cross-beta spines reveal varied steric zippers. *Nature*. 447: 453–7.
15. Kayed, R., E. Head, J.L. Thompson, T.M. McIntire, S.C. Milton, et al. 2003. Common structure of soluble amyloid oligomers implies common mechanism of pathogenesis. *Science*. 300: 486–9.
16. Ferreira, S.T., M.N.N. Vieira, and F.G. De Felice. 2007. Soluble protein oligomers as emerging toxins in Alzheimer's and other amyloid diseases. *IUBMB Life*. 59: 332–345.
17. Lorenzo, A., and B.A. Yankner. 1994. b-amyloid neurotoxicity requires fibril formation and is inhibited by Congo red. *Proc. Natl. Acad. Sci. USA*. 91: 12243–12247.
18. Lopes, D.H.J., C. Colin, T.L. Degaki, A.C. V De Sousa, M.N.N. Vieira, et al. 2001. Amyloidogenicity and cytotoxicity of recombinant mature human islet amyloid polypeptide (rhIAPP). *J. Biol. Chem*. 279: 42803–42810.
19. Glabe, C.G. 2006. Common mechanisms of amyloid oligomer pathogenesis in degenerative disease. *Neurobiol. Aging*. 27: 570–575.
20. Mattson, M.P., B. Cheng, D. Davis, K. Bryant, I. Lieberburg, et al. 1992. beta-Amyloid peptides destabilize calcium homeostasis and render human cortical neurons vulnerable to excitotoxicity. *J. Neurosci*. 12: 376–389.
21. Schubert, D., C. Behl, R. Lesley, A. Brack, R. Dargusch, et al. 1995. Amyloid peptides are toxic via a common oxidative mechanism. *Proc. Natl. Acad. Sci. U. S. A*. 92: 1989–1993.

22. Saitoh, T., K. Horsburgh, and E. Masliah. 1993. Hyperactivation of signal transduction systems in Alzheimer's disease. Ann. N. Y. Acad. Sci. 695: 34–41.
23. Shoffner, J.M. 1997. Oxidative phosphorylation defects and Alzheimer's disease. *Neurogenetics*. 1: 13–19.
24. Margarson, M.P., and N. Soni. 1998. Serum albumin: touchstone or totem? *Anaesthesia*. 53: 789–803.
25. Finn, T.E., A.C. Nunez, M. Sunde, and S.B. Easterbrook-Smith. 2012. Serum albumin prevents protein aggregation and amyloid formation and retains chaperone-like activity in the presence of physiological ligands. *J. Biol. Chem*. 287: 21530–40.
26. Hastings, G.E., and P.G. Wolf. 1995. The therapeutic use of albumin. *Int. J. Artif. Organs*. 1: 281–287.
27. Boada, M., P. Ortiz, F. Anaya, I. Hernández, J. Muñoz, et al. 2009. Amyloid-targeted therapeutics in Alzheimer's disease: use of human albumin in plasma exchange as a novel approach for Abeta mobilization. *Drug news Perspect*. 22: 325–339.
28. Costa, M., A.M. Ortiz, and J.I. Jorquera. 2010. The capacity of albumin to bind to beta-amyloid. *Rev. Neurol*. 50 Suppl 5: S1–S4.
29. Ginsberg, M.D., M.D. Hill, Y.Y. Palesch, K.J. Ryckborst, and D. Tamariz. 2006. The ALIAS Pilot Trial: a dose-escalation and safety study of albumin therapy for acute ischemic stroke--I: Physiological responses and safety results. *Stroke A J. Cereb. Circ.* **37,** 2100–2106 (2006)
30. Jalan, R., K. Schnurr, R.P. Mookerjee, S. Sen, L. Cheshire, et al. 2009. Alterations in the Functional Capacity of Albumin in Patients with Decompensated Cirrhosis Is Associated with Increased Mortality. *Hepatology*. 50: 555–564.
31. Hennebry, S.C. 2009. Evolutionary changes to transthyretin: structure and function of a transthyretin-like ancestral protein. *FEBS J*. 276: 5367–5379.
32. Westermark, P., K. Sletten, B. Johansson, and G.G. Cornwell. 1990. Fibril in senile systemic amyloidosis is derived from normal transthyretin. *Proc. Natl. Acad. Sci. U. S. A*. 87: 2843–2845.
33. Coelho, T. 1996. Familial amyloid polyneuropathy: new developments in genetics and treatment. *Curr. Opin. Neuro*l. 9: 355–359.
34. Saraiva, M.J. 1995. Transthyretin mutations in health and disease. *Hum. Mutat*. 5: 191–6.
35. Chiti, F., and C.M. Dobson. 2009. Amyloid formation by globular proteins under native conditions. *Nat. Chem. Biol*. 5: 15–22.
36. Kugimiya, T., H. Jono, S. Saito, T. Maruyama, D. Kadowaki, et al. 2011. Loss of functional albumin triggers acceleration of transthyretin amyloid fibril formation in familial amyloidotic polyneuropathy. *Lab. Invest*. 91: 1219–28.
37. Tennent, G.A., L.B. Lovat, and M.B. Pepys. 1995. Serum amyloid P component prevents proteolysis of the amyloid fibrils of Alzheimer disease and systemic amyloidosis. *Proc. Natl. Acad. Sci. U. S. A*. 92: 4299–4303.
38. Coria, F., E. Castaño, F. Prelli, M. Larrondo-Lillo, S. Van Duinen, et al. 1988. Isolation and characterization of amyloid P component from Alzheimer's disease and other types of cerebral amyloidosis. *Lab. Investig. a J. Tech. methods Pathol*. 58: 454–458.
39. Duong, T., E.C. Pommier, and A.B. Scheibel. 1989. Immunodetection of the amyloid P component in Alzheimer's disease. *Acta Neuropathol*. 78: 429–437.
40. Pepys, M.B., J. Herbert, W.L. Hutchinson, G.A. Tennent, H.J. Lachmann, et al. 2002. Targeted pharmacological depletion of serum amyloid P component for treatment of human amyloidosis. *Nature*. 417: 254–259.
41. Pinteric, L., and R.H. Painter. 1979. Electron microscopy of serum amyloid protein in the presence of calcium; alternative forms of assembly of pentagonal molecules in two-dimensional lattices. *Can. J. Biochem*. 57: 727–736.
42. Baltz, M.L., F.C. De Beer, A. Feinstein, and M.B. Pepys. 1982. Calcium-dependent aggregation of human serum amyloid P component. *Biochim. Biophys. Acta*. 701: 229–36.
43. Hutchinson, W.L., E. Hohenester, and M.B. Pepys. 2000. Human serum amyloid P component is a single uncomplexed pentamer in whole serum. *Mol. Med*. 6: 482–493.

44. Dergunov, A.D., and Y.Y. Vorotnikova. 1994. The interaction of human serum albumin in the native and fully reduced states with apolipoprotein E, serum amyloid protein and very low density lipoproteins from human plasma. *Int. J. Biochem.* 26: 933–942.
45. Wilcox, G. 2005. Insulin and insulin resistance. *Clin. Biochem. Rev.* 26: 19–39.
46. Menting, J.G., J. Whittaker, M.B. Margetts, L.J. Whittaker, G.K.-W. Kong, et al. 2013. How insulin engages its primary binding site on the insulin receptor. *Nature*. 493: 241–5.
47. Westermark, P., M.D. Benson, J.N. Buxbaum, A.S. Cohen, B. Frangione, et al. 2005. Amyloid: toward terminology clarification. Report from the Nomenclature Committee of the International Society of Amyloidosis. Amyloid Int. J. Exp. Clin. Investig. Off. J. Int. Soc. *Amyloidosis*. 12: 1–4.
48. Dische, F.E., C. Wernstedt, G.T. Westermark, P. Westermark, M.B. Pepys, et al. 1988. Insulin as an amyloid-fibril protein at sites of repeated insulin injections in a diabetic patient. .
49. Ivanova, M.I., S.A. Sievers, M.R. Sawaya, J.S. Wall, and D. Eisenberg. 2009. Molecular basis for insulin fibril assembly. *Proc. Natl. Acad. Sci. U. S. A.* 106: 18990–18995.
50. Waugh, D. 1946. A fibrous modification of insulin. I. The heat precipitate of insulin. *J. Am. Chem. Soc.* : 1944–1947.
51. Nielsen, L., S. Frokjaer, J.F. Carpenter, and J. Brange. 2001. Studies of the structure of insulin fibrils by Fourier transform infrared (FTIR) spectroscopy and electron microscopy. *J. Pharm. Sci.* 90: 29–37.
52. Paulsson, J.F., and G.T. Westermark. 2005. Aberrant processing of human proislet amyloid polypeptide results in increased amyloid formation. *Diabetes*. 54: 2117–25.
53. Muzaffar, M., and A. Ahmad. 2011. The mechanism of enhanced insulin amyloid fibril formation by NaCl is better explained by a conformational change model. *PLoS One*. 6: e27906.
54. Rasmussen, T., R. Tantipolphan, M. Van De Weert, and W. Jiskoot. 2010. The Molecular Chaperone α-Crystallin as an Excipient in an Insulin Formulation. *Pharm. Res.* 27: 1337–1347.
55. Glenner, G.G., and C.W. Wong. 1984. Alzheimer's disease: initial report of the purification and characterization of a novel cerebrovascular amyloid protein. *Biochem. Biophys. Res. Commun.* 120: 885–890.
56. De Strooper, B., and W. Annaert. 2000. Proteolytic processing and cell biological functions of the amyloid precursor protein. *J. Cell Sci.* 113 (Pt 1: 1857–1870.
57. Llewellyn, D.J., K.M. Langa, R.P. Friedland, and I.A. Lang. 2010. Serum albumin concentration and cognitive impairment. *Curr. Alzheimer Res.* 7: 91–96.
58. Anaya, F. 2010. [Therapeutic plasmapheresis and experience in Alzheimer's disease]. *Rev. Neurol.* 50 Suppl 5: S5–S8.
59. Milojevic, J., and G. Melacini. 2011. Stoichiometry and affinity of the human serum albumin-Alzheimer's Aβ peptide interactions. *Biophys. J.* 100: 183–192.
60. Rózga, M., M. Kłoniecki, A. Jabłonowska, M. Dadlez, and W. Bal. 2007. The binding constant for amyloid Abeta40 peptide interaction with human serum albumin. *Biochem. Biophys. Res. Commun.* 364: 714–718.
61. Boada-Rovira, M. 2010. Human Albumin Grifols 5% in plasmapheresis: a new therapy involving beta-amyloid mobilisation in Alzheimer's disease. *Rev. Neurol.* 50 Suppl 5: S9–S18.
62. Milojevic, J., V. Esposito, R. Das, and G. Melacini. 2007. Understanding the molecular basis for the inhibition of the Alzheimer's Abeta-peptide oligomerization by human serum albumin using saturation transfer difference and off-resonance relaxation NMR spectroscopy. *J. Am. Chem. Soc.* 129: 4282–4290.
63. Milojevic, J., V. Esposito, R. Das, and G. Melacini. 2007. Inhibition Alzheimer's Ab peptide oligomerization by human serum albumin using saturation transfer difference & off-resonance relaxation NMR. *J. Am. Chem. Soc.* 129: 4282–4290.
64. Stanyon, H.F., and J.H. Viles. 2012. Human serum albumin can regulate Amyloid-beta peptide fiber growth in the brain interstitium. Implications for Alzheimer's Disease. *J. Biol. Chem.* 287: 28163–28168.
65. Sen, P., S. Fatima, B. Ahmad, and R.H. Khan. 2009. Interactions of thioflavin T with serum albumins: spectroscopic analyses. *Spectrochim. acta Part A Mol. Biomol. Spectrosc.* 74: 94–99.

66. Milojevic, J., A. Raditsis, and G. Melacini. 2009. Human serum albumin inhibits Abeta fibrillization through a "monomer-competitor" mechanism. *Biophys. J.* 97: 2585–2594.
67. Bohrmann, B., L. Tjernberg, P. Kuner, S. Poli, B. Levet-Trafit, et al. 1999. Endogenous proteins controlling amyloid beta-peptide polymerization. Possible implications for beta-amyloid formation in the central nervous system and in peripheral tissues. *J. Biol. Chem.* 274: 15990–15995.
68. Reyes Barcelo, A.A., F.J. Gonzalez-Velasquez, and M.A. Moss. 2009. Soluble aggregates of the amyloid-β peptide are trapped by serum albumin to enhance amyloid-β activation of endothelial cells. *J. Biol. Eng.* 3: 5.
69. Simard, J.R., P.A. Zunszain, C.-E. Ha, J.S. Yang, N. V Bhagavan, et al. 2005. Locating high-affinity fatty acid-binding sites on albumin by x-ray crystallography and NMR spectroscopy. *Proc. Natl. Acad. Sci. U. S. A.* 102: 17958–17963.
70. Bhattacharya, a a, T. Grüne, and S. Curry. 2000. Crystallographic analysis reveals common modes of binding of medium and long-chain fatty acids to human serum albumin. *J. Mol. Biol.* 303: 721–32.
71. Curry, S., H. Mandelkow, P. Brick, and N. Franks. 1998. Crystal structure of human serum albumin complexed with fatty acid reveals an asymmetric distribution of binding sites. *Nat. Struct. Biol.* 5: 827–835.
72. Oida, T. 1986. 1H-NMR study on the interactions of human serum albumin with free fatty acid. *J. Biochem.* 100: 1533–1542.
73. Simard, J.R., P.A. Zunszain, C.-E. Ha, J.S. Yang, N. V Bhagavan, et al. 2005. Locating high-affinity fatty acid-binding sites on albumin by x-ray crystallography and NMR spectroscopy. *Proc. Natl. Acad. Sci. U. S. A.* 102: 17958–17963.
74. Krenzel, E.S., Z. Chen, and J.A. Hamilton. 2013. Correspondence of fatty acid and drug binding sites on human serum albumin: A two-dimensional nuclear magnetic resonance study. *Biochemistry.* 52: 1559–1567.
75. Simard, J.R., P.A. Zunszain, J.A. Hamilton, and S. Curry. 2006. Location of High and Low Affinity Fatty Acid Binding Sites on Human Serum Albumin Revealed by NMR Drug-competition *Analysis. J. Mol. Bio*l. 361: 336–351.
76. Thornalley, P.J., A. Langborg, and H.S. Minhas. 1999. Formation of glyoxal, methylglyoxal and 3-deoxyglucosone in the glycation of proteins by glucose. Biochem. J. 344 Pt 1: 109–116.
77. Vogt, W. 1995. Oxidation of methionyl residues in proteins: Tools, targets, and reversal. *Free Radic. Biol. Med.* 18: 93–105.
78. Benseny-Cases, N., M. Cócera, and J. Cladera. 2007. Conversion of non-fibrillar beta-sheet oligomers into amyloid fibrils in Alzheimer's disease amyloid peptide aggregation. *Biochem. Biophys. Res. Commun.* 361: 916–921.
79. Hou, L., I. Kang, R.E. Marchant, and M.G. Zagorski. 2002. Methionine 35 oxidation reduces fibril assembly of the amyloid abeta-(1-42) peptide of Alzheimer's disease. *J. Biol. Chem.* 277: 40173–6.

Mapping the Interactions between the Alzheimer's Aβ-Peptide and Human Serum Albumin beyond Domain Resolution

Chapter 2

Chapter 2 Preference

This work has been published:

Algamal, M., J. Milojevic, N. Jafari, W. Zhang and G. Melacini. Mapping the Interactions between the Alzheimer's Aβ-Peptide and Human Serum Albumin beyond Domain Resolution. *BiophysJ*. (105) 2013, pp. 1700-1709.

I conducted the experimental work and data analysis corresponding to Figures 2, 5 and 6 in the main text, in addition to all the supplementary Figures. Dr. Julijana Milojevic conducted the experimental work and data analysis corresponding to Figures 1, 3, and 4. Both of us contributed equally to the whole work presented here.

Mapping the Interactions between the Alzheimer's Aβ-Peptide and Human Serum Albumin beyond Domain Resolution

Moustafa Algamal, Julijana Milojevic, Naeimeh Jafari, William Zhang

and Giuseppe Melacini

Abstract

Human Serum Albumin (HSA) is a potent inhibitor of Aβ self-association and this novel function of HSA is of potential therapeutic interest for the treatment of Alzheimer's disease. It is known that HSA interacts with Aβ oligomers through binding sites evenly partitioned across the three albumin domains and with comparable affinities. However, no information is currently available on the HSA–Aβ interactions beyond domain resolution. Here, we map the HSA–Aβ interactions at sub-domain and peptide resolution. We show that each separate sub-domain of HSA domain 3 inhibits Aβ self-association. We also show that fatty acids (FAs) compete with Aβ oligomers for binding to domain 3, but the determinant of the HSA/Aβ oligomer interactions are markedly distinct from those of FAs. While salt bridges with the FA carboxylate determine the FA binding affinities, hydrophobic contacts are pivotal for Aβ oligomer recognition. Specifically, we identified a site of Aβ oligomer recognition that spans the HSA (494-515) region and aligns with the central hydrophobic core of Aβ. The HSA (495-515) segment includes residues affected by FA binding and is prone to self-associate into β-amyloids, suggesting that sites involved in fibrillization may provide a lead to develop inhibitors of Aβ self-association.

***Keywords**: Alzheimer's Disease, Amyloid, Inhibition, NMR, Oligomers, HSA*

Abbreviations: AD, Alzheimer's Disease; BBB, Blood Brain Barrier; CNS, Central Nervous System; CSF, Cerebrospinal Fluid; FA, Fatty Acid; HSA, Human Serum Albumin; ICP, Inductively Coupled Plasma; MA, Myristic Acid; SL, Spin-Lock; RC, Random Coil; STD, Saturation Transfer Difference; STR, Saturation Transfer Reference; WG; Watergate water-suppression NMR technique.

Introduction

Late-onset Alzheimer's disease (AD) is associated with impairment in the clearance of the amyloid beta (Aβ) peptide (1-8). The Aβ peptide clearance from the brain relies on the Aβ transport through the blood brain barrier (BBB) promoted by agents that do not penetrate the BBB, but bind Aβ in plasma. Such agents drive an equilibrium shift of Aβ from the brain toward the periphery, as posited by the 'peripheral sink' hypothesis (9). Since ~90% of circulating plasma Aβ is bound to human serum albumin (HSA), HSA is a key mediator of Aβ clearance. The pivotal role of albumin in Aβ clearance is also confirmed by recent clinical investigations showing that low concentrations of albumin in plasma are associated with cognitive impairment (10,11). Moreover, albumin replacement through plasma dialysis has been proposed as a promising strategy for the treatment of mild AD (12). Given the physiological and potential therapeutic relevance of the Aβ-albumin interactions, the stoichiometry and affinity of the Aβ-albumin complexes have been recently investigated (13). These investigations have revealed that albumin selectively targets Aβ oligomers (denoted here as $A\beta_n$) rather than Aβ monomers (denoted here as $A\beta_1$) (13). The Aβ oligomers are recognized by albumin through largely independent binding sites evenly partitioned across the three albumin domains (Fig. 1a) and with comparable dissociation constants in the sub μM range (13). Such degeneracy in the Aβ binding sites within albumin implies that each single albumin domain can be used as a model system to further probe the HSA/Aβ interactions. However, the binding sites for the Aβ oligomers within HSA have not been mapped

beyond domain resolution, due to experimental challenges arising from the transient nature and the high MW of the Aβ oligomers interacting with HSA.

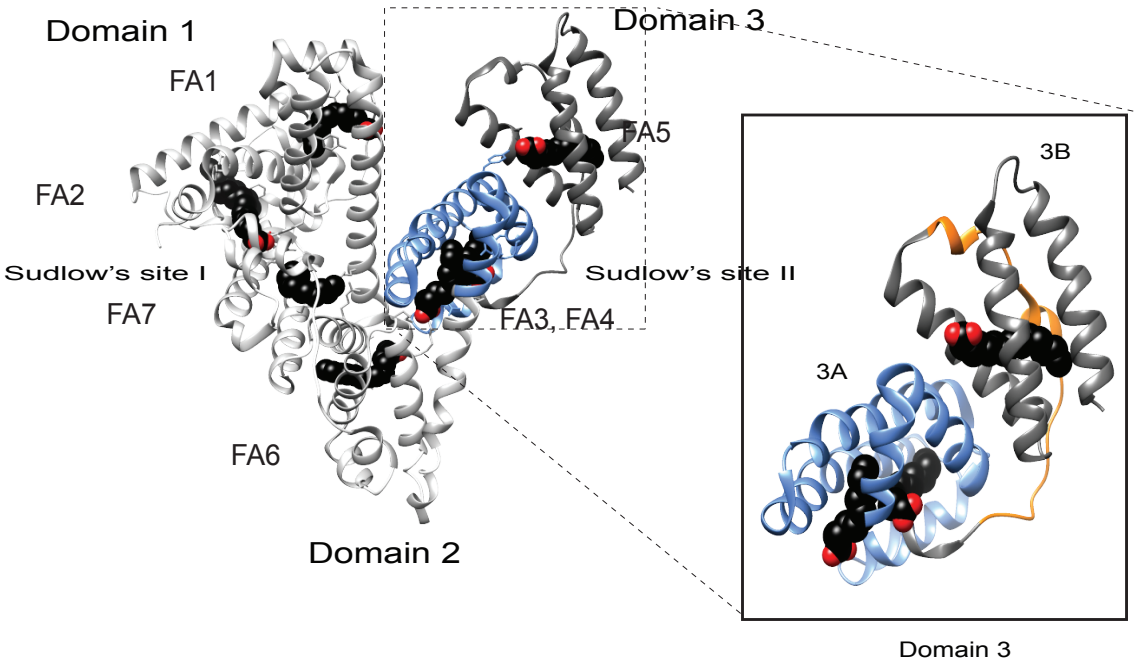

Figure 1. X-ray crystal structures of HSA bound Myristic acid (PDB: 1E7G). Myristate molecules are shown in space-filling representation and are colored by atom: carbon (black), oxygen (red). Major drug binding sites are labeled as Sudlow's sites I and II and their location in the 2A and 3A sub-domains, respectively, is indicated. A separate inset shows in greater detail the structures of domain 3, sub-domains 3A (blue), 3B and the HSA (495-515) segment (orange), for which the Aβ interactions were investigated here.

Here, we show how the interactions of domain 3 of HSA with Aβ oligomers can be mapped at sub-domain and peptide resolution. We specifically focus on domain 3 (i.e.

HSA 381-585), because it remains well structured and soluble even when in isolation (13,14). In addition, domain 3 includes high-affinity fatty-acid (FA) binding sites and therefore it is a suitable construct to explore the competition between Aβ oligomers and FAs, such as myristic acid (MA). Since the binding of MA to domain 3 has been structurally well characterized (Fig. 1b) (15-19), the MA vs. Aβ competition is an effective approach to start mapping the Aβ/domain 3 interactions. However, given the presence of multiple MA binding sites and the possibility of indirect allosteric effects, competitive binding and inhibition experiments alone are not sufficient to narrow down the Aβ binding sites within domain 3. We therefore complement the FA vs. Aβ competition experiments with comparative mutational analyses. Mutants include sub-domain deletions (*i.e.* sub-domains 3A and 3B) and point mutations within each sub-domain at sites of FA binding. The combination of comparative mutational analyses and competition experiments monitored by NMR provides a viable experimental strategy to effectively circumvent the challenges in mapping interactions with large and transient Aβ oligomers.

Our results show that FAs compete with Aβ oligomer for binding to domain 3 of HSA and that, similarly to FAs, Aβ oligomers interact with both sub-domains 3A and 3B, although not all the residues critical to bind FA interact with the Aβ oligomers. In addition, we took our reductionist approach one step further and we identified using a combination of bioinformatics and fluorescence a contiguous putative Aβ interaction site in sub-domain 3B. The sub-domain 3B peptide spanning the identified Aβ interaction site was synthesized and tested for self-association inhibitory potency. The selected domain 3

peptide inhibits Aβ self-association and interestingly matches well with a region of albumin prone to amyloid fibril formation. These results suggest the intriguing hypotheses that a sub-set of the putative sites of Aβ-binding proteins involved in inter-molecular contacts during protein self-association may also serve as possible Aβ recognition and inhibition sites.

Materials and Methods

Aβ (12-28) Peptide Sample Preparation. The Aβ (12-28) peptide used in this investigation was purchased from Pepnome Limited with a purity of 98 %. Lyophilized peptide was dissolved in 50 mM acetate buffer–d_4 at pH 4.7, with 10 % D_2O to a concentration of 1 mM. After the peptide was dissolved, the solution was filtered through a Ultrafree-MC Millipore filter with a 30 kDa cutoff in 5 min intervals at 3,000 rpm to remove aggregates formed during the peptide lyophilization and dissolution processes (13, 20-22). To induce aggregation a 1 M NaCl solution prepared in 50 mM acetate buffer at pH 4.7 was then added to the filtered peptide sample up to a final concentration of 40 mM NaCl followed by a 7 day incubation period at room temperature (13,21).

Aβ (1-42) Peptide Sample Preparation. The Alzheimer's peptide Aβ (1-42) was purchased from EZBiolab Inc., with a purity greater than 95 %. A stock Aβ (1-42) solution was prepared by dissolving 5 mg of the Aβ (1-42) peptide in 2.5 mL of 10 mM NaOH (13, 22). This stock solution was sonicated twice using 2 minute intervals followed by 2 minute incubation on ice. Immediately after sonication, the stock Aβ (1-42) solution

was divided into 100 μL aliquots and frozen at -20^{o}C. 100 μL of the Aβ (1-42) stock solution were thawed and sonicated twice for 2 min with 2 min incubation on ice in between before each experiment. 450 μL of wild type domain 3, domain 3 bound to myristic acid, and domain 3 mutant proteins in 20 mM sodium phosphate buffer at pH 7.4 were added to the sonicated peptides for collection of NMR spectra at 700 MHz with a TCI cyroprobe and at 37 ^{o}C. During the time between NMR data acquisition sessions, the NMR samples were stored in a water bath at 37 ^{o}C and were not stirred or mixed.

TFA Removal from the Aβ Samples. Although all peptides were commercially obtained with > 95% purity, they all contained residual TFA (trifluoroacetic acid), which is routinely used in the final stage of peptide purification. To avoid potential biases, TFA was removed from the Aβ samples prior to the addition of the domain 3 using at least three lyophilization steps in the presence of 50-100 mM HCl (23).

Preparation of HSA Peptides. HSA peptides, HSA (495-515), HSA (495-515) reversed and HSA (530-550) were purchased from (GenScript USA Inc) as a dry powder with purity higher than 95%. 0.5 mM Peptides stock solutions were prepared by dissolving the lyophilized powder in water and adding 50 mM NaOH until the peptides were fully solubilized. Peptides concentration was determined by measuring their UV absorbance at 280 nm using 1490 $M^{-1}cm^{-1}$ as extinction coefficient.

Preparation of Myristic Acid Stock: Myristic acid dry powder (Sigma 490873) was dissolved in DMSO–d_6 at 100 mM. Afterwards aliquots of myristic acid were diluted to 1.5 mM in 20 mM sodium phosphate, pH 7.4 at 70 ^{o}C. The stock was then cooled to 55^{o}C and stored at that temperature for use in subsequent experiments. The myristic acid concentration was confirmed based on the comparison of the methyl signal intensity of the myristic acid ^{1}H-NMR spectra to the methyl intensity of an octanoic acid internal standard (Sigma 153753).

Protein Sub-Cloning, Expression and Purification. The domain 3 gene flanked by the NdeI restriction enzyme site and six hystidines at the N–terminus was generated in the pet15B vector, as previously published (13). The Y411AR410A, R485AS489A and K525A mutants were generated following standard PCR protocols. The 3A subdomain was generated by mutating T496 into a stop codon using as a primer 5' GCTCTGGAAGTCGATGAATAATACGTTCCC 3'. The 3B construct was generated by mutating D494 and E495 into an NdeI restriction enzyme site. This was accomplished using the 5' CAGCTCTGGAAGTCCATATGACATACGTTCCC 3' primer. Since the 3A sub-domain was flanked by the NdeI site, digestion of this mutated DNA resulted in the excision of the 3A sub-domain from the domain 3 sequence. Subsequent ligation generated a 3B sub-domain DNA construct. The sequence of each constructs was

confirmed through PCR based sequencing. All proteins samples were expressed and purified as previously described (13,14).

NMR Spectroscopy. 1D-Saturation Transfer Difference (STD) and Reference (STR) experiments were used to monitor the effect of domain 3 mutants and deletion constructs on the Aβ (12-28) samples. In the STD measurements saturation is transferred through chemical exchange from the Aβ (12-28) oligomers to the monomeric, and thus NMR detectable, Aβ (12-28). Hence, the STD signal probes the interactions of monomeric Aβ (12-28) polypetide chains with the Aβ (12-28) assemblies. Albumin competes with monomeric Aβ (12-28) for binding to oligomeric Aβ (12-28), resulting in a loss of STD signal that is albumin concentration dependent and is exploited to measure the effective average affinity of albumin for the Aβ (12-28) assemblies. A previously published experimental set up was used (13) and therefore will not be further discussed here. The titration curves were fitted using a Scatchard-like model as previously explained (13). Due to the transient nature of the oligomers formed by the longer Aβ (1-42) peptide, the STD experiments were not performed for this longer peptide, however the intensities of 1D Watergate experiments are effective in probing aggregation of Aβ (1-42) (13,22). These experiments rely on the incorporation of a 30 ms long spin lock pulse prior to acquisition to suppress contributions from residual protein and selectively observe the monomeric and low MW Aβ signal. All experiments were acquired on a Bruker Avance 700 MHz spectrometer equipped with a 5 mm TCI Cyroprobe. The STD experiments

were performed at 20 ^{o}C, while 1D-WG experiments were performed at 37^{o}C. All spectra were processed with NMRPipe (24) and analyzed with Sparky (25).

ThT Fluorescence. ThT fluorescence spectra were recorded using a Tecan Safire fluorescence spectrometer and 96 well plates (half-area) with 155 μL sample volumes (22,26). The concentration of Aβ (1-42) in all samples was 70 mM, while the concentration of inhibitory and control peptides, *i.e.* HSA (494-515) and HSA (594-515) reversed, respectively, was set to 120 mM. Measurements were performed in 30 mM HEPES buffer with 20 mM of the Thioflavin T dye at pH 7.4. As a control, individual ThT fluorescence spectra were collected for HSA peptides samples. These values were subtracted from the values obtained from the HSA peptides:Aβ mixtures. For each sample at least three measurements were performed and the average values are reported. The error was calculated as the standard deviation of all measurements.

Bioinformatics analysis. Secondary structure elements and local (three residues) RMSD changes were calculated through the MOLMOL software (27) using PDB files (1AO6) and (1E7G) for apo and myristic acid bound HSA (18), respectively. The Waltz algorithm (http://waltz.switchlab.org/) was used to predict domain 3 regions prone to amyloid formation (28). For the Waltz profile the output with high sensitivity and pH 7 was chosen. The Waltz score was plotted against the residue number to show the residue-specific propensity of amyloid formation.

Results

Myristic acid and Aβ oligomers compete for binding to domain 3 of HSA. In order to probe the competition between myristic acid (MA) and Aβ binding, we measured the potency of HSA domain 3 in inhibiting Aβ (1-42) self-association in the presence and absence of MA. For this purpose, we monitored the loss of Aβ (1-42) 1D NMR signal intensity vs. time due to the formation of high-MW NMR-undetectable aggregates (Fig. 2a). In these experiments, the contributions to the NMR signal arising from HSA are effectively edited out through a spin-lock relaxation filter. This is a distinct advantage of NMR relative to other spectroscopies, such as ThT fluorescence, because the ThT fluorophore binds to HSA and therefore the addition of HSA may affect the detected fluorescence signal. In addition, the Aβ (1-42) 1D NMR signal intensity *vs.* time profiles appear more reproducible than those obtained using ThT fluorescence (13, 22, 29), thus facilitating the quantitative evaluation of self-association inhibitors through comparative analyses.

Fig. 2a shows that in the absence of HSA domain 3, the 1D NMR signal of Aβ (1-42) is rapidly lost over time, until a plateau is reached with the original intensity reduced by ~40 %. Upon addition of sub-stoichiometric amounts of apo HSA domain 3, the NMR signal intensity of Aβ (1-42) is dramatically increased both in the initial decay phase and in the final plateau region (Fig. 2a), clearly indicating that the isolated domain 3 functions as an effective Aβ self-association inhibitor. However, when HSA domain 3 was added

in the presence of excess myristic acid (MA), the inhibitory potency of domain 3 was significantly reduced resulting in Aβ (1-42) signal intensities that are intermediate between those of the two previous profiles (Fig. 2a). These variations in the 1D NMR signal vs. time profiles are attributable to either the competition between MA and Aβ (1-42) for binding to domain 3 and/or to potential interactions between free MA and Aβ (1-42). In order to rule out the latter explanation, we monitored the 1D NMR signal of Aβ (1-42) over time in the absence and presence of 30 μM of MA and no significant differences were observed upon addition of 30 μM of MA (Fig. S1). This MA concentration exceeds the concentration of free MA expected under the conditions of Fig. 2a (i.e. $[\text{HSA domain 3}]_{\text{Total}}$ = 25 μM and $[\text{MA}]_{\text{Total}}$ = 90 μM), because domain 3 is fully saturated by MA, as shown by saturation transfer difference NMR (Fig. 2b) and the HSA domain 3:MA specific binding stoichiometry is 1:3. We therefore conclude that the data of Fig. 2b point to competition between MA and Aβ (1-42) oligomers for binding to domain 3 of HSA.

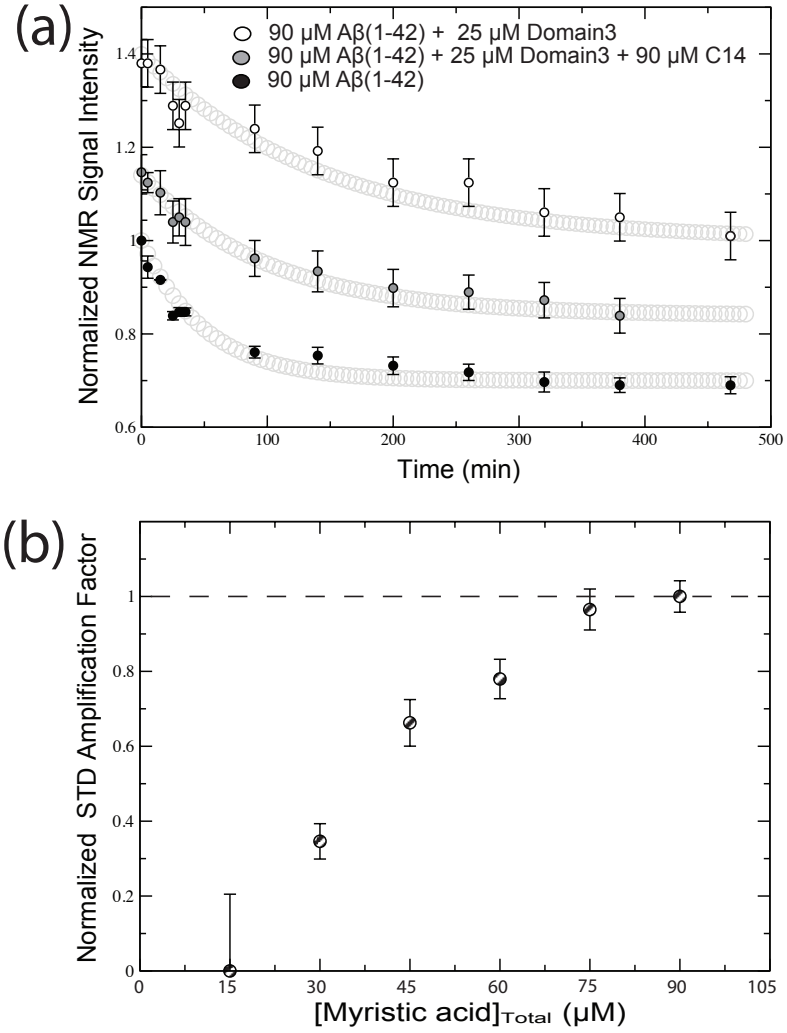

Figure 2. (a) Effect of myristic acid on the inhibition of Aβ (1-42) aggregation by HSA domain 3 (*i.e.* HSA 381-585). 1D ^{1}H-NMR signal intensities of 90 μM Aβ (1-42) recoded over time are shown in the absence (black circles) and in the presence of domain 3 either in the apo form (white circles) or saturated with myristic acid (gray circles). The initial (t = 0) amplitude quantifies the NMR detectable species present after the dead time of the experiment, *i.e.* the time interval elapsed between sample preparation and the beginning of the NMR data acquisition. The Aβ (1-42) concentration of 90 μM was chosen because under our experimental conditions it provides an optimal compromise between the signal-to-noise of each sampled spectrum and the time resolution of the decay. We recognize that this concentration is higher than those typically reported for *in vivo* Aβ (*i.e.* < nM in human plasma (10)). However, our *in vitro* conditions allowed us to test the effect of albumin on a wide range of Aβ assemblies from monomers to fibrils, increasing the likelihood to mimic also the Aβ association states relevant *in vivo*. (b) STD based dose-response curve for myristic acid binding to domain 3.

The MA *vs.* Aβ competition emerging from Fig. 2a suggests that at least some of the domain 3 residues affected by MA binding are also critical for Aβ self-association inhibition. The residues affected by MA binding include those in direct contact with MA as well as those indirectly affected by MA through local conformational changes (Fig. S2). Fig. S2 shows that the MA binding sites in domain 3 span both sub-domains (*i.e.* 3A and 3B) and that the sites directly or indirectly affected by MA binding are scattered through domain 3. Considering the abundance and wide distribution of domain 3 sites affected by MA (Fig. S2), we decided to further narrow down the location of sites critical for Aβ self-association inhibition by complementing the competition experiments of Fig. 2 with comparative mutational analyses.

The first set of mutants was designed to address the question as to whether Aβ binds both sub-domains (*i.e.* 3A and 3B), similarly to MA, or it is selective for a single sub-domain. For this purpose, we have sub-cloned, expressed and purified separate 3A and 3B sub-domain constructs and tested their interactions with two Aβ peptides, Aβ (12-28) and Aβ (1-42). The former peptide spans the central hydrophobic core of the Aβ peptide as well as key residues involved in HSA binding (13, 21, 22) and was included in the analyses, because unlike Aβ (1-42) forms stable soluble Aβ oligomers. Furthermore, the binding of Aβ (12-28) oligomers to albumin can be monitored by STD NMR experiments, resulting in albumin inhibition isotherms from which quantitative effective K_D values for the Aβ oligomer:HSA complexes are obtained based on Scatchard-like models, as previously explained (13). In addition, the Aβ (12-28) STD *vs.* [HSA] inhibition profiles exhibit a clear plateau whose starting point provides an estimation of

the effective concentration of protein (*i.e.* HSA) necessary to saturate the Aβ (12-28) oligomers binding sites (13).

Sub-domains 3A and 3B are minimal structural units that retain potency in inhibiting Aβ self-association. Figs. 3a and 3b show the concentration-dependent STD monitored Aβ (12-28) self-association inhibition profiles measured for sub-domains 3A and 3B. The STD-monitored titration data (Figs. 3a and 3b) display a typical dose-response pattern in which the I_{STD}/I_{STR} ratios decrease progressively as the sub-domain concentration increases, until a saturation plateau is reached, indicating that both sub-domains span specific Aβ oligomers binding sites. These interactions are compatible with at least two different stoichiometries for the domain 3:$A\beta_n$ complexes. In the first stoichiometry, a single Aβ oligomer interacts with both sub-domains. In this case, we expect that, in going from the integral domain 3 to the separate sub-domains, the average effective number of Aβ oligomers bound per molecule of albumin construct, defined as $n_{A\beta n}$, will remain largely unaffected, although the affinity may change. In the second putative stoichiometry, two distinct Aβ oligomers interact with the two sub-domains. In this case, we expect that, in going from the integral domain 3 to the separate sub-domains, $n_{A\beta nn}$ should approximately halve.

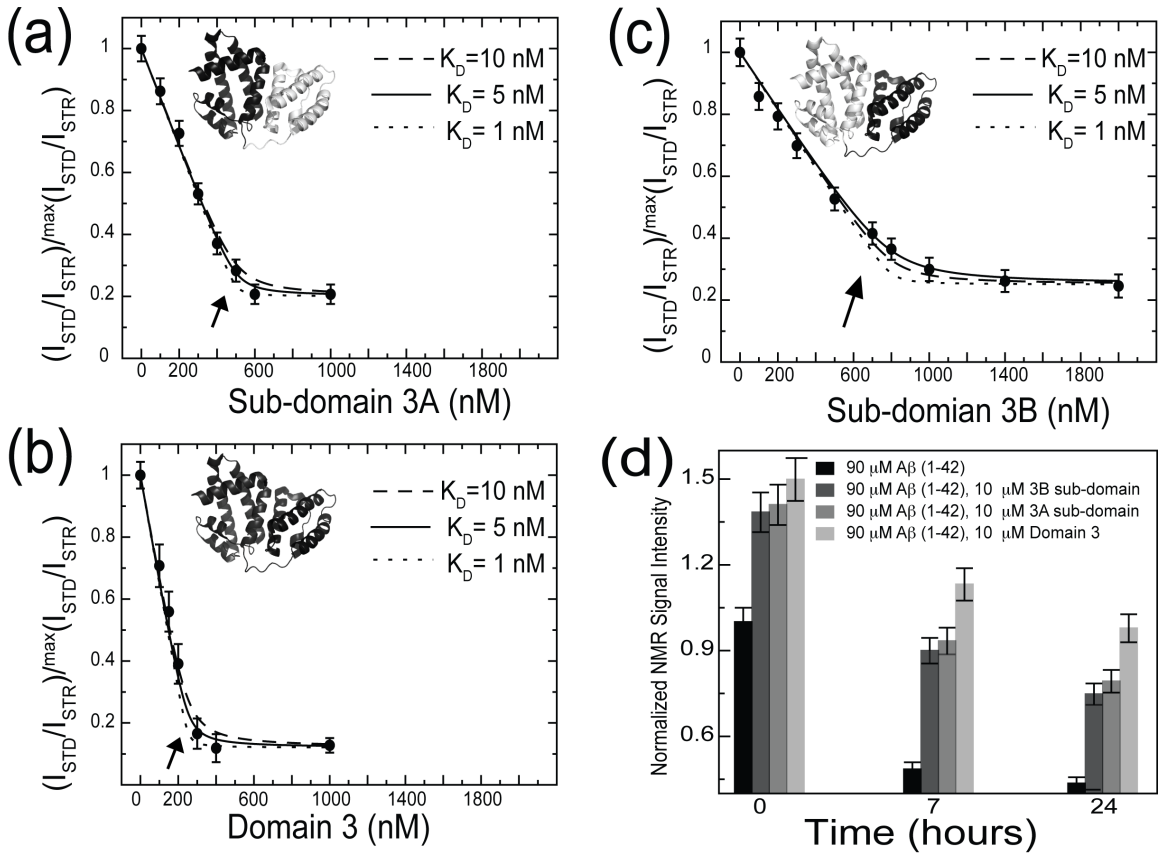

Figure 3. Inhibition of the Aβ self-association by domain 3 and its sub-domain deletion mutants monitored by dose-response Aβ (12-28) STD-based profiles (a-c) and by Aβ (1-42) 1D-NMR *vs.* time (d). Panels (a)-(c) illustrate the effect of the sub-domain deletion mutants (*i.e.* 3A and 3B) and the full length domain 3, respectively, on the relative I_{STD}/I_{STR} ratios measured for a filtered 1 mM Aβ (12-28) peptide sample aggregated through addition of 40 mM of NaCl. In panels (a)-(c), dotted, dashed and full lines correspond to dose-response curves back-calculated using a Scatchard-like model. In each panel the structure of domain 3 is shown (PDB: 1A06) and the construct used in the titration is colored in black. The $<[A\beta_n]_{Tot.}>$ the average effective total concentration of albumin-binding competent Aβ oligomers and $\gamma = n_{protein} / n_{A\beta n}$, where $n_{protein}$ is the average effective number of albumin protein construct molecules (*i.e.* domain 3 or sub-domain 3A or 3B) bound per Aβ oligomer and $n_{A\beta n}$ is the average effective number of Aβ oligomers bound per molecule of albumin protein construct. In (d), 0.1 mM Aβ (1-42) samples were incubated with 10 μM of domain 3 constructs and changes in the intensities of the methyl region of 1D-WG spectra with time are reported. All intensities were normalized to the 0.1 mM Aβ (1-42) sample acquired for the first incubation time point.

To discriminate between the two possible domain 3:$A\beta_n$ stoichiometries discussed above, we also measured as a reference the Aβ (12-28) self-association inhibition STD profile for the integral domain 3 (Fig. 3c). All three STD profiles of Fig. 3a-c were fitted to a Scatchard-like model, which provides the $\gamma<[A_n]_{Tot.}>$ product (13), where $<[A_n]_{Tot.}>$ is the average effective total concentration of albumin-binding competent Aβ oligomers and $\gamma = n_{protein} / n_{A\beta_n}$, where $n_{protein}$ is the average effective number of albumin protein construct molecules (*i.e.* domain 3 or sub-domain 3A or 3B) bound per Aβ oligomer and $n_{A\beta_n}$ is defined as above, *i.e.* the average effective number of Aβ oligomers bound per molecule of albumin construct (13). Since the measurements in Fig. 3a-c were recorded utilizing the same Aβ stock solution, $<[A\beta_n]_{Tot.}>$ does not change appreciably in the inhibition STD profiles of domain 3 and sub-domains 3A and 3B (Fig. 3a-c). Similarly, $n_{protein}$ is not expected to vary in going from panels a, b to c of Fig. 3 and to be ~1, as previously reported (13). As a result, variations in the fitted $\gamma<[A\beta_n]_{Tot.}>$ product across the three panels of Fig. 3a-c report primarily on changes in $n_{A\beta_n}$, allowing to differentiate between the two proposed putative stoichiometries for binding of Aβ oligomers to domain 3 of albumin.

The comparison of the STD profile in Fig. 3c with those in Figs. 3a and 3b clearly shows that in going from domain 3 to the either one of the two separate sub-domains $\gamma<[A_n]_{Tot.}>$ is doubled (Fig. 3a-c), as expected if the $n_{A\beta_n}$ value of domain 3 is about twice as the $n_{A\beta_n}$ value for the isolated 3A or 3B sub-domains. These observations support the

second stoichiometric pattern, whereby each sub-domain binds a different Aβ (12-28) oligomer. This conclusion is also consistent with the inhibitory potencies measured for the two sub-domains using the longer Aβ (1-42) peptide (Fig. 3d). Fig. 3d consistently indicates that domain 3 exhibits higher inhibition potency than the individual sub-domains, corroborating that both sub-domains, 3A and 3B, are involved in Aβ oligomer binding. Given that each sub-domain interacts with $A\beta_n$, the next open question we focused on pertains to the specific $A\beta_n$ contact sites within each HSA sub-domain.

Comparison of Aβ and Fatty Acid (FA) binding modes: effects of hydrogen-bonding perturbing mutations. Given the competition between FAs and Aβ oligomers supported by Fig. 2, we hypothesized that Aβ and FAs might share common binding determinants. In order to test this hypothesis, we investigated the interaction between Aβ and domain 3 mutants that hamper FA binding by removing side-chains involved in hydrogen-bonds to the FA carboxylate. For instance, the R410A/Y411A and R485A/S489A double mutations (Fig. 4b,d) drastically reduce fatty acid binding to sub-domain 3A (Fig. S3a,b), while K525A (Fig. 4f) markedly decreases FA binding to sub-domain 3B (Fig. S3c) (17). Therefore, we tested the interactions of these three sets of domain 3 mutants (*i.e.* R410A/Y411A, R485A/S489A and K525A) with Aβ oligomers. Fig. 4a,c,e report the STD-monitored titration of Aβ (12-28) with the R410A/Y411A, R485A/S489A and K525A domain 3 mutants. The STD profiles shown in Fig. 4a,c,e (black dots) indicate that all three domain 3 mutants are active inhibitors of Aβ (12-28) self-association. Furthermore, no significant differences were observed when the titration profile of each mutant was compared to the corresponding profile for the WT domain 3

(Fig. 4a,c,e, red dots). These results suggest that mutations that disrupt the interactions of domain 3 with FAs (Fig. S3) do not necessarily affect Aβ (12-28) oligomer binding, pointing to marked differences between the HSA binding determinants for FAs and those for the Aβ (12-28) oligomers. In order to confirm the validity of this conclusion for longer and more physiologically relevant Aβ peptides, we also tested the interactions between the three domain 3 mutants and Aβ (1-42).

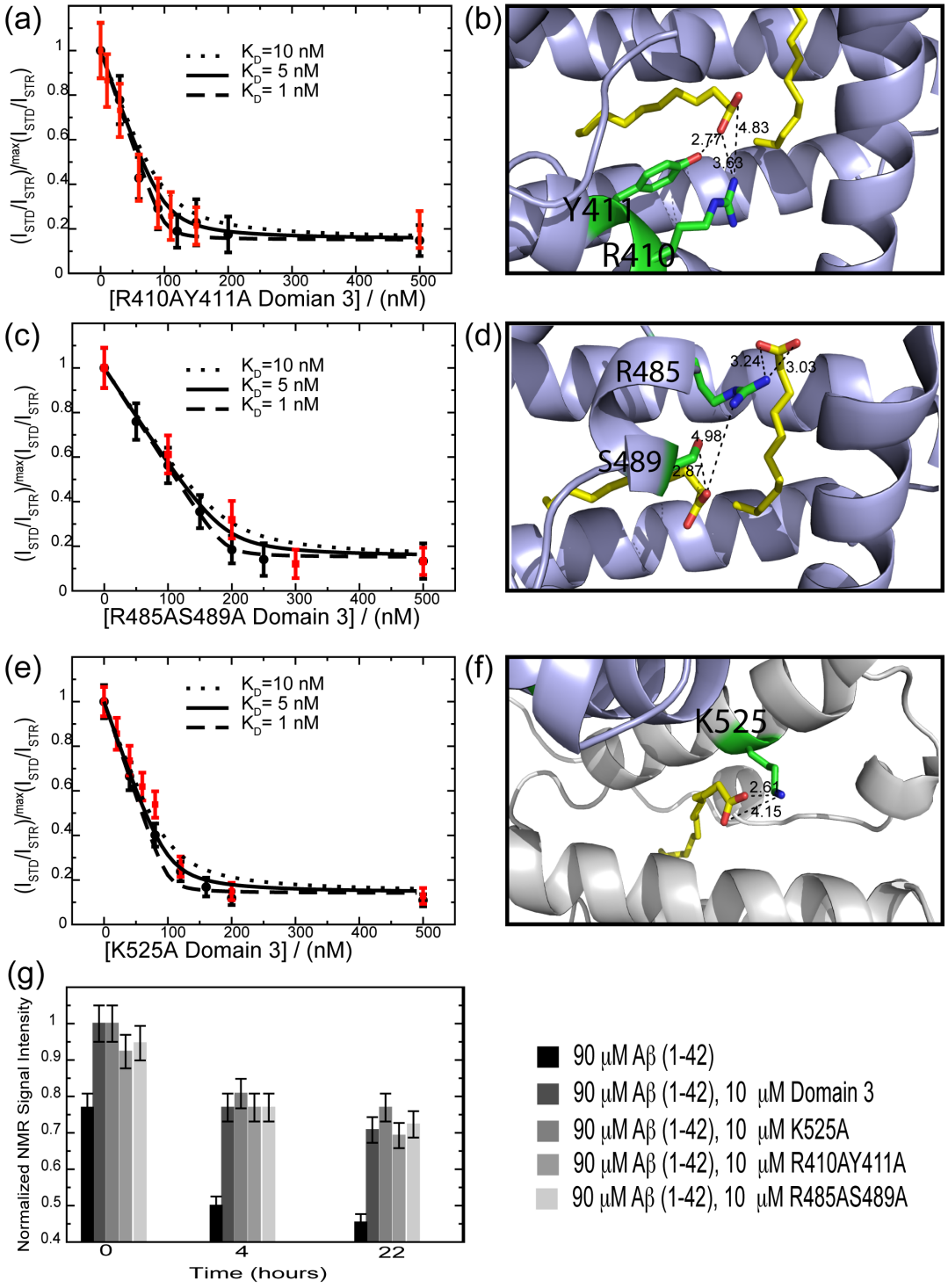

Figure 4. Inhibition of the Aβ self-association by fatty-acidic silencing domain 3 point mutants monitored by dose-response Aβ (12-28) STD-based profiles (a-f) and by Aβ (1-42) 1D-NMR *vs.* time (g). In panels (a), (c) and (e), all ratios were normalized to their

maximum value measured before protein addition and dashed, full and dotted lines correspond to dose-response curves back-calculated using a Scatchard-like model and K_D values of 1, 5 and 10 nM, respectively. For reference purposes, the titration profile of wild-type domain 3, measured using the same Aβ (12-28) peptide batch as the mutated protein, is shown in each panel in red color. In panels (b), (d) and (f), the side chains of the mutated residues interacting with fatty acids are shown. Bound fatty acids are displayed in yellow. Hydrogen bonds to the fatty acid are indicated by dashed lines and their lengths are reported in Å. For (d), experiments were acquired at 700 MHz at 310 K in 20 mM potassium phosphate, pH 7.4, 10% D_2O, 0.05% NaN_3. A 50 ms long spin lock was used to suppress residual protein signal. Color coding is as per the legend in the Figure.

The experiments on the Aβ (1-42) peptide (Fig. 4g) confirmed the differences between the Aβ and FA binding modes already emerged from the STD experiments on Aβ (12-28) (Fig. 4a,c,e). Specifically, Fig. 4g indicates that the incubation of Aβ (1-42) at 37 ^oC results in peptide aggregation and consequent losses in the Aβ NMR signal over time. These signal losses are significantly reduced in the presence of WT domain 3 (Fig. 4g). A similar reduction in aggregation is observed for all domain 3 mutants, suggesting that the mutations did not significantly perturb binding of the Aβ oligomers to domain 3 (Fig. 4g), although they had a marked effect on FA binding (Fig. S3) (17). We conclude that the mutated residues (*i.e.* R410, Y411, S489, R485 and K525), while involved in hydrogen-bonds with albumin-bound FAs, are not part of the HSA domain 3 determinants for Aβ binding. In order to further dissect the domain 3 residues involved in Aβ binding, we focused on sub-domain 3B, because it provides a minimal structural unit that still inhibits Aβ self-association (Fig. 3a,d) and it includes only a single well-defined FA binding site.

Dissecting the sub-domain 3B determinants for Aβ binding. As a first step towards narrowing down the Aβ binding sites within sub-domain 3B, we verified that this construct retains FA binding capacity and that FA binding competes with Aβ binding. Fig. S4a shows the STD amplification factor for a titration of MA into sub-domain 3B. A clear dose-response pattern with plateau is observed, confirming that MA binds specifically to our 3B construct. Furthermore, Fig. S4b, similarly to Fig. 2a, clearly shows that MA binding decreases the Aβ self-association inhibitory potency of the 3B construct, indicating that the MA vs. Aβ oligomer competition occurs also at the level of sub-domain 3B. This observation suggests that the 3B residues interacting with the Aβ oligomers are either in direct contact with the FA (Fig. S2, open circles) and/or are indirectly affected by FA binding through conformational changes (Fig. S2, local RMSD).

In order to further screen for the 3B sites that recognize Aβ oligomers, we hypothesized that, since Aβ monomers and HSA compete for the same binding partner (i.e. Aβ oligomers), the recognition of Aβ oligomers by HSA should to some extent resemble the recognition of Aβ oligomers by Aβ monomers. Based on this hypothesis, HSA residues with high propensity to bind to Aβ oligomers and proto-fibrils should meet two additional criteria. First, they should fall in regions of HSA prone to adopt a β-strand conformation and to self-associate into amyloid fibrils. For instance, the Waltz algorithm (28) predicts that three distinct segments of sub-domain 3B are likely to be involved in HSA self-association (Fig. 5b), with the longest region spanning residues 494-515.

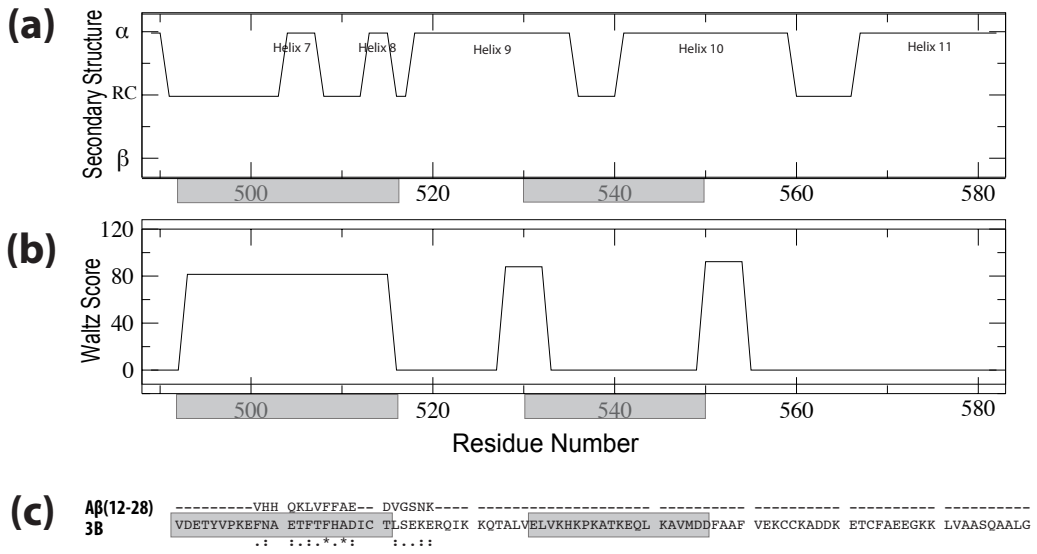

Figure 5. (a) Sub-domain 3B secondary structure (PDB: 1E7G). (b) WALTZ scores, which predict amyloid propensity. (c) Clustaw sequence alignment of sub-doamin 3B and Aβ (12-28). Residues of no consensus are indicated as black dash, single, fully conserved residues are indicated in stars, while strong and weak conserved residues are indicated as semicolons and dots respectively. The domain 3 regions corresponding to the HSA peptides (494-515) and (530-550) used in Fig. 6 are highlighted in grey.

Second, sites that recognize Aβ assemblies are likely to align in sequence with the Aβ residues involved in self-recognition. For instance, the central hydrophobic core of Aβ (i.e. L17VFFA21) is known to be critical for Aβ self-association and aligns well with several residues in the 494-515 segment of HSA (Fig. 5c). Interestingly, the 494-515 region also includes several loci of FA-dependent conformational change (Fig. S2). Overall, the 494-515 HSA segment emerges as a consensus sequence for Aβ oligomer binding, which is consistent with the MA competition data (Fig. S4) and meets the two bioinformatic criteria of amyloid propensity and Aβ alignment (Fig. 5b,c). Based on these observations, we hypothesized that the HSA (494-515) peptide retains Aβ self-association inhibitory potency. In order to test this hypothesis, we measured the

inhibitory potencies of the HSA (494-515) synthetic peptide using both the Aβ (12-28) and Aβ (1-42) systems. We also included in our measurements two negative controls, i.e. the reversed HSA (494-515) peptide, to check the specificity of the HSA peptide/Aβ interactions, and the HSA (530-550) peptide, which spans a region of sub-domain 3B that does not meet our two bioinformatic criteria (Fig. 5b,c).

Fig. 6a shows the effect of the HSA (494-515) peptide on the Aβ (12-28) self-association as monitored by STD. The STD vs. [HSA (494-515)] profile conforms to a clear does-response pattern with a well-defined plateau (Fig. 6a), pointing to specific interactions between this HSA peptide and Aβ (12-28). The specificity of these interactions is further confirmed by the dramatically reduced affinity for Aβ (12-28) observed for the reversed HSA (494-515) peptide (Fig. 6a), which results in an effective Kd about one-order of magnitude higher than that measured for the wt HSA (494-515) counterpart (Fig. 6a). In addition, as expected, no Aβ (12-28) self-association inhibition was observed for the other negative control peptide, i.e. HSA (530-550) (Fig. 6a), confirming the usefulness of the bioinformatic selection criteria.

The results obtained for Aβ (12-28) (Fig. 6a) were confirmed when the HSA peptides were tested on Aβ (1-42) (Fig. 6b). The self-association of Aβ (1-42) was not monitored by NMR intensity losses because of the overlap between the NMR signals of the Aβ (1-42) and the HSA (494-515) peptides. The sharp and intense NMR lines of the flexible HSA (494-515) peptide are not easily edited out through a spin-lock relaxation filter without significant intensity losses for the Aβ (1-42) peptide as well, unlike the case of larger and well-structured HSA constructs. However, unlike full length HSA, the HSA

(494-515) peptide under our experimental conditions does not affect the fluorescence of ThT in the absence of Aβ (1-42) (Fig. S5). We therefore resorted to ThT fluorescence to monitor the formation of cross-b amyloid assemblies (Fig. 6b). Fig. 6b shows that the HSA (494-515) peptide significantly reduces the ThT fluorescence arising from the Aβ (1-42) cross-b amyloids formed during a 15 h incubation period. This inhibitory effect is completely lost when the HSA (494-515) sequence is reversed (Fig. 6b). Overall, the data for Aβ (12-28) and Aβ (1-42) (Fig. 6a,b) consistently point to the HSA (494-515) region as a site of specific HSA/Aβ contacts, confirming our hypothesis based on the FA competition experiments and bioinformatic analyses (Fig. 5).

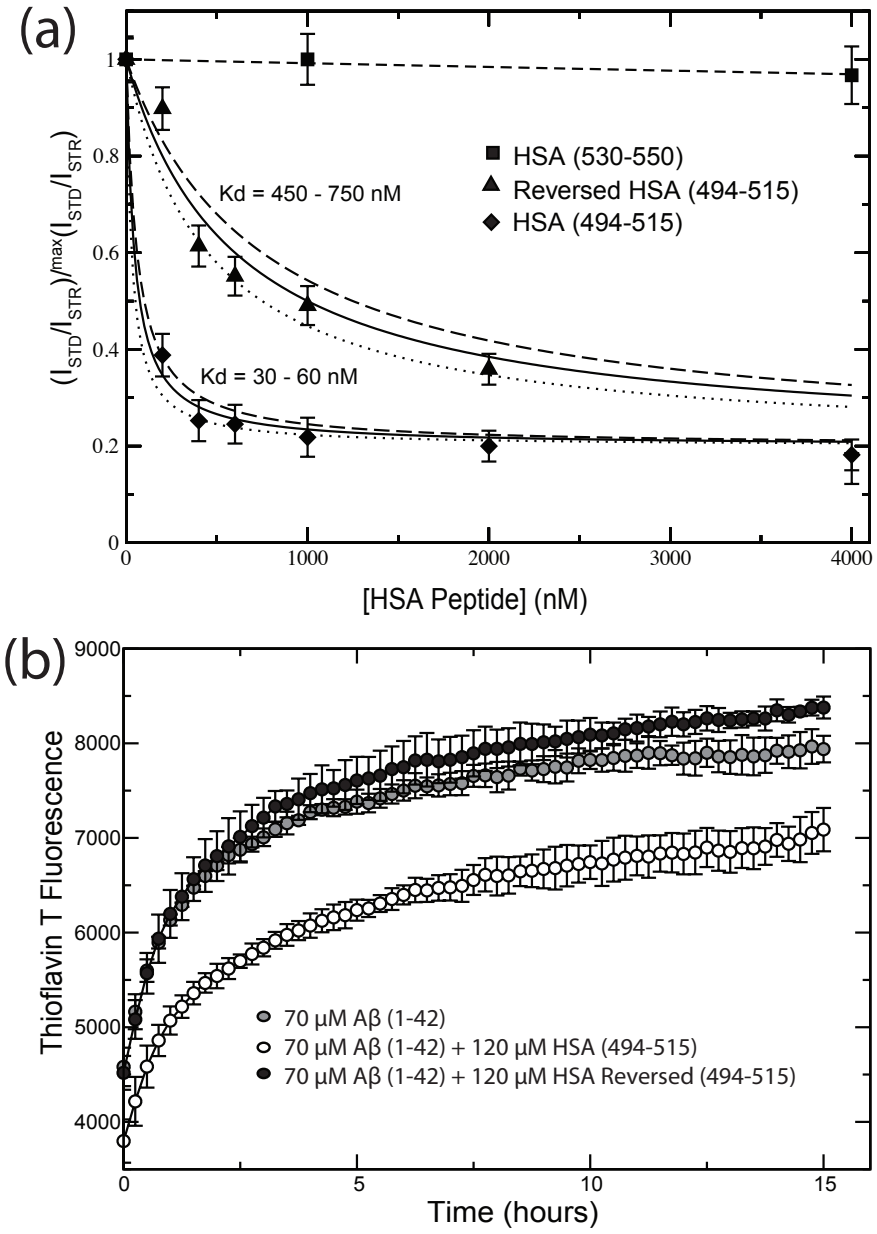

Figure 6. (a) Dose-response STD-based profiles for the inhibition of the Aβ (12-28) self-association by three HSA domain 3-derived peptides, *i.e.* HSA (494-515) (black diamonds), HSA (494-515) with reversed sequence (black triangles) and HSA (530-550) (black squares). The latter two peptides serve as negative controls. (b) Inhibition of Aβ (1-42) aggregation by HSA (494-515) (white circles) and HSA (494-515) with reversed sequence (black circles), as monitored by ThT fluorescence. The aggregation profile for Aβ (1-42) alone is shown as grey circles.

Discussion

The consensus model emerging from the data presented here provides unprecedented insight about the HSA:Aβ oligomer interactions well beyond the previously available domain resolution. We show that each separate sub-domain of HSA domain 3 retains Aβ self-association inhibitory potency and is able to bind Aβ oligomers with a sub-μM affinity (Fig. 3). The FA binding sites are also located in both sub-domains 3A and 3B (Fig. 1) and FAs compete with Aβ oligomers for binding to domain 3 (Fig. 2 and Fig. S4). However, the determinant of the HSA/Aβ oligomers interactions are markedly distinct from those of FAs (Fig. 4). For FAs, although extensive hydrophobic contacts are common, it is the strength of hydrogen bonds/salt bridges formed between the albumin amino acid side chains and the fatty acid carboxylate groups that determines the binding affinities (Fig. S3) (15,16). For Aβ, the relevance of these specific polar/ionic interactions becomes marginal (Fig. 4), but hydrophobic contacts appear to play a pivotal role for Aβ oligomer recognition (Fig. 5 and Fig. 6). For instance, in the case of sub-domain 3B, a site of Aβ oligomer recognition spans the HSA (494-515) region, which includes hydrophobic sites in contact with the aliphatic tail of MA and subject to changes in conformation upon FA binding (Fig. S2). The (494-515) HSA region thus explains the competition between FA and Aβ oligomer for binding to HSA sub-domain 3B, although at the present stage we cannot rule out that other HSA sites may also contribute to the observed FA vs. $A\beta_n$ competition. Interestingly, the (494-515) segment includes also several residues that align to the central hydrophobic core sequence of Aβ (i.e. L17VFFA21, Fig. 5c).

The importance of the hydrophobic effect in the binding of Aβ oligomers is supported by the observation that several other Aβ binding proteins, such as sLRP (30), clusterin (31,32) and ApoE (33), are also involved in lipid binding. Additionally, it was recently shown that binding of Aβ to proteins not involved in lipid metabolism, such as ABAD and affibody ZAb3, is accompanied by a favorable entropic change, consistent with hydrophobically driven protein:Aβ interactions (34-36). Furthermore, the solution structure of the complex between Aβ and the affibody ZAb3 dimer revealed a large hydrophobic cavity, which is required for high Aβ affinity (36).

The observation that the HSA (494-515) peptide inhibits Aβ self-association (Fig. 6) and is also prone to self-association into cross-β fibrils (Fig. 5b) suggest the hypothesis that protein segments prone to β-strand formation and self-association into amyloid deposits may also serve as sites that target Aβ oligomers at their growing loci, where Aβ monomers would otherwise bind. This notion is supported by the structure of the affibody Z_{Ab3} bound to Aβ, revealing that the Aβ peptide interacts with a β-strand of Z_{Ab3} (36). Overall, the criteria of hydrophobicity, β-strand propensity and involvement in protein:protein self-association emerging from our investigation of albumin:$Aβ_n$ interactions will facilitate the initial screening for peptide regions that may serve as potential inhibitors of Aβ fibrillization. In addition, we anticipate that the methods and experimental approaches utilized here to map the albumin:$Aβ_n$ interactions will be at least in part transferable to other amyloid inhibitory systems (30-38).

Acknowledgements:

This work was possible through the financial support of the National Science and Engineering Research Council (NSERC).

References

1. Mawuenyega, K.G., W. Sigurdson, V. Ovod, L. Munsell, T. Kasten, et al. 2010. Decreased clearance of CNS β-amyloid in Alzheimer's disease. *Science*. 330: 1774-1774.
2. Miller, Y., B. Ma, and R. Nussinov. 2010. Polymorphism in Alzheimer Abeta amyloid organization reflects conformational selection in a rugged energy landscape. *Chemical reviews*. 110: 4820–38.
3. Zheng, J., B. Ma, Y. Chang, and R. Nussinov. 2008. Molecular dynamics simulations of Alzheimer Aβ40 elongation and lateral association. *Frontiers in bioscience a journal and virtual library*. 13: 3919–3930.
4. Brubaker, W.D., J.A. Freites, K.J. Golchert, R.A. Shapiro, V. Morikis, et al. 2011. Separating instability from aggregation propensity in γS-crystallin variants. *Biophysical Journal*. 100: 498–506.
5. Detoma, A.S., S. Salamekh, A. Ramamoorthy, and M.H. Lim. 2011. Misfolded proteins in Alzheimer's disease and type II diabetes. *Chemical Society Reviews*. 41: 608–621.
6. Choi, J.-S., J.J. Braymer, R.P.R. Nanga, A. Ramamoorthy, and M.H. Lim. 2010. Design of small molecules that target metal-Aβ species and regulate metal-induced Aβ aggregation and neurotoxicity. *Proceedings of the National Academy of Sciences of the United States of America*. 107: 21990–21995.
7. Hindo, S.S., A.M. Mancino, J.J. Braymer, Y. Liu, S. Vivekanandan, et al. 2009. Small molecule modulators of copper-induced Aβ aggregation. *Journal of the American Chemical Society*. 131: 16663–5.
8. Zlokovic, B. V. 2004. Clearing amyloid through the blood-brain barrier. *Journal of Neurochemistry*. 89: 807–811.
9. Demattos, R.B., K.R. Bales, D.J. Cummins, J. Dodart, S.M. Paul, et al. 2001. Peripheral anti-A $^{N}_{L}$ antibody alters CNS and plasma A $^{N}_{L}$ clearance and decreases brain A $^{N}_{L}$ burden in a mouse model of Alzheimer ' s disease. *PNAS*. 98: 8850–8855.
10. Biere, A.L., B. Ostaszewski, E.R. Stimson, B.T. Hyman, J.E. Maggio, et al. 1996. Amyloid β-peptide is transported on lipoproteins and albumin in human plasma. *The Journal of Biological Chemistry*. 271: 32916–32922.
11. Llewellyn, D.J., K.M. Langa, R.P. Friedland, and I.A. Lang. 2010. Serum albumin concentration and cognitive impairment. *Current Alzheimer Research*. 7: 91–96.
12. Boada, M., P. Ortiz, F. Anaya, I. Hernández, J. Muñoz, et al. 2009. Amyloid-targeted therapeutics in Alzheimer's disease: use of human albumin in plasma exchange as a novel approach for Aβ mobilization. *Drug news perspectives*. 22: 325–339.
13. Milojevic, J., and G. Melacini. 2011. Stoichiometry and affinity of the human serum albumin-Alzheimer's Aβ peptide interactions. *Biophysical Journal*. 100: 183–192.
14. Mao, H., A.H. Gunasekera, and S.W. Fesik. 2000. Expression, refolding, and isotopic labeling of human serum albumin domains for NMR spectroscopy. *Protein Expression and Purification*. 20: 492–499.
15. Petitpas, I., T. Grüne, A.A. Bhattacharya, and S. Curry. 2001. Crystal structures of human serum albumin complexed with monounsaturated and polyunsaturated fatty acids. *Journal of Molecular Biology*. 314: 955–960.

16. Curry, S., H. Mandelkow, P. Brick, and N. Franks. 1998. Crystal structure of human serum albumin complexed with fatty acid reveals an asymmetric distribution of binding sites. *Nature Structural Biology*. 5: 827–835.
17. Simard, J.R., P.A. Zunszain, C.-E. Ha, J.S. Yang, N. V Bhagavan, et al. 2005. Locating high-affinity fatty acid-binding sites on albumin by x-ray crystallography and NMR spectroscopy. *Proceedings of the National Academy of Sciences of the United States of America*. 102: 17958–17963.
18. Bhattacharya, a a, T. Grüne, and S. Curry. 2000. Crystallographic analysis reveals common modes of binding of medium and long-chain fatty acids to human serum albumin. *Journal of molecular biology*. 303: 721–32.
19. Sugio, S., A. Kashima, S. Mochizuki, M. Noda, and K. Kobayashi. 1999. Crystal Structure of Human Serum Albumin at 2.5 Å. *Protein Engineering*. 12: 439–446.
20. Jarvet, J., P. Damberg, K. Bodell, L.E. Göran Eriksson, and A. Gräslund. 2000. Reversible Random Coil to β-Sheet Transition and the Early Stage of Aggregation of the Aβ(12–28) Fragment from the Alzheimer Peptide. *Journal of the American Chemical Society*. 122: 4261–4268.
21. Milojevic, J., V. Esposito, R. Das, and G. Melacini. 2007. Inhibition Alzheimer's Aβ peptide oligomerization by human serum albumin using saturation transfer difference & off-resonance relaxation NMR. *Journal of the American Chemical Society*. 129: 4282–4290.
22. Milojevic, J., A. Raditsis, and G. Melacini. 2009. Human serum albumin inhibits Aβ fibrillization through a "monomer-competitor" mechanism. *Biophysical Journal*. 97: 2585–2594.
23. Andrushchenko, V. V, H.J. Vogel, and E.J. Prenner. 2007. Optimization of the hydrochloric acid concentration used for trifluoroacetate removal from synthetic peptides. *Journal of Peptide Science*. 13: 37–43.
24. Delaglio, F., S. Grzesiek, G.W. Vuister, G. Zhu, J. Pfeifer, et al. 1995. A multidimensional spectral processing system based on pipes. Journal of *Biomolecular NMR*. 6: 277–293.
25. Kneller, D.G., and I.D. Kuntz. 1993. UCSF Sparky: An NMR Display, Annotation and Assignment Tool. *Journal of Cellular Biochemistry*. 53 (S17C): 254.
26. Benseny-Cases, N., M. Cócera, and J. Cladera. 2007. Conversion of non-fibrillar β-sheet oligomers into amyloid fibrils in Alzheimer's disease amyloid peptide aggregation. *Biochemical and Biophysical Research Communications*. 361: 916–921.
27. Koradi, R., M. Billeter, and K. Wüthrich. 1996. MOLMOL: a program for display and analysis of macromolecular structures. *Journal of molecular graphics*. 14: 51–5, 29–32.
28. Maurer-Stroh, S., M. Debulpaep, N. Kuemmerer, M. Lopez de la Paz, I.C. Martins, et al. 2010. Exploring the sequence determinants of amyloid structure using position-specific scoring matrices. *Nature methods*. 7: 237–42.
29. Stanyon, H.F., and J.H. Viles. 2012. Human serum albumin can regulate Amyloid-β peptide fiber growth in the brain interstitium. Implications for Alzheimer's Disease. *The Journal of biological chemistry*. 287: 28163–28168.
30. Sagare, A., R. Deane, R.D. Bell, B. Johnson, K. Hamm, et al. 2007. Clearance of amyloid-β by circulating lipoprotein receptors. *Nature Medicine*. 13: 1029–1031.
31. Matsubara, E., B. Frangione, and J. Ghiso. 1995. Characterization of apolipoprotein J-Alzheimer's Aβ interaction. *The Journal of Biological Chemistry*. 270: 7563–7567.
32. Calero, M., A. Rostagno, E. Matsubara, B. Zlokovic, B. Frangione, et al. 2000. Apolipoprotein J (clusterin) and Alzheimer's disease. *Microscopy research …*. 315: 305–315.
33. Petrlova, J., H.-S. Hong, D.A. Bricarello, G. Harishchandra, G.A. Lorigan, et al. 2011. A differential association of Apolipoprotein E isoforms with the amyloid-β oligomer in solution. *Proteins*. 79: 402–416.
34. Lustbader, J.W., M. Cirilli, C. Lin, H.W. Xu, K. Takuma, et al. 2004. ABAD directly links Aβ to mitochondrial toxicity in Alzheimer's disease. *Science*. 304: 448–52.
35. Hoyer, W., and T. Härd. 2008. Interaction of Alzheimer's Aβ peptide with an engineered binding protein--thermodynamics and kinetics of coupled folding-binding. *Journal of Molecular Biology*. 378: 398–411.

36. Hoyer, W., C. Grönwall, A. Jonsson, S. Ståhl, and T. Härd. 2008. Stabilization of a β-hairpin in monomeric Alzheimer's amyloid-β peptide inhibits amyloid formation. *Proceedings of the National Academy of Sciences of the United States of America*. 105: 5099–5104.
37. Raditsis, A.V., Milojevic, J., Melacini, G. 2013. Aβ association inhibition by transferrin. *Biophys J*. 105(2):473-80.
38. Ramamoorthy, A., Lim, M.H. 2013. Structural Characterization and Inhibition of Toxic Amyloid-β Oligomeric Intermediates. *Biophys J*. 105(2):287-88.
39. Moreland, J.L., Gramada, A., Buzko, O. V., Zhang, Q., Bourne, P.E.. 2005. The Molecular Biology Toolkit (MBT): a modular platform for developing molecular visualization applications. *BMC bioinformatics*. 6: 21.

Supplementary Material

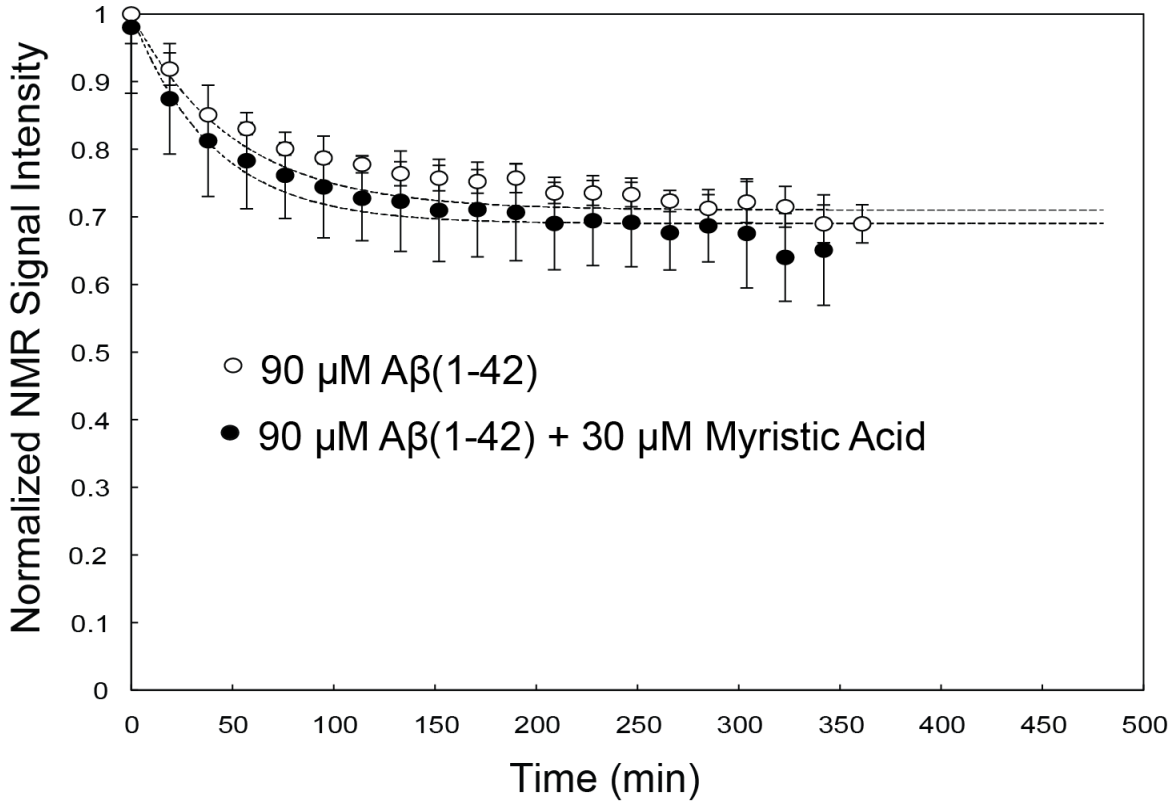

Figure S1. Effect of free myristic acid on the Aβ (1-42) aggregation profile. White circles represent the 1D NMR signal intensities of 90 μM Aβ (1-42) *vs.* time, while the black circles represent the 1D NMR signal intensities of 90 μM Aβ in the presence of 30 μM myristic acid. Signal intensities were measured using a Bruker Avance 700 MHz spectrometer equipped with a 5 mm TCI Cyroprobe at 37 ^{o}C.

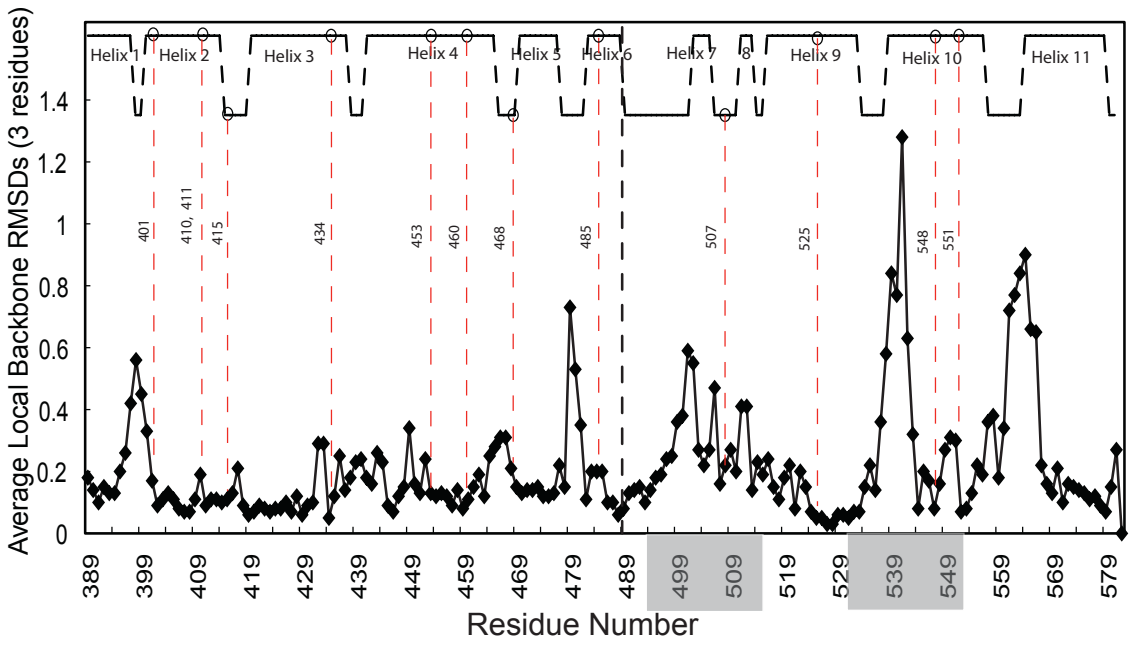

Figure S2. Three residue average local backbone RMSDs computed for domain 3 using the structures of HSA in the apo and myristic acid-bound forms (PDB codes 1AO6 and 1E7G, respectively). Secondary structure elements of domain 3 are shown in the upper area, while residues in direct contact with myristic acid are indicated using circles and dotted red lines. Local RMSDs were calculated using MOLMOL (27), while contact residues were extracted from the PDB files using Ligand Explorer Software (39). The black dotted vertical line indicates the sub-domain 3A / 3B boundary, while residues highlighted in grey indicate the HSA derived peptides used in this study (Figures 5 and 6).

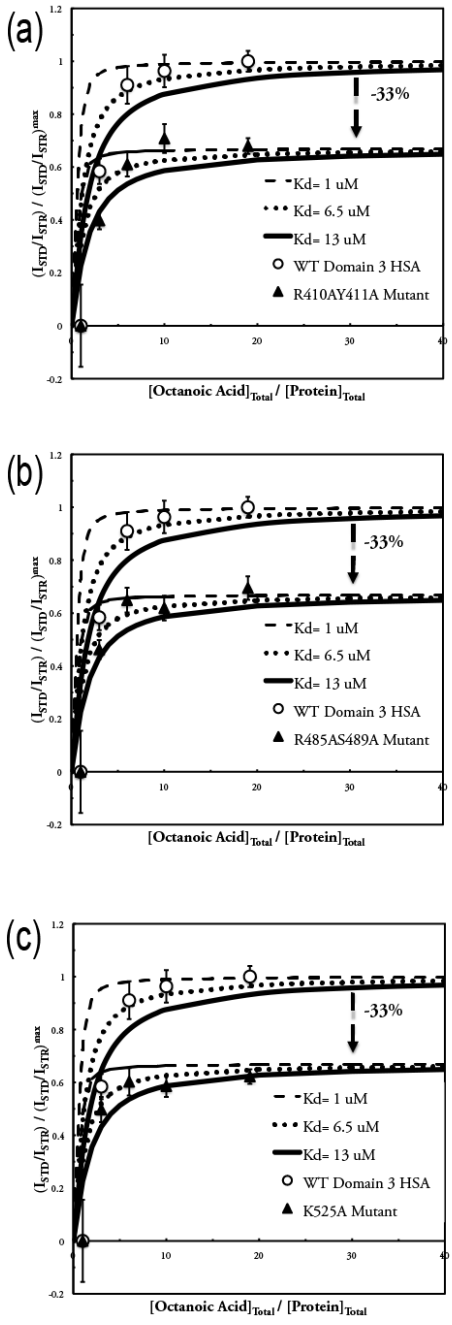

Figure S3. Binding of octanoic acid to 10 μM wild-type domain 3 and fatty acid silencing mutants as monitored by STD NMR titration in D_2O. The black triangles in panels (a), (b) and (c) represent dose-response curves for octanoic acid binding to K525A, R410AY411A and R485AS489A domain 3 mutants, respectively. As a reference, the wild type domain 3 dose-response STD curve is shown in white circles for each mutant. All the mutants showed a one third drop in their saturation regions relative to wild type.

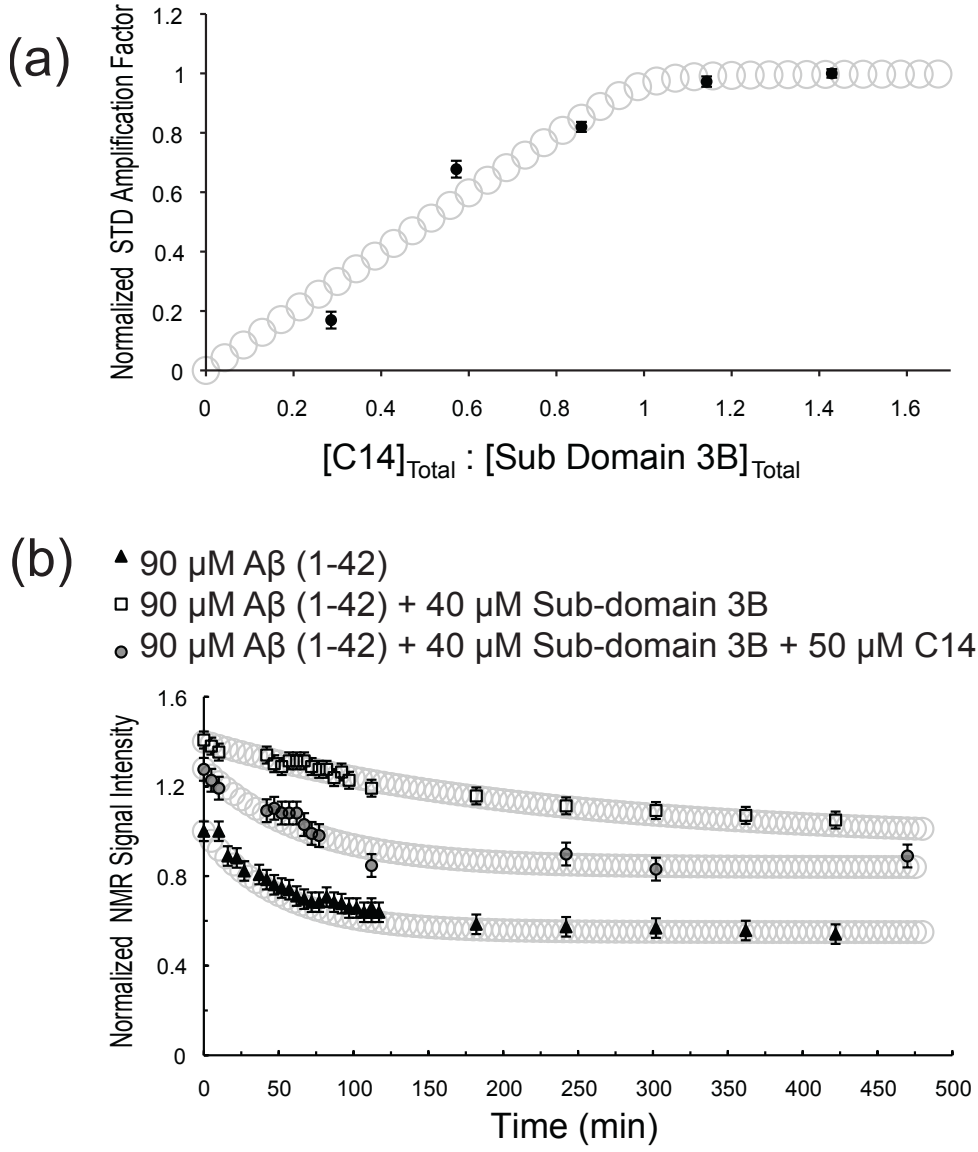

Figure S4. (a) STD based dose-response curve for myristic acid binding to sub-domain 3B. (b) Effect of myristic acid on the inhibition of Aβ (1-42) aggregation by HSA sub-domain 3B. 1D ^{1}H-NMR signal intensities of 90 μM Aβ (1-42) recoded over time are shown in the absence (filled triangles) and in the presence of sub-domain 3B either in the apo form (open squares) or bound to myristic acid (filled circles).

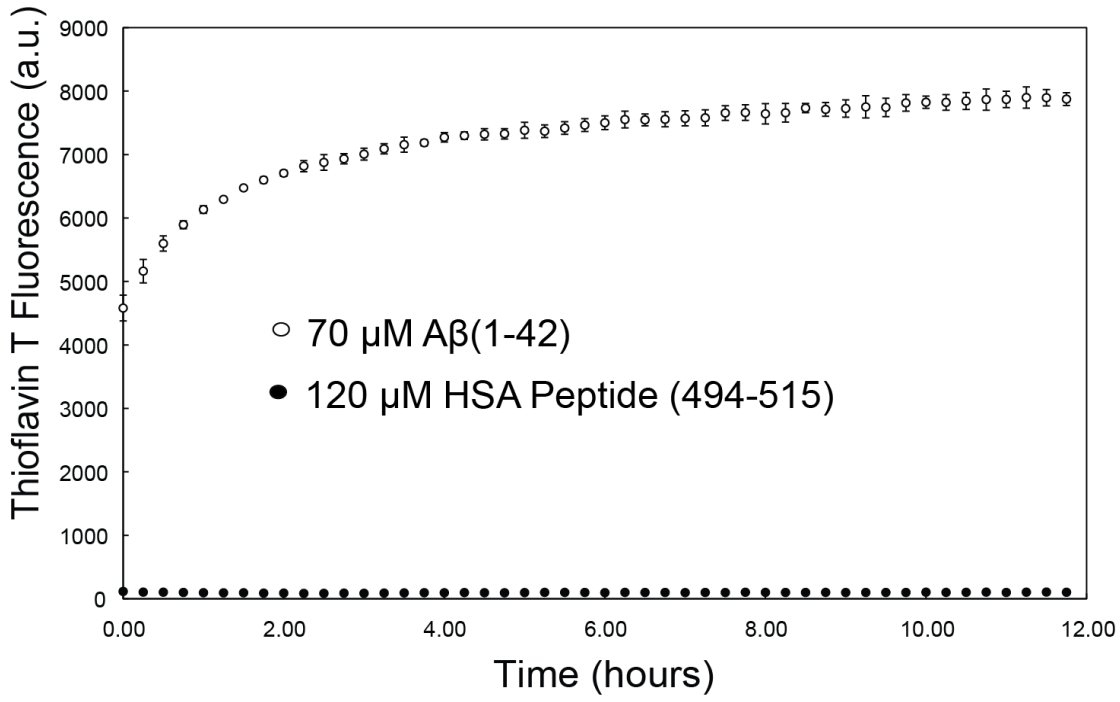

Figure S5. ThT fluorescence for the HSA (494-515) peptide (black circles) at 120 μM, showing that this peptide does not form cross-β amyloid fibrils under our experimental conditions. These conditions differ markedly from those used in the original Waltz protocol (28) in which higher concentrations of peptide and buffer (500 mM phosphate buffer) were employed, explaining why under our experimental conditions no cross-β amyloid fibrils were observed for HSA (494-515). The ThT fluorescence of 90 μM Aβ (1-42) alone (Figure 6) is reported here as well (white circles) for the convenience of comparison.

Aβ Peptides Binds HSA via a Dual Mechanism

Chapter 3

Chapter 3 Preference

This work hasn't been published yet:

Algamal, M., Ahsan, B., Ortega, J. & Melacini, G. (2014). *Aβ Peptides Interact with HSA via Dual Binding Mechanism*. Unpublished manuscript.

I did all the work and data analysis presented in this chapter except for the Electron Microscopy experiments, which has been done by Bilal Ahsan.

Aβ Peptides Binds HSA via a Dual Mechanism

Moustafa Algamal, Bilal Ahsan, Joaquin Ortega, and Giuseppe Melacini

Abstract: Self-association of the Aβ peptides is linked to the pathogenesis of Alzheimer's disease. A key regulator of Aβ self-association in plasma is Human Serum Albumin (HSA), which binds up to 95 % of circulating Aβ peptides. It is also known that HSA binds Aβ oligomers with higher affinity than Aβ monomers. However the exact molecular mechanism by which HSA binds the oligomers is still not fully understood due to the their transient and elusive nature. In order to explore the mechanism of interaction between HSA and Aβ peptides at atomic resolution, we examined the effect of HSA on a pseudo-equilibrium state of Aβ (1-40) monomers and protofibrils using Nuclear Magnetic Resonance (NMR) saturation transfer and T_2 relaxation experiments, complemented by Dynamic Light Scattering (DLS) and Electron Microscopy (EM). Our results show that HSA binds to Aβ (1-40) via a dual mechanism. In the first mechanism, HSA binds weakly to Aβ monomers at sites responsible for nucleation. Although these interactions are weak (Kd ~ 0.1-1 mM), they are still physiologically relevant owing to the high concentration of HSA in the plasma. In the second mechanism, HSA targets the sites of Aβ (1-40) growth at the edges of the protofibrils with two to three orders of magnitude higher affinity (Kd ~ μM). In both cases HSA is able to compete with Aβ self-association by targeting Aβ residues that are critical for the next step along the Aβ fibrillization pathway.

Introduction

The exact etiology of Alzheimer's disease is not fully understood, but the amyloid cascade hypothesis provides one of the plausible explanations for the pathology of Alzheimer's disease (1). The amyloid hypothesis states that the aggregation of short peptides (Aβ) in the brain is a driving factor for neuronal death and brain damage typically observed in Alzheimer's patients. The Aβ peptides are present in both the cerebrospinal fluid (CSF) and in blood plasma, but in the latter the self-association of Aβ into amyloids is inhibited primarily by human serum albumin (HSA), which binds ~90 % of plasma Aβ (2,3). The inhibition of Aβ self-association has both pathological and therapeutic potential (4-7). Low serum albumin concentrations are associated with increased cognitive impairment in elderly patients (4) and plasmapheresis with therapeutic albumin is currently being assessed in clinical trials as a potential treatment for mild to moderate Alzheimer's disease. The pathological and therapeutic potential for HSA warrants a comprehensive understanding of the molecular mechanism underlying the HSA – Aβ interactions, not only to improve the HSA therapeutic efficiency, but also to elucidate basic principles of amyloid inhibition and facilitate the design of new Ab amyloid inhibitors (8-11).

While it has been shown that HSA binds Aβ oligomers with higher affinity than Aβ monomers, several questions remain open about the mechanism through which HSA prevents Aβ aggregation (8-11), First, due to the transient and elusive nature of the oligomers formed under physiological conditions by the two major physiological species

of Aβ, *i.e.* 1-40 and 1-42, it is currently not fully understood how these oligomers are perturbed by HSA. Second, although it is known that the affinity of HSA for Aβ monomers is weak (K_d > mM), it is currently unknown if monomeric Aβ peptides bind HSA in plasma, where the HSA concentration is high (~0.6 mM) and weak interactions with HSA ($K_d \leq$ mM) are of potential physiological relevance. In order to address these questions, we have prepared solutions of Aβ (1-40) either diluted to the monomeric form or in a dynamic monomer – oligomer equilibrium, stabilized through the use of low temperatures and desalting, as recently described (12). Under these experimental conditions, the interactions between monomeric Aβ ($Aβ40_1$) and the surface of protofibrillar Aβ oligomers with aggregate MW > 1 MDa ($Aβ40_n$) are effectively probed at atomic resolution by a combination of ^{15}N T_2 relaxation experiments and selective ^{15}N saturation transfer, as implemented through the DEST (dark-state exchange saturation transfer) NMR pulse sequence (12). Here, we utilize these experiments to monitor the interactions between unlabeled HSA and ^{15}N-labeled Aβ(1-40). Based on these data, we propose a dual mechanism for the inhibition of Aβ self-association by HSA, whereby under plasma conditions the latter interacts with both $Aβ40_1$ and $Aβ40_n$. When HSA binds monomeric Aβ40, it targets primarily a C-terminal Aβ nucleation site, but when HSA binds oligomeric Aβ40, it targets primarily Aβ growth sites at the edges of protofibrils. Hence, in both cases HSA is able to compete with the addition of Aβ monomers by targeting Aβ residues that are critical for the next step along the Aβ self-association pathway.

Materials and Methods

Sample Preparation. Peptides were prepared as described by Fawzi et al., 2011 (13). In brief, the Aβ (1-40) peptides (Rpeptides Inc.) were dissolved in 3 mM NaOH at a concentration of 1 mg/mL with the pH value adjusted to 11 using 50 mM NaOH. Peptide solutions were then divided into aliquots equivalent to 50, 150, and 300 μM in a 500 μL volume and freeze dried. The lyophilized powder equivalent to each final peptide concentration was re-solublized using 250 μL of 3 mM Tris:HCl and buffer exchanged was a Zeba desalting column pre-quilibrated with Tris buffer. Desalted solutions were adjusted to 50 mM HEPES buffer, 10 % D_2O pH 6.8 by the addition of 250 μL of 100 mM HEPES buffer, 20 % D_2O pH 6.3 and, if necessary, up to 30 μL amounts of 100 mM HEPES buffer pH 6.8. A 3 mM HSA solution was prepared by dissolving lyophilized HSA, essentially fatty acid and globulin free (Sigma, A3782), in 50 mM HEPES buffer, 10 % D_2O pH 6.8 . The HSA concentration was confirmed by measuring the absorbance at 280 nm using an extinction coefficient of 34445 $M^{-1}cm^{-1}$. (14). Aβ peptides concentration was determined by UV absorption at 280 nm with an extinction coefficient of 1490 $M^{-1}cm^{-1}$.(13)

NMR Spectroscopy – Dark-state Exchange Saturation Transfer (DEST) Experiment. All NMR experiments were acquired at 10 °C on an Avance 700 MHz Bruker spectrometer equipped with a 5-mm TCI CyroProbe (Bruker BioSpin). The DEST was implemented starting from a ^{15}N T_1 relaxation experiment and inserting within the relaxation delay period a continuous wave ^{15}N selective saturation pulse (12). The ^{15}N saturation pulse

was applied at four different radiofrequency offsets (35, 4, -4, -45) KHz at a 350 Hz radiofrequency field strength. Two-dimensional DEST data were collected as four interleaved hetero-nuclear single quantum coherence correlation (HSQC) data sets (corresponding to the four frequency offsets) with spectral widths of 22583 Hz (31.8 ppm) and 10000 Hz (14.28 ppm) and using 200 and 1900 complex data points in the indirect ^{15}N and direct ^{1}H dimensions, respectively. 2D-HSQC spectra were aquired using identical parameters as in the DEST experiment. Data were processed using Topspin 2.1, then transferred to Sparky for the determination of fit heights after applying Gaussian line fitting. The noise level in the HSQC spectra was estimated using Sparky ,which calculates the median of 30 randomly sampled absolute value data heights, and used as a measure of random error in the signal intensities.

NMR Spectroscopy – ^{15}N-R_2 Experiments. ^{15}N-R_2 relaxation experiments were acquired using a standard two-dimensional sensitivity and gradient enhanced ^{1}H–^{15}N HSQC-based NMR pulse sequence for the flowing samples, 300 μM Aβ (1-40), 60 μM Aβ (1-40) in the absence and presence of 60 μM HSA. Data were processed using Topspin 2.1 and the peak heights were fitted to a decaying exponential using Sparky in order to calculate R_2 rates.

NMR Spectroscopy –2D Saturation Transfer Difference (STD) Experiments.

STD pulse sequence was generated by combining the conventional 1D STD pulse sequence with an HSQC. A train of 40 Gaussian–shaped pulses of 50 ms each separated by 1 ms inter-pulse delay was applied to introduce selective saturation. The strength of

each Gaussian pulse was 119 Hz with a 1 % truncation and 1000 digitization points. The train of Gaussian pulses was preceded by a 100 ms delay in all STD experiments. The spectral widths were 9842.52 Hz and 2258.35 Hz for direct and indirect dimensions respectively and were digitized using 1900 t2 by 200 t1 complex points. The on-resonance irradiation was applied at ~0.75 ppm.. The off resonance control irradiation was performed at 30 ppm. The saturation transfer difference (STD) spectrum was obtained by phase cycling subtraction of the on-resonance and off resonance data acquired in interleaved mode. The number of scans and dummy scans in the 2D-STD experiments were 16 and 64, respectively. Separate reference ST experiments were also acquired with 4 scans and 64 dummy scans.

Electron Microscopy. Using a protocol similar to the one used for the NMR experiments, 300 μM Aβ (1-40) samples were prepared and 50 μM HSA was added to an aliquot of the Aβ (1-40) sample after seven days. Then both samples with and without HAS were imaged using Transmission Electron Microscopy (TEM) using negative staining to visualize fibril formation, as previously described (15). A volume of 5 μL of the NMR sample was applied to a freshly prepared carbon coated grid after glow discharge. After two minutes the grids were blotted and stained with 1% uranyl acetate for 1 minute. Specimens were imaged using a JEOL TEMSCAN electron microscope operated at 80 kV using nominal magnifications of 1000X, 4000X and 150,000X.

Dynamic Light Scattering (DLS). DLS samples were prepared following the same protcol used for the samples imaged by TEM. DLS measurements were preformed using a Zetasizer Nano S Instrument (Malvern Instruments, Malvern UK). Autocorrelation functions were accumulated for 5 minutes at 10 °C and with an angle θ of 173° with a 4 mW He-Ne laser operating at a wavelength of 633 nm. All measurements were performed using a 12 μL (ZEN2112) quartz cell. The particle diameter detection limit was 0.6 – 6 μm. The viscosity value for water was used in the analysis of all measurements. All the samples were centrifuged for 10 min at 13,000 rpm prior to DLS measurements.

Results

The interaction between monomeric Aβ (1-40) (Aβ40$_1$) and HSA is weak (K_d ~ 0.1 - 1 mM), but specific and physiologically relevant.

In order to test the hypothesis that HSA binds weakly Aβ40$_1$ with K_d values in the μM - mM range and build a complete binding isotherm, at least one of the interacting partners needs to reach mM concentrations. This is unattainable for Aβ40$_1$, as it would be challenging to preserve the monomeric form of Aβ (1-40) at mM concentrations. On the contrary, HSA is highly soluble and can reach mM concentrations. However, highly concentrated solutions of albumin are known to give rise to non-specific binding (NSB), albumin self-association and/or crowding, with the latter including both enhanced viscosity and excluded volume effects. To minimize these potential biases, we have probed the interactions between HSA and monomeric ^{15}N-labeled Aβ(1-40) through the

comparative analysis of ^{15}N T_2 relaxation rates, which are known to sense the presence of minor populations of HSA-bound Aβ(1-40) occurring at HSA concentrations << mM thus avoiding NSB and crowding. For this purpose, we prepared a dilute (50-60 μM) solution of ^{15}N-labeled Aβ(1-40), in which the peptide is primarily monomeric, and acquired HSQC and ^{15}N T_2 relaxation data both in the absence and presence of equimolar amounts of HSA (Figure 1 and Figure 2).

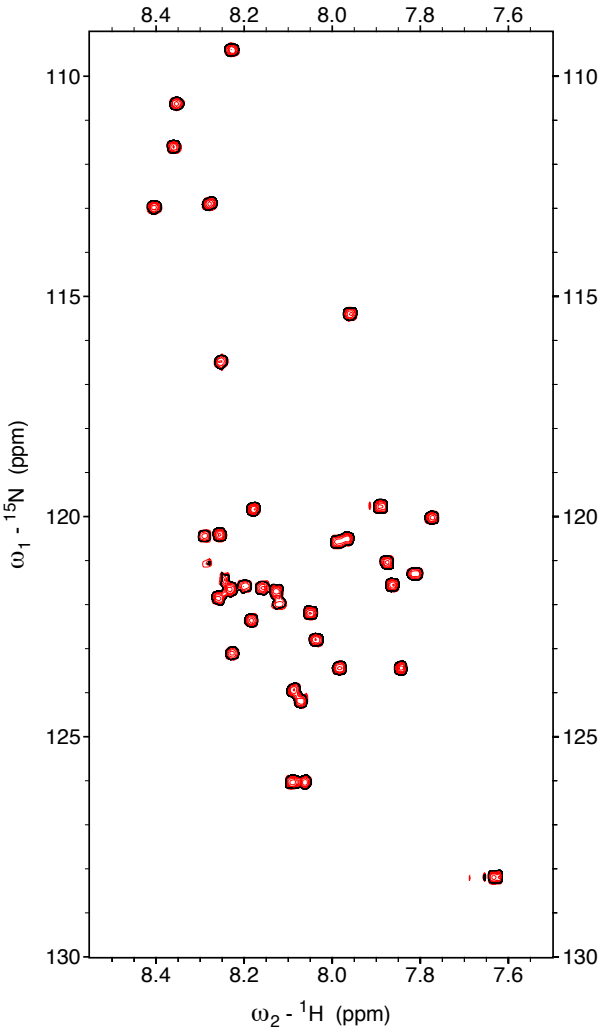

Figure 1. *Effect of HSA on Aβ (1-40) monomers as monitored by HSQC spectra.* 2D HSQC spectra of 50 μM Aβ (1-40) in the absence (multiple red-orange contours) and presence of 50 μM HSA (single black circles). No significant chemical shift changes are observed in the overlay of the two spectra.

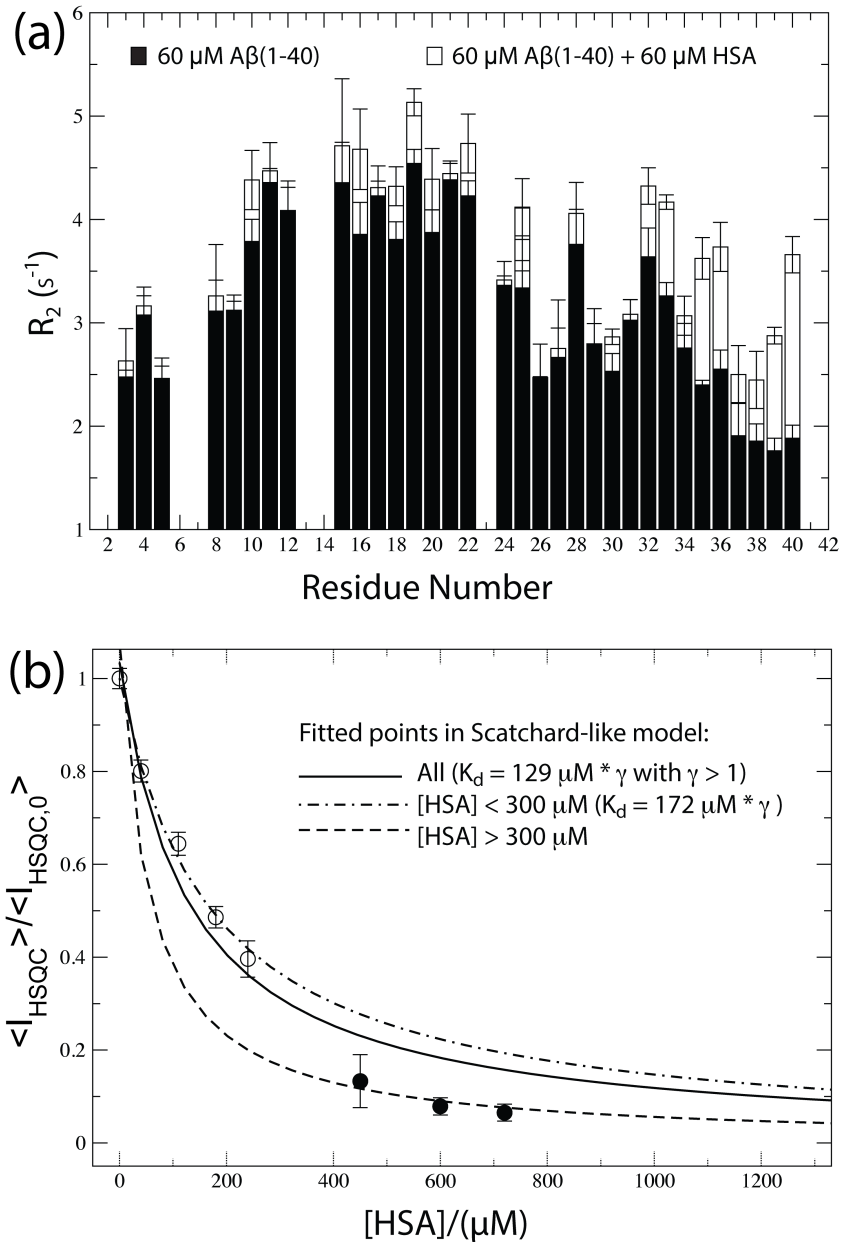

Figure 2. *Effect of HSA on Aβ (1-40) monomers as monitored by ^{15}N R_2 relaxation*. **(a)** ^{15}N R_2 relaxation rates of 60 μM Aβ (1-40), which is mostly monomeric, in the absence (solid black bars) and presence of 60 μM HSA (empty bars). No major change is observed for most of the N-terminal and central hydrophobic core residues, while the C-terminal residues *i.e.,* (I32:V40) exhibit significantly elevated N15 R_2 rates. **(b)** Titrationof HSA into a solution of 40 μM ^{15}N-labeled Aβ (1-40) monitored through HSQC intensity losses quantified as the $<I_{HSQC}>/<_{IHSQC,0}>$ ratio. $<I_{HSQC}>$ is the average signal intensity of the last five residues (*i.e.* V36-V40), after correction for dilution effects. These residues are those most affected by HSA. $<I_{HSQC,0}>$ is the $<I_{HSQC}>$ value

measured in the absence of HSA. Data were fitted using a Scatchard-like model, where γ represents the number of independent and equivalent binding sites for monomeric Aβ (1-40) within HSA. If each sub-domain of HSA binds monomeric Aβ (1-40), γ reaches a value of ~6. K_d is the site-specific dissociation constant obtained through non-linear curve fitting of the $\langle I_{HSQC}\rangle/\langle I_{HSQC,0}\rangle$ *vs.* [HSA] data to the Scatchard-like function: $\langle I_{HSQC}\rangle/\langle I_{HSQC,0}\rangle = \alpha*(1 - ([HSA]/(K_{d'}+[HSA])))$, where α and $K_{d'}$ are the fitted parameters, $K_{d'} = K_d/\gamma$ and [HSA] is approximated by the total concentration of HSA, reported on the horizontal axis. This equation assumes that the HSQC intensity losses are proportional to the fraction of HSA-bound Aβ (1-40). Although this Scatchard-like approach represents one of the simplest models of a binding isotherm, the data acquired at [HSA] > 300 μM appear as a clear outlier, possibly due to the presence of crowding and/or non-specific binding effects caused by HSA or HSA self-association. Hence, model fitting was repeated twice using either the data collected at [HSA] < 300 μM (empty circles, dot-dashed line) or the data acquired at [HSA] > 300 μM (solid circles, dashed line).

In order to better estimate the K_d values for the HSA-Aβ40$_1$ interactions, a dilute solution of ^{15}N-labeled Aβ (1-40) monomers was titrated with increasing concentrations of HSA and the titration was monitored through the HSQC intensity losses caused by the HSA-induced ^{15}N-R_2 enhancements for the C-terminal residues V36-V40 (Figure 2b). As shown in Figure 2b, as the HSA concentration increases the signal intensity of the C-terminal residues decreases in a dose dependant manner until a plateau value is reached at an HSA concentration of ~0.6 mM. When these data are fitted using a Scatchard-like model, K_d values in the 0.1 – 1 mM range are obtained (Figure 2b). However, the exact values of the fitted K_d (Figure 2b) should be interpreted be interpreted with caution, because data at high concentrations of HSA ([HSA] > 300 μM) appear as a clear outlier (Figure 2b) pointing to the presence of non-specific binding and/or crowding effects, which are negligible at lower HSA concentrations. In addition, the exact site-specific affinities (K_d) depend also on the stoichiometry of the Aβ (1-40) : HSA complex. For

instance, if only a single molecule of monomeric Aβ (1-40) binds each molecule of HSA (*i.e.* γ = 1 in Figure 2b), K_d ~ 0.1-0.2 mM, but if each subdomain of HSA binds monomeric Aβ (1-40) (*i.e.* γ = 6 in Figure 8b), then K_d ~ 0.7-1.0 mM (Figure 8b). Overall, the data of Figure 2b suggest that the last five residues of monomeric Aβ (1-40) bind HSA with K_d values in the 0.1 – 1 mM range. In order to investigate to what extent these conclusions about the Aβ residue profile and affinity range can be extended from the Aβ monomers to oligomers, we proceeded to investigate the effect of HSA on more concentrated solutions of Aβ (1-40), in which Aβ monomers are in dynamic equilibrium with Aβ assemblies.

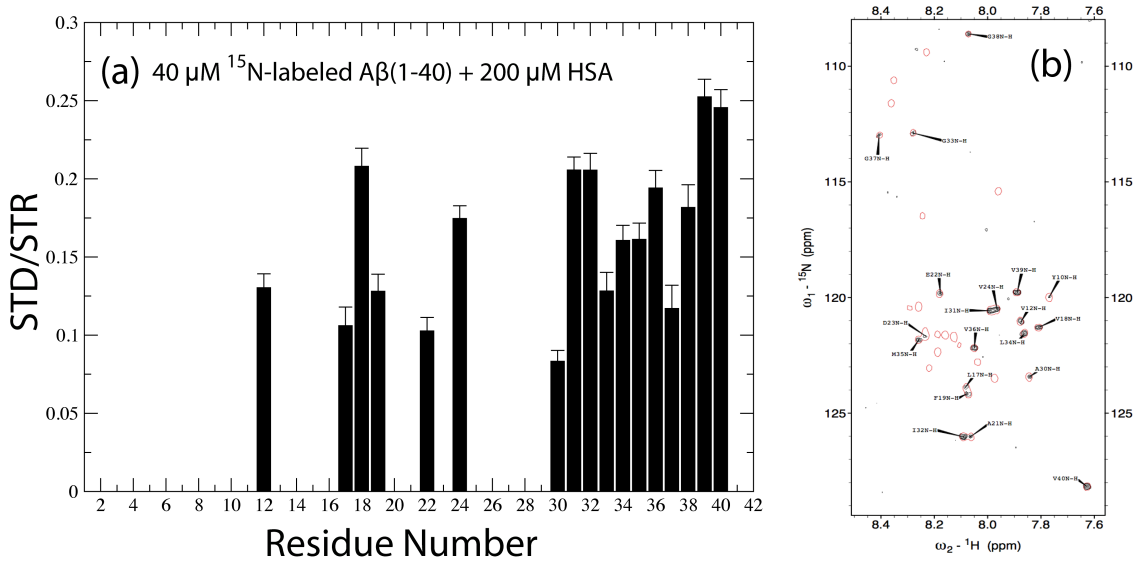

Figure 3. *Effect of HSA on Aβ (1-40) monomers as monitored by STD-HSQC. Panel (a) depicts the* STD/STR ratios measured for 40 μM ^{15}N-labeled Aβ (1-40) in the presence of 200 μM HSA, while panel (b) shows the overlay of the STD_HSQC spectrum (multiple black contours) over the STR_HSQC spectrum (single red circles). STD and STR stand for saturation transfer difference and reference, respectively.

Preparation of Aβ (1-40) oligomers ($A\beta 40_n$)

In order to examine the effect of HSA on the Aβ monomer – oligomer exchange process, we prepared a solution of 300 μM ^{15}N-labeled Aβ (1-40). Aβ peptides are known to form large amyloid protofibrils spontaneously when dissolved at concentrations higher than 100 μM (12). In addition, when the sample at these concentrations is left to equilibrate for 7 to 10 days at low temperature (4-10 ^{o}C), a pseudo-equilibrium is reached in which Aβ monomers are in dynamic exchange with protofibrillar oligomers ($A\beta 40_n$) (12). Indeed, after 7 days of incubation at 4 ^{o}C, our 300 μM Aβ (1-40) solution contained large (~100 nm) worm-like aggregates, as shown by dynamic light scattering (Figure 4a) and electron microscopy (Figure 5a). The sample didn't contain any observable mature fibers (Figure 4a), as previously observed for Aβ (1-40) in similar conditions (12). Moreover, the average difference in NMR ^{15}N transverse relaxation rates (ΔR_2) between the 300 μM and the diluted reference 60 μM Aβ (1-40) solutions is greater than 1 s^{-1} (*i.e.* 1.45 s^{-1}), which has been shown to be indicative of the presence of NMR-invisible ('dark') protofibrils in dynamic exchange with NMR-visible Aβ monomers in the concentrated sample (12). The pseudo first-order rate constant $k_{on,app}$ for the conversion from NMR-visible to invisible species is estimated using the maximum value of ΔR_2 (12), which based on Figure 6 is ~2 s^{-1}. We then investigated how the dynamic steady state $A\beta 40_1$ - $A\beta 40_n$ exchange is affected by HSA.

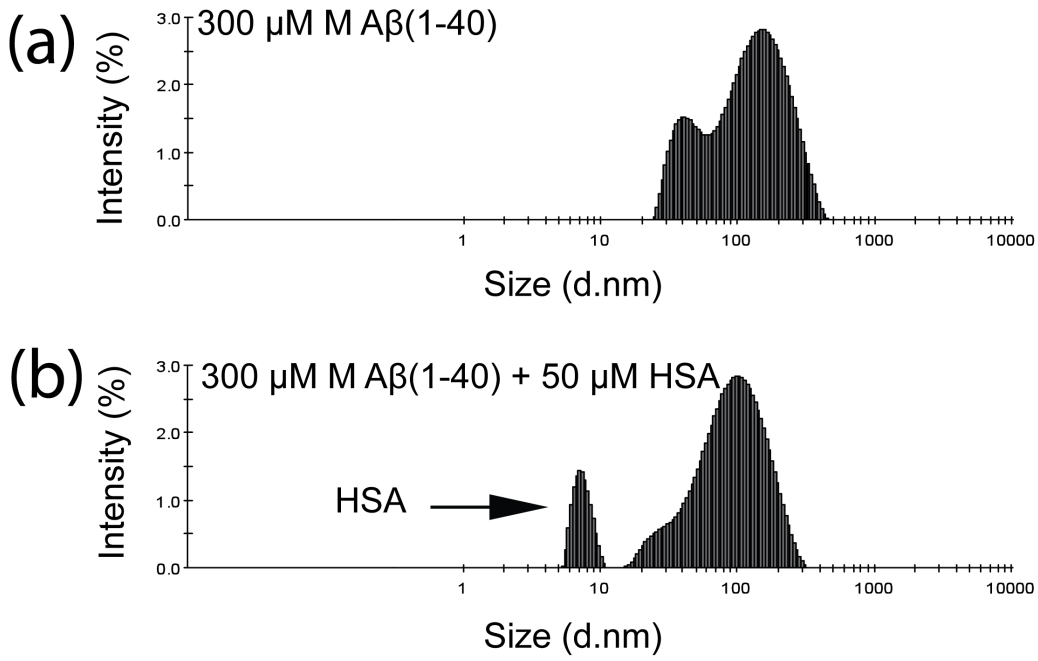

Figure 4. *Monitoring Aβ (1-40) protofibril formation through dynamic light scattering (DLS)*. Intensity *vs*. size DLS plots for 300 μM Aβ (1-40) incubated at 10 ºC for 10 days **(a)**, and 300 μM Aβ(1-40) with 50 μM HSA added at the 7th day of incubation and kept at 10 ºC for a total time of 10 days **(b)**. A black arrow indicates the peak corresponding to HSA close to 10 nm. All measurements were performed using 12 μL volume cells and a Zetasizer Nano S system at 10 ^{o}C.

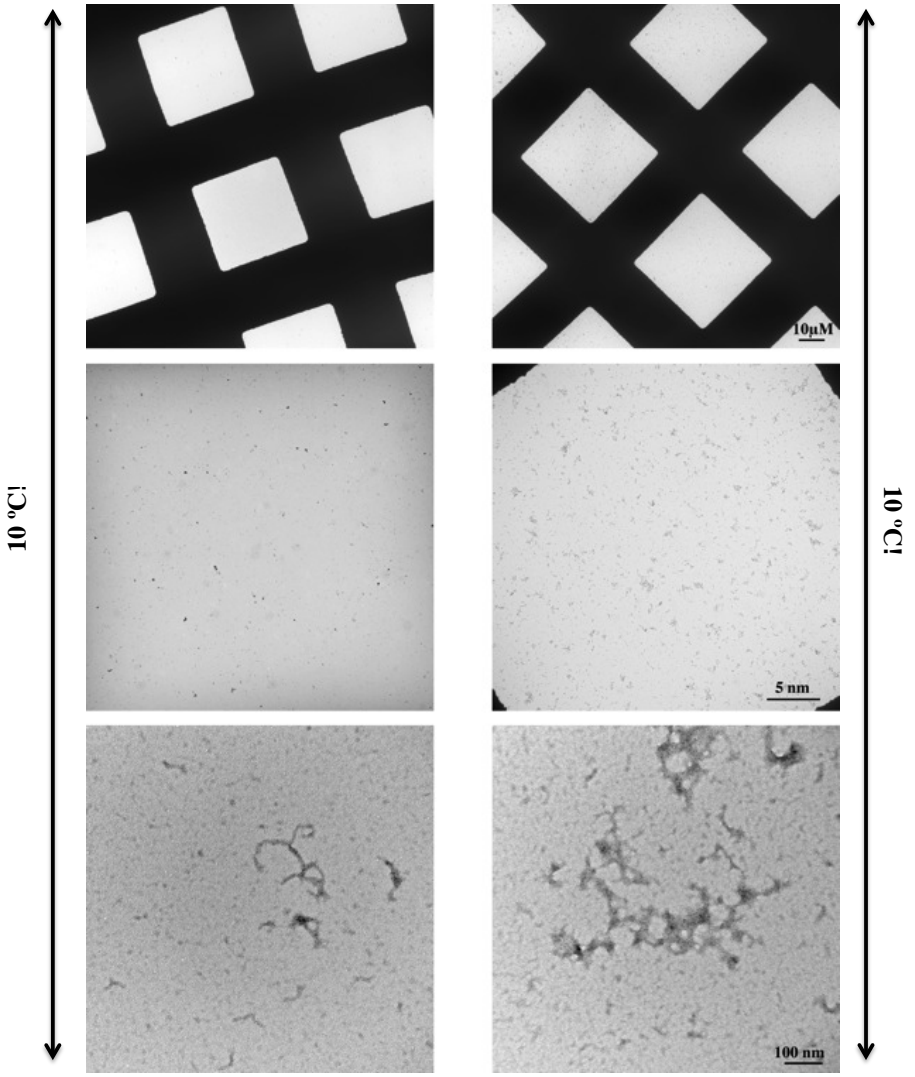

Figure 5. *Monitoring Aβ (1-40) protofibril formation through electron microscopic (EM).* EM Charge-Coupled Device CCD pictures of Aβ (1-40) peptides after performing negative stain using 1 % uranyl acetate. Images (top to bottom) were acquired at a magnification of 1K, 4K and 150K, respectively. **(a)** Images of 300 µM Aβ (1-40) incubated at 10 ºC for 10 days. **(b)** Images of 300 µM Aβ (1-40) with 50 µM HSA added at the 7th day of incubation and kept at 10 ºC for a total time of 10 days.

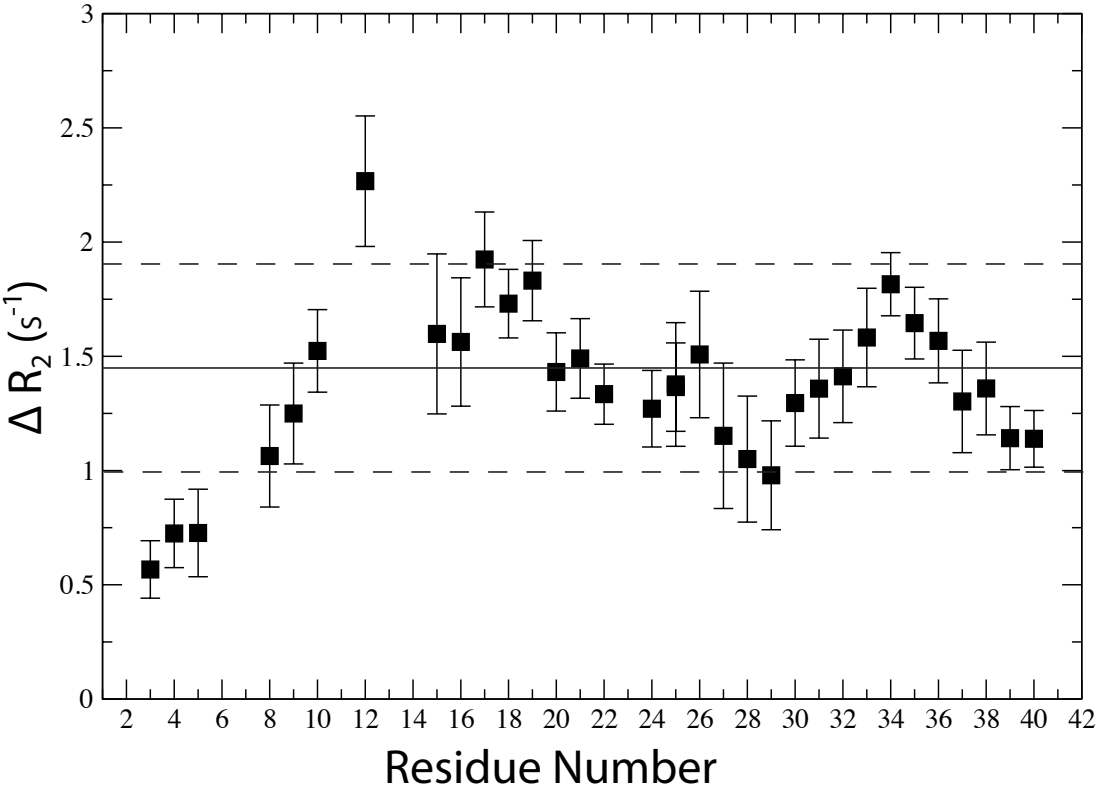

Figure 6. *Monitoring Aβ (1-40) protofibril formation through ^{15}N R_2 relaxation*. Residue-specific differences in ^{15}N R_2 relaxation rates of 300 μM and 60 μM Aβ (1-40). The increase in ^{15}N R_2 values is attributed to the presence of Aβ protofibrils in the concentrated sample. Solid and dashed lines represent the average and the standard deviation of the ΔR_2 values, respectively.

An approach to probe how HSA perturbs the Aβ40$_1$ - Aβ40$_n$ interactions: the Θ values

The ΔR_2 *vs.* residue profile measured for concentrated (> 100 μM) Aβ samples is typically combined with DEST data from ^{15}N-selective saturation experiments at multiple offsets and simultaneously fitted to the McConnel equations (12). The combined analysis of the ΔR_2 and DEST profiles provides a residue specific constant, defined as $K_{3,i}$, which

quantifies the partitioning of a given Aβ residue *i* between direct- and tethered-contacts with the Aβ protofibril surface. However, the extension of this approach to Aβ solutions containing HSA is challenging, due the major effect of HSA on the ^{15}N R_2 rates of monomeric Aβ, which remain the most abundant species even in the concentrated (300 μM) Aβ (1-40) sample. In order to circumvent this challenge and probe how HSA perturbs the Aβ monomer – oligomer equilibrium and the direct *vs.* tethered-contact partitioning, we calculated the DEST Difference (or Θ), defined as the normalized difference between the DEST cross-peak intensities measured using selective ^{15}N-saturation at two frequency offsets, one set far off-resonance (*e.g.* 35 KHz), which serves as a reference, and the other set closer to the ^{15}N carrier frequency, to better saturate Aβ oligomers, but still sufficiently far from the ^{15}N resonance frequencies of monomeric Aβ to minimize direct saturation of Aβ monomers (*e.g.* 2-8 KHz).

The DEST data were analyzed similarly to the analysis of the traditional ^{1}H Saturation Transfer Difference (STD) experiment, and the DEST Difference (Θ) was defined according to the following equation:

$$\Theta = \frac{\sum \pm I^{\circ} - \sum \pm Ist}{\sum \pm I^{\circ}}$$

Where I° refers to the DEST intensities measured at far off-resonance frequency offsets, while *Ist* refers to the DEST intensities measured at frequency offsets closer to the carrier frequency ('near off-resonance offsets'), at which a saturation transfer effect is detected.

The Σ± notation indicates that the intensities at the positive and negative offset values were averaged.

In order to test the effectiveness of the DEST Difference (Θ) method in probing the Aβ40$_1$ - Aβ40$_n$ interactions, we computed the Θ values using previously acquired Aβ (1-40) DEST data, for which the K_3 direct- *vs.* tethered-contact partitioning coefficients determined through the combined DEST/ΔR_2 McConnell fitting are available (16). The Θ values were computed utilizing DEST intensities measured with a 350 Hz ^{15}N saturating field strength at three different offset pairs differing in the near off-resonance values: {±35 KHz, ±2 KHz}, {±35 KHz, ±4 KHz} and {±35 KHz, ±8 KHz}, (Figure 6a). Figure 7a shows that the Θ *vs.* profiles calculated using different near off-resonance values, *i.e.* ±2 KHz, ±4 KHz and ±8 KHz, exhibit similar patterns, with maxima located at the same residue numbers. Given these similarities, we opted for ±4 KHz as an optimal near off-resonance saturation frequency, since it provides the advantage of a balanced compromise between adequate saturation of the Aβ oligomers, resulting in significant cross-peak attenuation (up to ~40%, Figure 7a) and optimal Aβ oligomer *vs.* monomer selectivity (16). The minimal effect of the selective ^{15}N saturation at ±4 KHz on the Aβ monomer is proven by the negligible Θ values measured for a dilute (60 μM) solution of Aβ (1-40) (Figure 8, black bars).

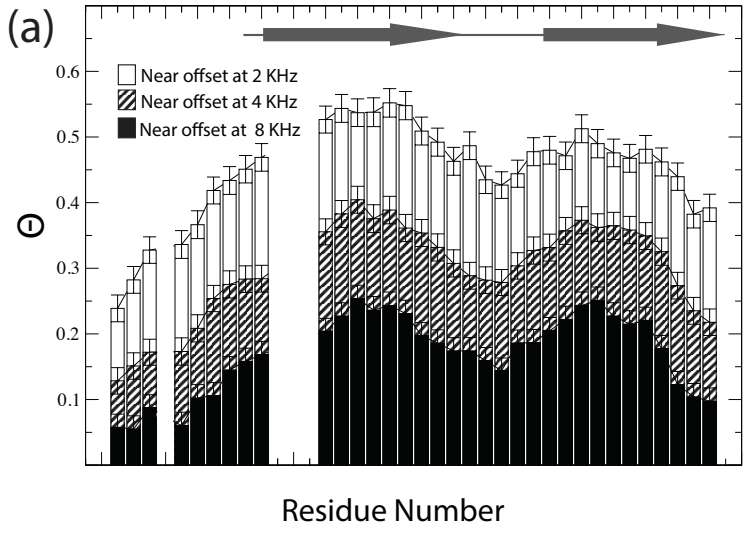
(a)
Near offset at 2 KHz
Near offset at 4 KHz
Near offset at 8 KHz
Θ
Residue Number

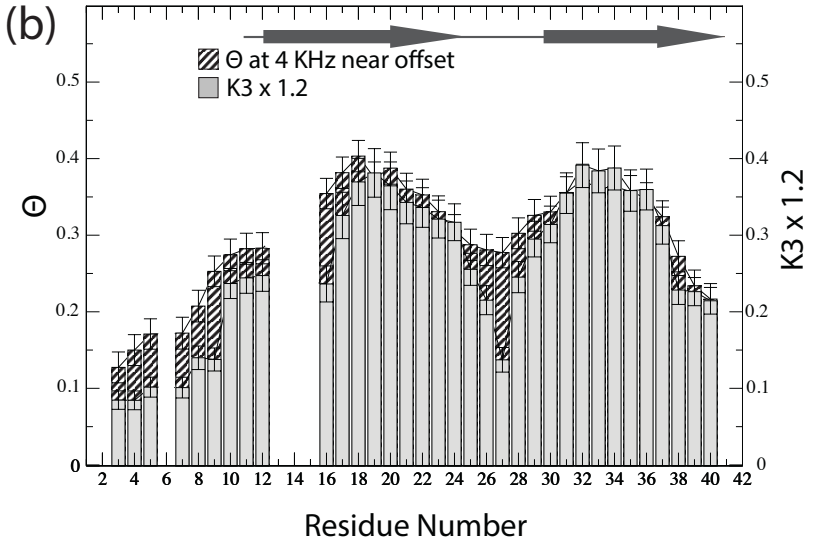
(b)
Θ at 4 KHz near offset
K3 x 1.2
Θ
K3 x 1.2
Residue Number

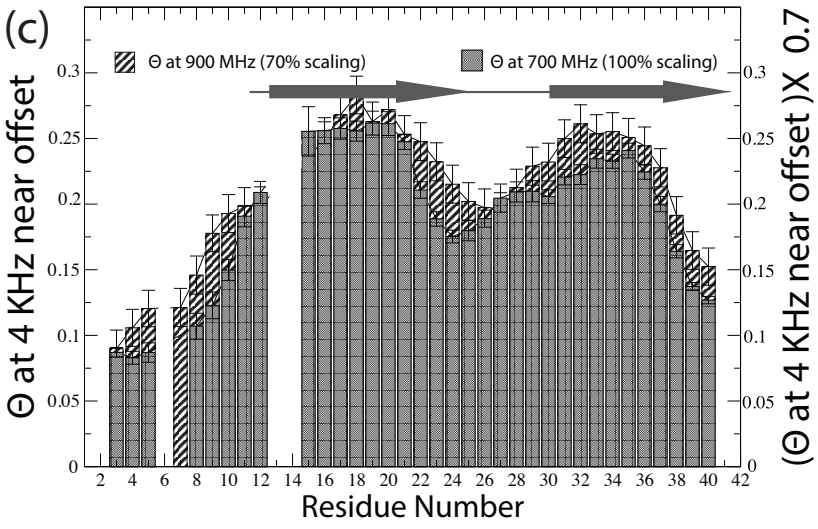
(c)
Θ at 900 MHz (70% scaling)
Θ at 700 MHz (100% scaling)
Θ at 4 KHz near offset
(Θ at 4 KHz near offset)X 0.7
Residue Number

Figure 7. *Validation of the DEST Difference (Θ) Approach.* Using Θ to estimate the DEST profiles width and the K3 values. The Data provided by the DESTfitting_v1.9 software was used to generate panels a, b, and c (16). **(a)** Effect of the near-off resonance offset on the Θ values. Solid Black, segmented, and empty bars represent data acquired using ±8 KHz, ±4 KHz, and ±2 KHz as near off resonance frequencies, respectively. In all cases 35 KHz was used as a far off resonance frequency. **(b)** Comparison between the Θ values at ±4KHz (segmented bars) and the calculated K_3 values (grey bars). **(c)** Comparison between the published Θ data for 270 μM Aβ (1-40) at ±4 KHz saturation frequencies and 900 MHz (segmented bars) and our experimental data at ±4 KHz saturation frequencies and 700 MHz (dark grey bars). Red arrows indicate the regions of Aβ (1-40) adopting a β-strand conformation in the Aβ fibrils (23). The Θ values under our experimental conditions show less saturation transfer, because the saturation pulse was applied farther off resonance (57 ppm) on a spectrometer operating at 700 MHz, while the published data were acquired on a spectrometer operating at 900 MHz. Hence, 900 MHz data were scaled to 70% of its original values. Data were smoothed using three-residue averaging, *i.e.* each specific value represents the average values of that specific residue, the one preceding and the one following in sequence. However, two-residue averaging was used for the terminal residues and residues followed or proceeded by absent data. We decided to use |4 KHz| as a saturation frequency at 700 MHz, since it provides a good compromise between adequate partial saturation of the protofibrils (attenuation in the cross peaks signals of ~20-30%) and sufficient selectivity for the Aβ (1-40) protofibrils *vs.* monomers by being far from the 2 KHz window of the monomers.

In order to test the suitability of Θ values at ±4 KHz to estimate K_3 values, we overlaid the residue profile for both Θ and K_3 as shown in Figure 6b. The Θ *vs.* K_3 comparison (Figure 7b) indicates that the two parameters exhibit similar trends, with both profiles featuring maxima with comparable widths and at similar residue positions. Hence, the Θ residue profile provides an approximation of the relative K_3 values without the need of T_2 measurements. Next, we checked whether the Θ parameter is field dependent. For this purpose, the DEST differences (Θ) were measured at ±4 KHz and 700 MHz for a concentrated (300 μM) Aβ (1-40) solution equilibrated for seven days at 4 ^{o}C and compared to those computed using the published data acquired for a similar Aβ (1-40) sample at ±4 KHz and 900 MHz (14, 15) (Figure 7c). Despite the difference in

field and consequently in relative offsets, the two plots in Figure 7c exhibit overall similar relative trends with two maxima centered at residues ~18 and ~32, showing that the N-terminal residues prefer tethered states, while the central hydrophobic core and part of the C-terminal residues are more likely to be in direct contact with the protofibril surface.

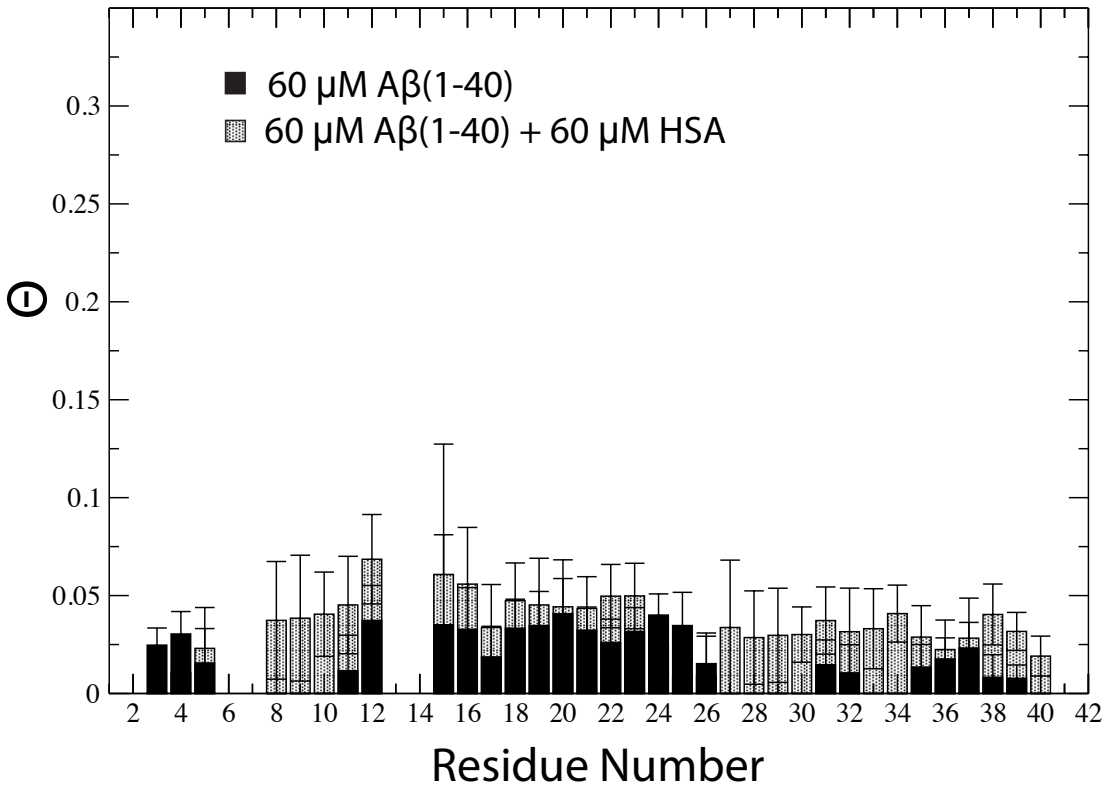

Figure 8. *The DEST difference (Θ) for diluted Aβ (1-40)*. Θ values at |4 KHz| for monomeric Aβ (1-40) samples in the absence (solid black bars) and presence (black dotted bars) of HSA. As expected for monomeric peptides, negligible or marginal Θ values are observed for diluted Aβ (1-40) and the Θ pattern typical for the dark state samples (Figure 7) is absent.

Using the Θ values to probe how HSA interacts with Aβ40$_n$ protofibrils

The Θ profile was measured again after adding 70 μM of unlabeled HSA to the equilibrated 300 μM ^{15}N-labeled Aβ (1-40) solution and significant reductions in Θ values were observed for several Aβ residues (Figure 9a, b). The HSA-induced Θ changes arise either from HSA interactions with Aβ40$_n$ and/or Aβ40$_1$ or from fragmentation of Aβ40$_n$ protofibrils caused by HSA. In order to test the latter explanation, we examined the size distribution and appearance of the protofibrils in the 300 μM Aβ (1-40) samples in the presence and absence of HSA using DLS and TEM. No major changes in the protofibril integrity were observed under our experimental conditions after adding HSA as monitored by DLS and TEM (Figures 4 and 5, respectively). These data suggest that the HSA-induced Θ reduction (Figure 8) reflects direct interactions of HSA with Aβ40$_n$ and/or Aβ40$_1$. The contribution of HSA - Aβ40$_1$ binding to the HSA-dependent Θ changes observed in Figure 9 is expected to be negligible based on two main lines of evidence. First, the fraction of Aβ40$_1$ bound to HSA is minimal due to its weak affinity. Second, when unlabeled HSA is added to a solution of ^{15}N-labeled Aβ40$_1$, no significant changes were observed in the DEST profile (Figure 8). These observations suggest that the HSA-dependent Θ changes observed in Figure 9 is primarily caused by direct interactions between HSA and the Aβ40$_n$ oligomers. Hence, the residue-specific Θ variations caused by HSA (Figure 9b) are a valuable indicator of how HSA affects the direct *vs*. tethered-contact partitioning of Aβ (1-40) monomers at the surface of the Aβ40$_n$ protofibrils. Moreover HSA binds Aβ40$_n$ in a specific and a dose dependant manner, as suggested by the 1D DEST-monitored titration of Aβ40$_n$ with HSA (Figure 10). Figure 10

shows that addition of HSA decreases the 1D Θ values measured for Aβ40$_n$ in a dose dependent manner until a plateau is reached at 50 - 60 μM HSA.

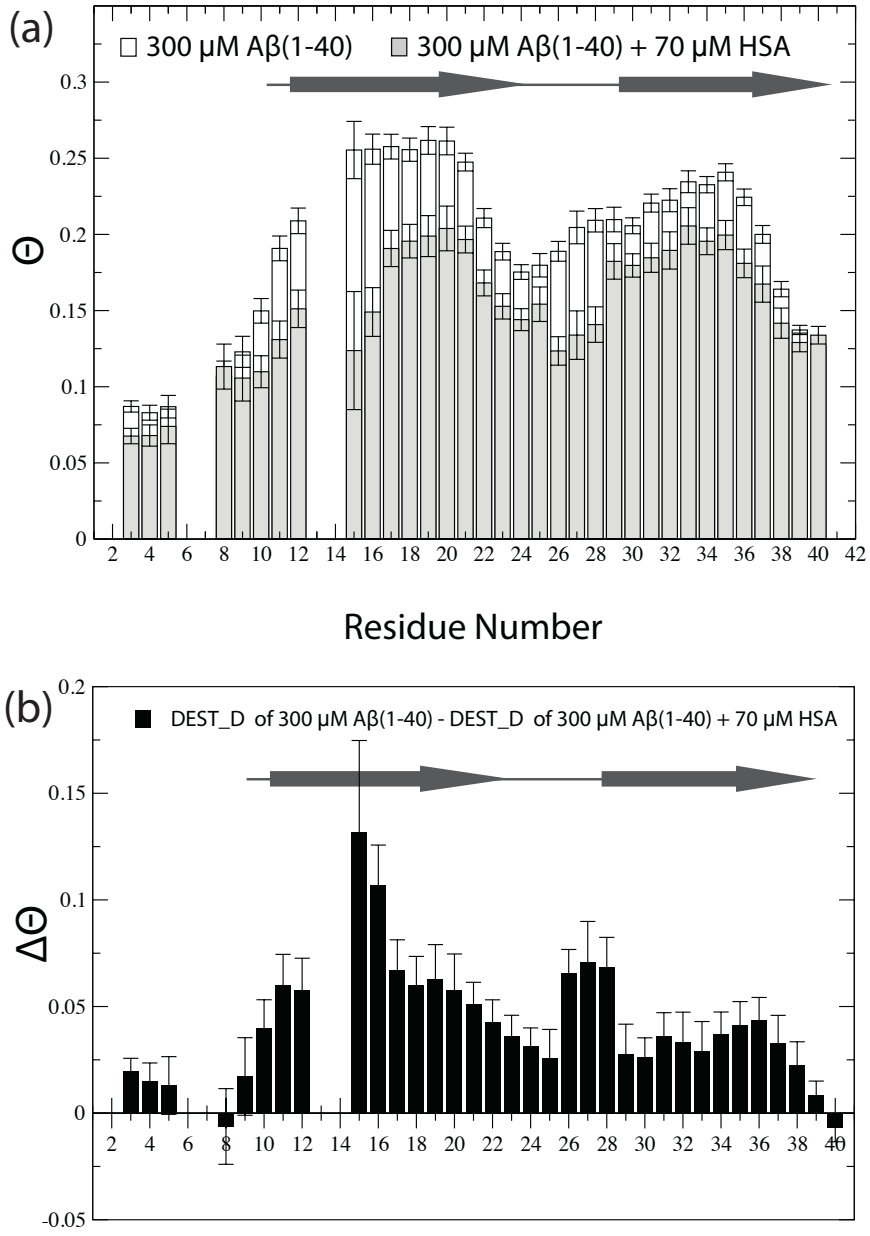

Figure 9. *The DEST difference (Θ) for concentrated Aβ (1-40)*. Effect of HSA on the Θ values of Aβ (1-40) under pseudo-equilibrium state between monomers and protofibrils.

(a) Θ values for 300 μM Aβ (1-40) in the absence (white bars), and presence (grey) of 70 μM HSA. **(b)** Residue-specific differences between the two Θ values of panel (a). HSA causes a significant Θ decrease for most of the residues, except for the N- and C-terminal regions. Horizontal arrows indicate the regions of Aβ (1-40) adopting a β-strand conformation in the Aβ fibrils.

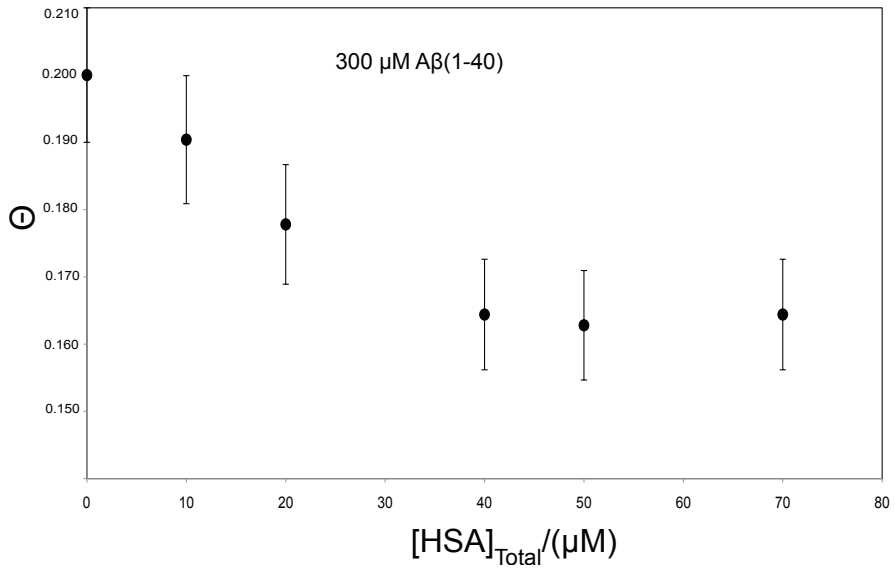

Figure 10. *1D DEST-monitored titration of Aβ (1-40) protofibrils with HSA*. HSA was added to a 300 μM Aβ (1-40) sample containing Aβ protofibrils. Increasing the HSA concentration resulted in a decrease in the overall Θ values at |4 KHz|, until a plateau is reached at ~ 40 μM HSA.

HSA promotes a switch from direct to tethered-contacts for the Aβ(1-40) residues involved in protofibril growth.

As shown in Figure 9b, the Θ values for the majority of Aβ (1-40) residues are decreased in the presence of HSA, with the most significant differences observed for the central hydrophobic core and the region preceding the C-terminus, at or near the in-register b-sheets of the protofibril structure. Minimal or no differences were observed for the N-terminus and the last five C-terminal residues (Figure 9b). The decrease in Θ values

upon HSA addition suggests that HSA promotes a switch from the direct to the tethered-contact states of the $A\beta40_1$ monomers contacts with the $A\beta40_n$ protofibril surface.

In order to probe to what extent the switch form the direct to the tethered-contact states promoted by HSA resembles that caused by the dilution of the concentrated (300 μM) and $A\beta40_n$ protofibril-containing Aβ (1-40) sample, we compared the Θ change measured upon HSA addition on the concentrated 300 μM Aβ (1-40) sample (ΔΘ (+/-) HSA) to the Θ change observed upon dilution of the 300 μM Aβ (1-40) sample in the absence of HSA (ΔΘ Aβ (1-40) dilution) (Figure 11). As shown in Figure 11a, if all Aβ (1-40) residues are included in the comparison, the ΔΘ (+/-) HSA and ΔΘ Aβ(1-40) dilution values appear poorly correlated (R^2=0.61). However, when the ΔΘ plots are confined to selected Aβ (1-40) segments, such as L17-V24 and I31-V40, a significantly higher degree of correlation is observed (Figure 11c,d), suggesting that in these regions the effect of HSA is comparable to that of Aβ dilution. Interestingly, these two segments span the C-terminal halves of the in-register b-sheets involved in protofibril cross-β strand growth.

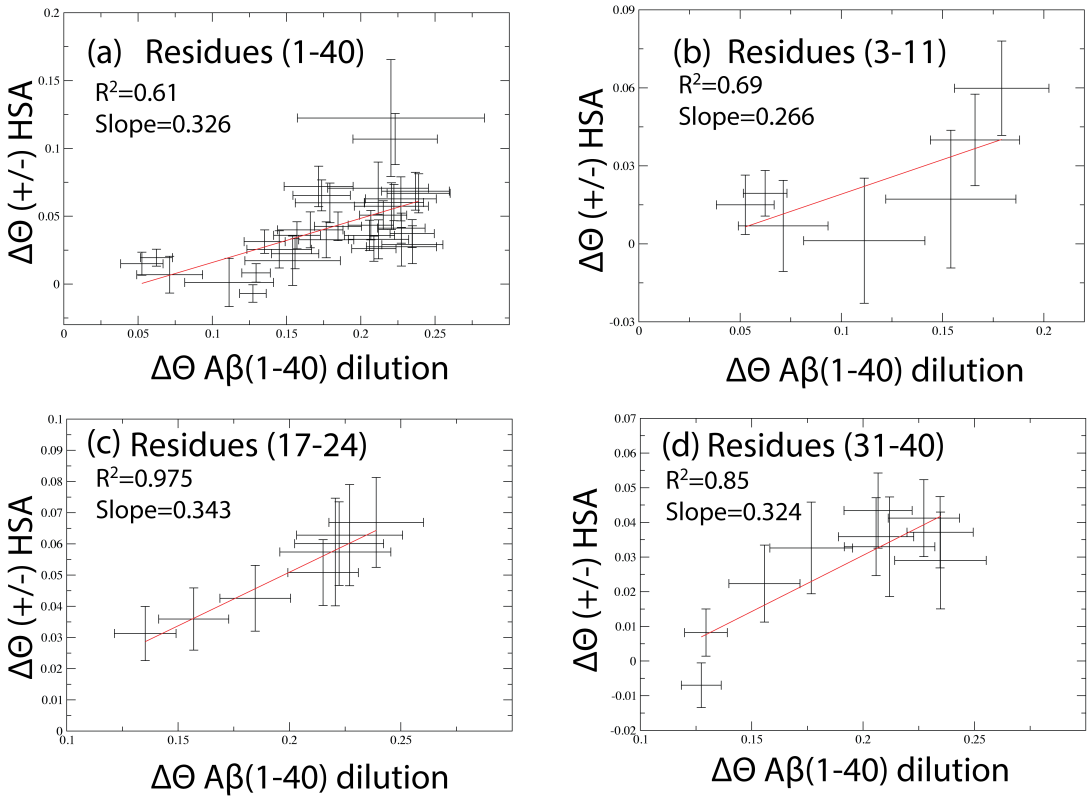

Figure 11. *Correlation between the Θ changes caused by HSA addition to Aβ (1-40) protofibrils and the Θ changes caused by dilution to monomeric Aβ (1-40).* **(a)** Correlation for the full-length Aβ (1-40) peptide. **(b-d)** Correlations for selected segments; E3-E11, L17-V24, and I31-V40, respectively. The ΔΘ (+/-) HSA values are the difference between the Θ values measured for 300 μM Aβ(1-40) before and after the addition of 70 μM HSA, while the ΔΘ Aβ(1-40) dilution values were calculated by subtracting the Θ values measured for 60 μM Aβ(1-40) from those observed at 300 μM Aβ(1-40).

Discussion

The work presented here has shown, for the first time, that Aβ (1-40) bind to HSA via a dual mechanism involving both Aβ (1-40) monomers and oligomers (Figure 12). Previous studies have shown that HSA selectively binds to Aβ oligomers (9, 11, 17),

while others have suggested that interactions with the monomers were dominating (18,19). Our results show that HSA binds Aβ (1-40) monomers and oligomers but with markedly different affinities. The former exhibit a ~two to three-order of magnitude lower affinity relative to the latter (Kd ~ 0.1-1 mM *vs*. μM). In contrast to what have been suggested by Rózga et al.(18) and Stanyon et al.(19) we didn't detect any μM affinity between Aβ monomers and HSA. On the other hand, the findings presented here are consistent with our previous work suggesting higher affinity between HSA and Aβ oligomers or higher molecular weight aggregates, and absence of interaction between HSA and Aβ monomers in the μM range (8, 10, 11). Moreover, Since the physiological HSA concentration in the plasma is ~0.6 mM, the majority of plasma Aβ monomers is expected to be bound to HSA. In addition, our results show that, when HSA binds Aβ (1-40) monomers, it targets primarily their C-terminal region (*i.e.* I32-V40), a segment previously shown to include sites responsible for Aβ (1-42) nucleation (Figure 12a) (20). This observation suggests that the plasma HSA - $A\beta40_1$ interactions may interfere with the nucleation of Aβ (1-40) fibrils, explaining why amyloid deposits are rarely found in peripheral tissues (21). However, in the brain cerebrospinal fluid (CSF), the HSA concentration drops to ~3 μM (22), making the fraction of Aβ (1-40) monomers bound to HSA negligible. However, the HSA concentration in the CSF is still sufficiently high to result in significant binding of HSA to $A\beta40_n$ oligomers.

Our results show that the HSA - $A\beta40_n$ interactions target preferentially Aβ (1-40) residues involved in protofibril cross-β strand growth and promote a switch of these Aβ (1-40) monomer – oligomer contacts from a direct to a tethered state (Figure 9b). These

observations can be interpreted as HSA shielding the protofibril edges at the sites of cross-β strand growth and competing with further Aβ (1-40) monomer addition to the oligomers (Figure 12b), thus inhibiting protofibril growth into mature Aβ (1-40) fibrils. Overall, the model emerging from our data (Figure 12) is useful to understand the physiological role of HSA as an endogenous anti-Aβ amyloid agent. In plasma, where HSA reaches sub-mM concentrations, HSA is able to inhibit the formation of Aβ (1-40) nuclei by targeting through weak interactions C-terminal Aβ (1-40) nucleation sites. Unlike plasma, in the CSF, where the HSA concentrations is limited to the mM range, the inhibition of nucleation is less efficient, but HSA is still effective in inhibiting protofibril growth by shielding the Aβ (1-40) oligomer sites of cross-β strand growth and outcompeting direct monomer addition.

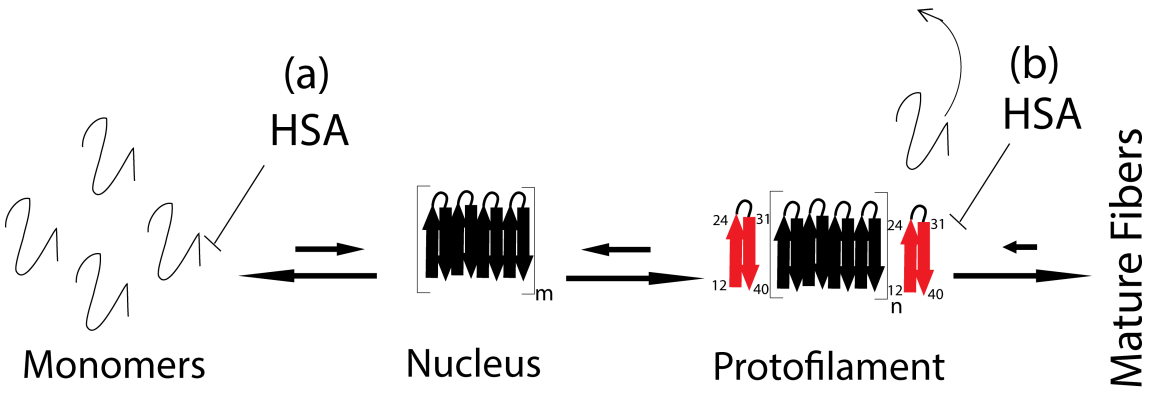

Figure 12. *Schematic model for the mechanism of Aβ (1-40) inhibition by HSA*. **(a)** HSA binds weakly but specifically to Aβ monomers at sites important for nucleation, such as the C-terminal residues 31-40. **(b)** HSA competes with Aβ (1-40) monomers for binding at the edges of protofibrils, thus preventing further fibril growth. The Aβ residues involved in cross-β structures are represented by thick arrows. Red arrows represent β strands at the edges of protofibrils and span Aβ regions interacting with HSA.

References

1. Karran, E., M. Mercken, and B. De Strooper. 2011. The amyloid cascade hypothesis for Alzheimer's disease: an appraisal for the development of therapeutics. *Nat. Rev. Drug Discov*. 10: 698–712.

2. Biere, A.L., B. Ostaszewski, E.R. Stimson, B.T. Hyman, J.E. Maggio, et al. 1996. Amyloid beta-peptide is transported on lipoproteins and albumin in human plasma. *J. Biol. Chem*. 271: 32916–32922.

3. Bohrmann, B., L. Tjernberg, P. Kuner, S. Poli, B. Levet-Trafit, et al. 1999. Endogenous proteins controlling amyloid beta-peptide polymerization. Possible implications for beta-amyloid formation in the central nervous system and in peripheral tissues. *J. Biol. Chem*. 274: 15990–15995.

4. Llewellyn, D.J., K.M. Langa, R.P. Friedland, and I.A. Lang. 2010. Serum albumin concentration and cognitive impairment. *Curr. Alzheimer Res*. 7: 91–96.

5. Boada, M., P. Ortiz, F. Anaya, I. Hernández, J. Muñoz, et al. 2009. Amyloid-targeted therapeutics in Alzheimer's disease: use of human albumin in plasma exchange as a novel approach for Abeta mobilization. *Drug news Perspect*. 22: 325–339.

6. Boada-Rovira, M. 2010. Human Albumin Grifols 5% in plasmapheresis: a new therapy involving beta-amyloid mobilisation in Alzheimer's disease. *Rev. Neurol*. 50 Suppl 5: S9–S18.

7. Anaya, F. 2010. [Therapeutic plasmapheresis and experience in Alzheimer's disease]. *Rev. Neuro*l. 50 Suppl 5: S5–S8.

8. Milojevic, J., V. Esposito, R. Das, and G. Melacini. 2007. Understanding the molecular basis for the inhibition of the Alzheimer's Abeta-peptide oligomerization by human serum albumin using saturation transfer difference and off-resonance relaxation NMR spectroscopy. *J. Am. Chem. Soc*. 129: 4282–4290.

9. Milojevic, J., and G. Melacini. 2011. Stoichiometry and affinity of the human serum albumin-Alzheimer's Aβ peptide interactions. *Biophys. J*. 100: 183–192.

10. Milojevic, J. 2012. Understanding the Inhibition of the Alzheimer's Ab peptide by Human Serum Albumin. .

11. Milojevic, J., A. Raditsis, and G. Melacini. 2009. Human serum albumin inhibits Abeta fibrillization through a "monomer-competitor" mechanism. *Biophys. J*. 97: 2585–2594.

12. Fawzi, N.L., J. Ying, R. Ghirlando, D. a Torchia, and G.M. Clore. 2011. Atomic-resolution dynamics on the surface of amyloid-β protofibrils probed by solution NMR. *Nature*. 480: 268–72.

13. Fawzi, N.L., J. Ying, D.A. Torchia, and G.M. Clore. 2010. Kinetics of amyloid ?? monomer-to-oligomer exchange by NMR relaxation. J. Am. Chem. Soc. 132: 9948–9951.

14. Pace, C.N., F. Vajdos, L. Fee, G. Grimsley, and T. Gray. 1995. How to measure and predict the molar absorption coefficient of a protein. Protein Sci. 4: 2411–2423.

15. Ortega, J., S.K. Singh, T. Ishikawa, M.R. Maurizi, and A.C. Steven. 2000. Visualization of substrate binding and translocation by the ATP-dependent protease, ClpXP. Mol. Cell. 6: 1515–1521.

16. Fawzi, N.L., J. Ying, D.A. Torchia, and G.M. Clore. 2012. Probing exchange kinetics and atomic resolution dynamics in high-molecular-weight complexes using dark-state exchange saturation transfer NMR spectroscopy. *Nat. Protoc*. 7: 1523–1533.

17. Milojevic, J., V. Esposito, R. Das, and G. Melacini. 2007. Inhibition Alzheimer's Ab peptide oligomerization by human serum albumin using saturation transfer difference & off-resonance relaxation NMR. *J. Am. Chem. Soc*. 129: 4282–4290.

18. Rózga, M., M. Kłoniecki, A. Jabłonowska, M. Dadlez, and W. Bal. 2007. The binding constant for amyloid Abeta40 peptide interaction with human serum albumin. *Biochem. Biophys. Res. Commun*. 364: 714–718.

19. Stanyon, H.F., and J.H. Viles. 2012. Human serum albumin can regulate Amyloid-beta peptide fiber growth in the brain interstitium. Implications for Alzheimer's Disease. *J. Biol. Chem*. 287: 28163–28168.

20. Lazo, N.D., M.A. Grant, M.C. Condron, A.C. Rigby, and D.B. Teplow. 2005. On the nucleation of amyloid beta-protein monomer folding. *Protein Sci*. 14: 1581–1596.

21. Selkoe, D.J. 1989. The deposition of amyloid proteins in the aging mammalian brain: implications for Alzheimer's disease. *Ann. Med*. 21: 73–76.

22. Stevens, R.W., D. Elmendorf, M. Gourlay, E. Stroebel, and H. a Gaafar. 1979. Application of fluoroimmunoassay to cerebrospinal fluid immunoglobulin G and albumin. *J. Clin. Microbiol*. 10: 346–50.

23. Petkova, A.T., Y. Ishii, J.J. Balbach, O.N. Antzutkin, R.D. Leapman, et al. 2002. A structural model for Alzheimer's beta -amyloid fibrils based on experimental constraints from solid state NMR. *Proc. Natl. Acad. Sci. U. S. A*. 99: 16742–16747.

Promising Leads and Future Outlook

Chapter 4

Promising Leads and Future Outlook

This chapter will focus on the future outlook of the HSA/Aβ project by highlighting some research leads that were generated during the course of this thesis. The future leads can be partitioned in four major groups. The first group contains different strategies to study the interaction between HSA and fatty acids (FA) and their application in studying the competition between Aβ and FA for HSA binding sites. The second group discusses the effect of glycation on HSA efficiency to inhibit Aβ aggregation. The third group will examine the effect of oxidation on Aβ aggregation propensity using Thioflavin T Fluorescence. The fourth section pertains to follow up work that will be needed to expand on the results of Chapter 3. The first group of leads is one of the main part of this chapter and can be further divided into three sub-sections: 1) using intrinsic HSA fluorescence to monitor FA binding to HSA; 2) studying the partitioning of ^{13}C labeled fatty acids within HSA binding sites using conventional 1D ^{13}C-NMR spectra; and 3) monitoring the competition of Aβ *vs.* short-medium chain FA for binding to HSA using 1D ^{1}H-NMR spectra. These sections are discussed in greater detail in the remaining part of this chapter.

4.1.1. Strategies to Examine the Effect of FA Binding to HSA.

In Chapter 2 we used FA competition as a tool to map Aβ binding to HSA domains and subdomains. For this purpose, we used saturation transfer different experiments (STD) as a strategy to quantitatively monitor FA binding to HSA constructs. However, using STD experiments to examine FA binding to full-length HSA is challenging, because high (*i.e.* >100 μM) FA total concentrations are needed to saturate all seven HSA binding sites. Using high FA concentrations is problematic due to the possibility of micelle formation, which complicate the analysis of STD data. On the other hand, lowering HSA concentration to avoid the need to use higher FA concentrations gives rise to sensitivity problems, *i.e.* at least 10 μM HSA solution is needed to have appropriate signal to noise ratios in the STD spectra under our experimental conditions. Moreover, STD experiments sense the binding of FA to all seven, non-equivalent binding sites, which might give rise to complex binding isotherms due to possible cooperativity between the binding sites, thus complicating the measurement of site-specific K_d values.

An alternative approach to study FA binding to HSA is to use the intrinsic tryptophan fluorescence of HSA. HSA has one tryptophan residue (W214), which can be excited at λ = 310 nm to result in a fluorescence spectrum with maximum emission intensity at 350 nm (Fig. 1a). Binding of FA to HSA causes a change in the local environment of tryptophan 214, which in turn results in a blue shift in the emission maximum from 350 nm to 335 nm (Fig. 1a). In addition, FA binding also causes an

increase in fluorescence intensity at 335 nm, as shown for myristate (C14) in Figure 1a. The increase in the fluorescence intensity at 335 can be utilized to build a binding isotherm of myristic acid binding to HSA. As shown in Figure 1b, myristic acid binds to HSA in a dose dependant manner until a plateau is reached.

Establishing a FA binding isotherm using tryptophan fluorescence (1) has two advantages over using STD. First, fluorescence is a very sensitive spectroscopy compared to NMR, which means that low HSA concentrations *e.g.* 1 μM can be used to monitor the binding of FA, thus eliminating the problems associated with the use of high FA concentrations. Second, tryptophan 214 is located in HSA domain 2 and, based on preliminary data obtained using domain 1-2 and 2-3 deletion constructs (Figure 2), the blue shift observed for its emission maximum in the presence of FA does not depend on FA binding to domain 1 or 3. Since HSA domain 2 contains only weak affinity FA binding sites (one in subdomain 2A and one in 2B) (69), and since it is assumed that in first approximation low affinity binding sites will be filled after the higher affinity ones are occupied, the blue shift observed represents a good estimate of the saturation.

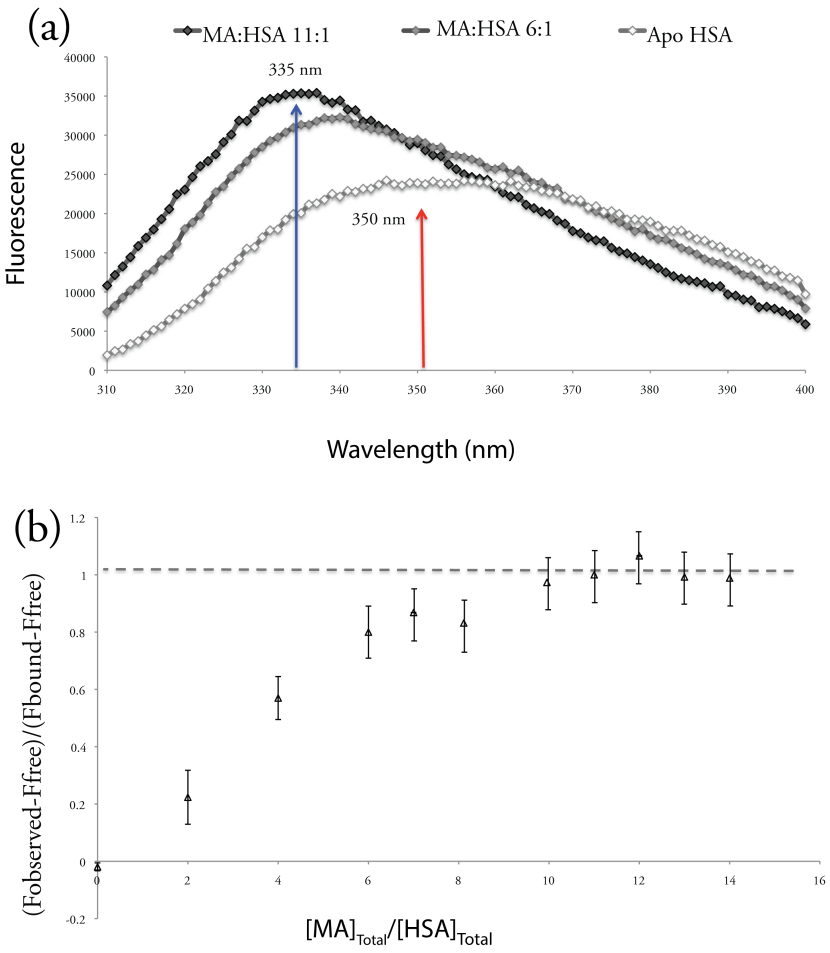

Figure 1. Using Intrinsic HSA fluorescence to monitor myristic acid (MA) binding to HSA. Panel (a) illustrates the blue shift observed upon binding of myristic acid to HSA. In the absence of myristic acid, the Trp 214 emission maximum is at λ = 350 nm. Binding of myristic cause a blue shift in Trp 214 emission spectra with maximum emission observed at λ = 335 nm. Panel (b) depicts the binding isotherm of myristic acid (C14). Using the fluorescence intensity at 335 nm, the fraction of myristic acid bound (<v>) at various C14:HSA ratios was measured using the relation:

<v>= (Fobserved - Ffree)/(Fbound - Ffree)

Where Fobserved represents the measured florescence intensity at 335 nm for each titration point, Fbound represents the maximum fluorescence intensity observed, and Ffree is the intensity of apo HSA. The dashed line shows the saturation plateau.

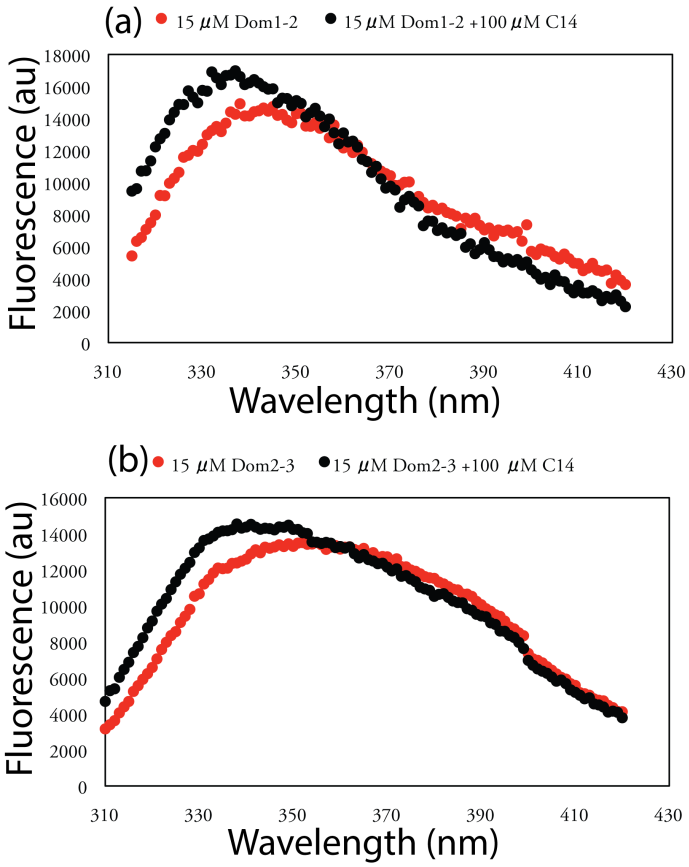

Figure 2. Using Intrinsic HSA fluorescence to monitor myristic acid (MA) binding to HSA deletion constructs; domain 1-2, and domain2-3. Panel (a) illustrates the blue shift observed upon addition of 100 μM myristic acid to Dom1-2, while panel (b) depicts the effect of adding 100 μM myristic acid to dom2-3. The blue shift of Trp214 fluorescence was observed in both cases.

The next step was to test the effect of adding Aβ oligomers on the tryptophan fluorescence spectra of HSA in the presence and absence of myristic acid. In order to examine this, 90 μM Aβ (1-42) was incubated at 37 ^{o}C for 3 hours and then added to either *apo* HSA or HSA saturated with C14. As shown in Figure 3, in the absence of C14, addition of Aβ oligomers to HSA causes quenching in the emission intensity of W214(66). On the contrary, addition of the oligomers to HSA pre-saturated with C14 did

not result in a similar quenching effect. These data are in agreement with the conclusions of Chapter 2 in which we show that there is a partial overlap between the binding sites of myristic acid and Aβ oligomers within HSA.

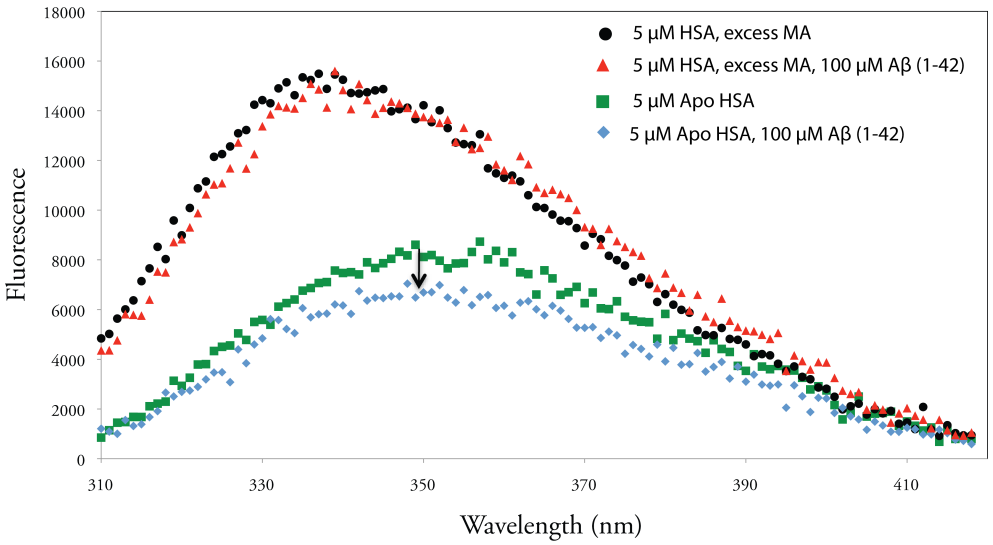

Figure 3. Probing the competition between Aβ (1-42) and myristic acid (MA or C14) using HSA Trp214. Binding of Aβ oligomers to HSA causes a quenching in the intrinsic fluorescence of HSA Trp214. The green squares represent the Trp-fluorescence emission spectrum of 5 µM HSA, while the blue diamonds represent Trp-fluorescence emission spectrum of 5 µM HSA in the presence of 90 µM Aβ (1-42) incubated for 3 hours at 37 °C. The black arrow shows the decrease in fluorescence intensity of Trp 214 due to the Aβ (1-42) quenching effect. Black circles represent the Trp-fluorescence emission spectrum of 10 µM HSA bound to MA with emission maximum at 335 nm. Addition of 90 µM Aβ (1-42) oligomers to the HSA-C14 complex didn't quench the emission intensity to the same extent observed in the absence of C14.

4.1.2. Characterizing FA Binding Sites within HSA using ^{13}C-Labeled FA.

Crystal structures of FA-bound HSA reviled seven distinct binding sites for medium to long chain fatty acids (70, 71). The interaction between FA and HSA has been

characterized also using NMR spectroscopy for several FAs with different chain lengths(72–75). Upon binding to different sites within HSA, FAs are surrounded by different binding environments, which in turn affect the ^{13}C chemical shift of the ^{3}C-labeled FA. Here we use ^{13}C enriched [1-^{13}C] palmitic acid (PA) and [18-^{13}C] oleic acid (OA) to define FA binding sites within HSA and to examine the effect of adding Aβ oligomers to the FA-HSA complexes. This protocol was applied in order to identify potential binding sites for the Aβ oligomers. For example, as shown in Figure 3, [1-^{13}C] PA binds to HSA and shows distinct 1D ^{13}C signals that correspond to various FA binding sites. Addition of 100 μM Aβ (1-42) to the PA-HSA complex caused a reduction in the signals corresponding to site 4 and 5 FA binding sites located in domain 3 HSA (Figure 4a). However, the data can't be simply interpreted as a direct competitive displacement between and Aβ the FAs, since Aβ peptides contain some residual trifluoroacetic acid (TFA) that interacts with HSA. Figure 4b show the effect of TFA addition on the 1D ^{13}C spectrum of PA-HSA complex. Figure 4b suggests that the reduction in peaks 4 and 5 upon Aβ addition (Figure 4a) was most likely caused by TFA.

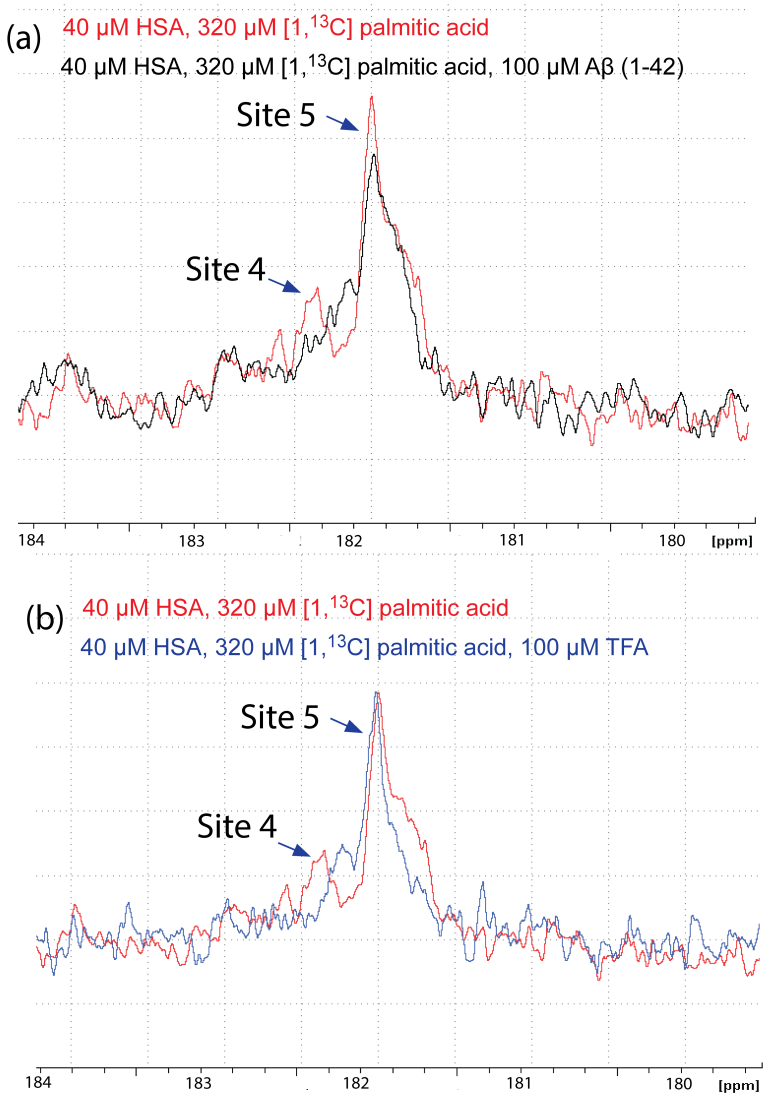

Figure 4. Comparison between 13C 1D NMR spectra of [1-13C] PA-HSA complex in the presence and absence of Aβ (1-42). Panel (a) illustrates the effect of adding 100 μM Aβ (1-42) to a solution of the PA-HSA complex; the solution contained 8 molar equiv of [1-13C] PA to 1 molar equiv of HSA at 40 μM HSA concentration, red spectrum. Addition of 100 μM Aβ (1-42) affected mainly sites 4 (located in sub-domain 3A) and site 5 (located in sub-domain 3B) (black spectrum). Panel (b) shows the effect of adding triflouroacetic (TFA) acid to the PA-HSA complex (blue spectrum). Only the carbonyl region is shown.

Another similar series of experiments was implemented by replacing PA with oleic acid (OA) 13C-labeled at the methyl position. First, four molar equivalents of OA were added to one molar equivalent of HSA as previously described (74). The 1D ^{13}C spectrum of the complex showed seven distinct OA signals, which correspond to the seven FA binding sites within HSA (Figure 5a). It is important to note that there was no detectable free OA in the solution containing the HSA complex described above. This is proven by Figure 5a (lower panel), which shows the 1D ^{13}C spectrum of free OA with only a single signal for the OA C18 methyl carbon. This signal doesn't correspond to any of the seven signals observed in the 4:1 OA-HSA complex solution.

We then examined the effect of Aβ oligomers on the distribution of OA signals. For this purpose, we prepared a 100 μM TFA free-Aβ (1-42) solution as described in Chapter 2. As shown in Figure 5a, addition of Aβ (1-42) oligomers resulted in a possibly partial reduction in one specific OA signal without major effects on the other signals. In order to corroborate this finding, we examined the effect of Aβ oligomers on the partitioning of OA molecules within domain 3 HSA.

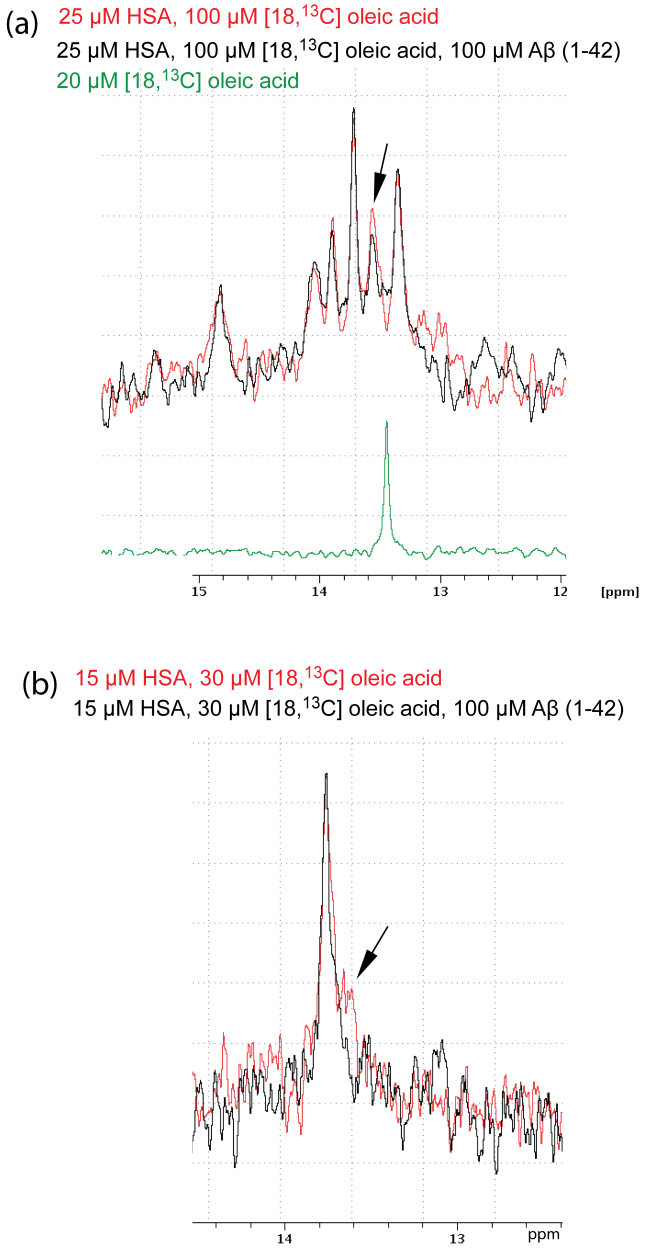

Figure 5. Comparison between the 13C 1D NMR spectra of [18-13C] OA-HSA and [18-13C] OA-domain 3 complexes in the presence and absence of Aβ (1-42). Panel (a) shows the overlay of the spectra of OA-HSA complex at a 4:1 ratio in the absence (red) and presence (black) of 100 μM Aβ (1-42). The spectrum representing free OA is shown in green. Panel (b) depicts the overlay of the spectra of the OA-domain 3 complex at a 2:1 ratio in the absence (red) and presence (black) of 100 μM Aβ (1-42). The signal potentially affected by Aβ addition are indicated by black arrows.

The crystal structure of HSA complexed with OA (PDB, 1GNI) shows that domain 3 contains OA-binding sites 3-5 with sites 4 and 5 reported as high affinity (69, 70). Using 2:1 molar ratios of OA:domain 3, we observed two distinct signals for OA (Figure 5b), which most likely correspond to the high affinity binding sites (*i.e.*, sites 4 and 5). The absence of a third signal that corresponds to site 3 can be due to incomplete formation of the binding pocket after truncation of domain 3 and/or due to the low affinity of OA to site 3. which would require higher OA: HSA stoichiometric ratios to start filling the binding site 3. Interestingly, addition of Aβ oligomers to the OA-domain 3 complex decreased the signal intensity of the OA signal corresponding to site 4 (Figure 5b), which could help to explain the results shown for full length HSA (Figure 5a). However, reaching a conclusive interpretation of the OA acid data is hard since the interactions between OA and Aβ oligomers or higher molecular weight aggregates was not fully covered in the current study. For instance, a possible cause for the decrease in the signal intensity of OA could be the direct interactions between the fatty acid and the large Aβ assemblies. Although this alternative interpretation can be dismissed assuming that FA from the lowest affinity binding sites would be recruited first into the Aβ assemblies, additional studies will be required to establish the significance of ^{13}C-OA signal changes upon Aβ addition.

4.1.3. Short to Medium Chain Fatty Acids and Aβ Oligomers Compete for Bbinding to HSA.

We have shown in Chapter 2 that myristic acid and Aβ oligomers compete for domain 3 binding sites. However, the competition between shorter chain fatty acids and the oligomers for HSA binding sites haven't been fully examined yet. Hence, HSA was loaded with very high stoichiometric ratios of octanoic acid, decanoic acid, and myristic acid (*i.e.* >1:10), then their efficiency in preventing Aβ aggregation was monitored using the same approach outlined in Chapter2. Figure 6 shows that in the absence of HSA , the 1D ^{1}H NMR signal of Aβ (1-42) is lost over time, until a plateau is reached with the intensity reduced by ~40 %. Upon addition of sub-stoichiometric amounts of apo HSA , the NMR signal intensity of Aβ (1-42) is dramatically increased both in the initial decay phase and in the final plateau region (Fig. 6). However, when HSA was added in the presence of excess, octanoic, decanoic or myristic acid, the inhibitory potency of HSA was significantly reduced resulting in Aβ (1-42) signal intensities that are intermediate between those of the two previous profiles (Fig. 6).

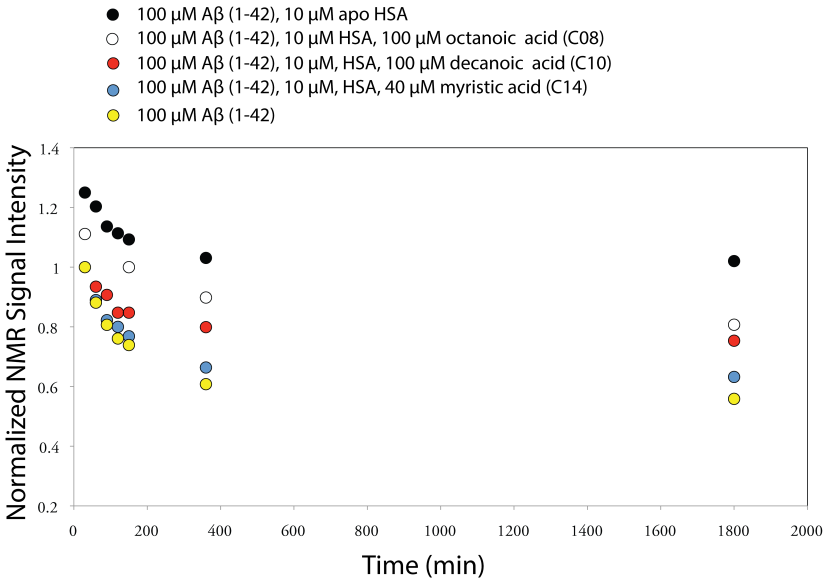

Figure 6. Effect of HSA saturation with fatty acids on the inhibition of Aβ (1-42) aggregation by HSA. 1D 1H-NMR signal intensities of 100 µM Aβ (1-42) recoded over time are shown in the absence (yellow circles) and in the presence of HSA either in the apo form (black circles) or in the presence of excess saturated fatty acids (white, red, and blue circles). White, red, and blue circles correspond to 100 µM excess octanoic acid (C08), 100 µM excess decanoic acid (C10), and 40 µM excess myristic acid (C14), respectively. Signal intensities were measured using a Bruker Avance 700 MHz spectrometer equipped with a 5 mm TCI Cyroprobe at 37 oC.

These variations in the 1D NMR signal *vs.* time profiles are attributable to either the competition between FA and Aβ (1-42) for binding to HSA and/or to potential direct interactions between free FA and Aβ (1-42). In order to rule out the latter explanation, we monitored the 1D NMR signal of Aβ (1-42) over time in the absence and presence of 40-100 µM of FA and no significant differences were observed upon addition of 40-100 µM of FA (Fig. 7).

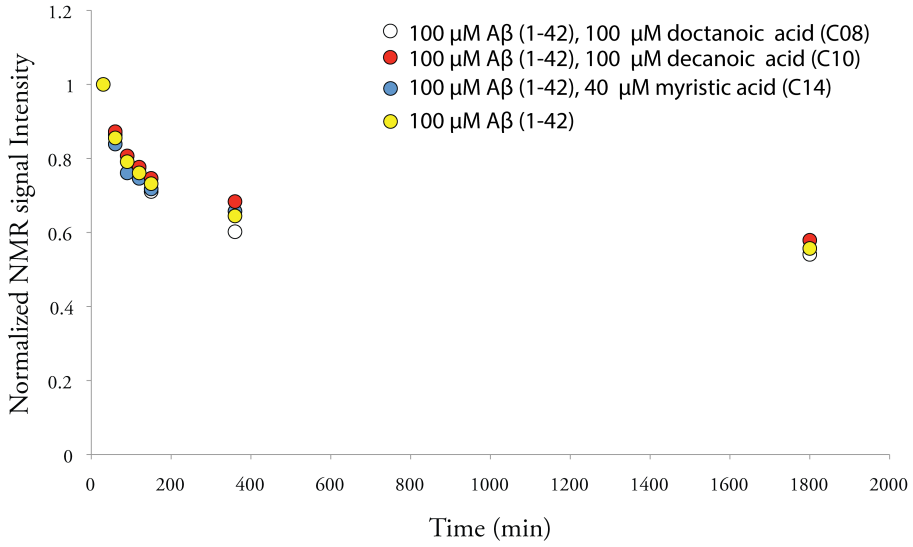

Figure 7. Effect of free fatty acids on the Aβ (1-42) aggregation profile. Yellow circles represent the 1D NMR signal intensities of 90 μM Aβ (1-42) vs. time, while the white, red and blue circles represent the 1D NMR signal intensities of 90 μM Aβ in the presence of 100 μM octanoic acid (C08), 100 μM decanoic acid (C10), and 40 μM myristic acid (C14), respectively.

4.2. Examining the Effect of Glycation on the Efficiency of HSA to Prevent Aβ Aggregation.

HSA is subject to non-enzymatic glycation, *i.e.* the covalent linkage of a sugar molecule, *e.g.* glucose(76). Blood sugar levels can be elevated in diseases like diabetes and increase the rate of glycation of plasma proteins such as HSA. Glycation of HSA can occur at one or multiple sites and has been correlated with several pathological effects. However, the effect of HSA glycation on its Ab-self-association inhibitory potency is currently unknown. Hence, glycated HSA that contains 1-5 molecules of sugar per HSA was purchased from Sigma (A3782) and tested for its efficiency in preventing Aβ aggregation. As shown in Figure 8, glycated HSA is less efficient in preventing HSA aggregation. However, the amount of fatty acids bound to glycated HSA is currently unknown and needs to be probed before firm conclusions on the effect of glycation on the Ab inhibitiory potency can be drawn. If, after the control experiments to assess the amount of FA bound to glycated HSA, it is determined that glycation does indeed reduce the Ab inhibitiory potency of HSA, two important questions will be opened: 1) In a clinical setting, is there a relation between the degree of HSA glycation, *i.e*. diabetes, and the prognosis of Alzheimer's disease? 2) At a molecular level, is there an overlap between Aβ binding sites and the sites of glycation within has or is glycation indirectly affecting Aβ binding through partial unfolding, for instance?

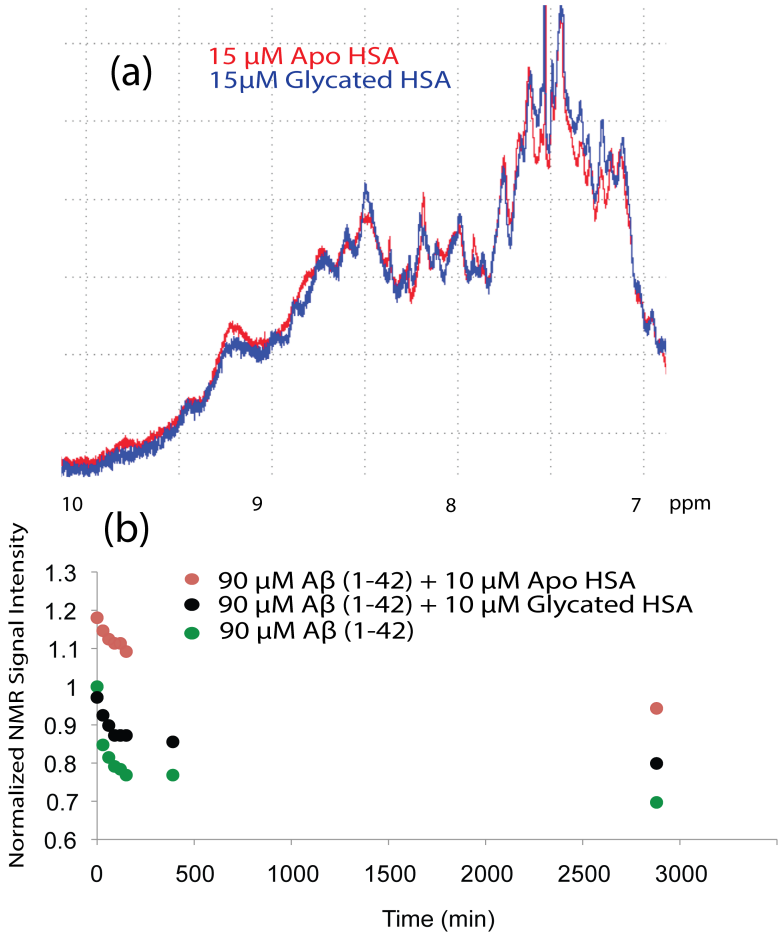

Figure 8. Effect of Glycation on the efficiency of HSA as an inhibitor for Aβ aggregation. Panel (a) depicts the aromatic regions of the 1D 1H-NMR spectrum of apo HSA (Sigma A3782) (red), and glycated HSA (Sigma A8301) (blue). Panel (b) shows the effect of HSA with and without glycation on Aβ (1-42) aggregation. In the absence of HSA, the proton 1D signal intensity of 90 µM Aβ (1-42) decreases rapidly, due to the formation of NMR invisible high molecular weight aggregates (green circles). In the presence of 10 µM apo HSA, the Aβ (1-42) signal intensity was higher (red circles). However, addition of 10 µM glycated is not as effective as addition of non-glycated HSA.

4.3. Probing the Effect of Met 35 Oxidation on the Aggregation Propensity of Aβ Peptides Variants.

Alzheimer's disease pathogenesis has been linked to the oxidation status of methionine 35 of Aβ peptides, since it represents the residue most prone to oxidation "in vivo"(77). We assessed the aggregation propensity of different Aβ peptides variants (with and without Met oxidation) using ThT fluorescence, which can monitor the formation of cross-β amyloid assemblies (Figure 9)(78). We prepared solutions for four Aβ variants: Aβ (1-40), Aβ (1-40) $Met35^{OX}$, Aβ (1-42), and Aβ (1-42) $Met35^{OX}$ under similar experimental conditions and measured their ability to form cross-β structures by monitoring the ThT fluorescence intensity over a 40 h incubation period at room temperature. At the concentration used, *i.e.* 50 μM, only Aβ (1-42) and Aβ (1-42) $Met35^{OX}$ were able to form amyloid aggregates that bind ThT dye. Figure 9 shows that methionine oxidation of Aβ (1-42) decreases its ability to form amyloid aggregates as evident by the significant decrease in ThT fluorescence. Future work should be directed towards optimizing the experimental conditions, *e.g.* concentration, temperature, etc, in order to find the suitable conditions that promote Aβ (1-40) aggregation without drastically increasing the aggregation rate of Aβ (1-42).

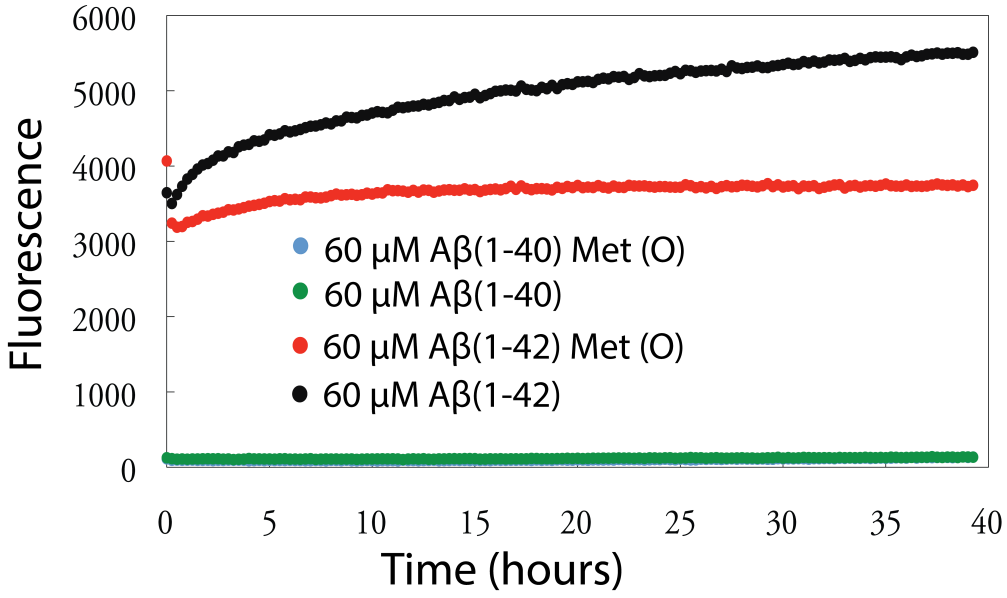

Figure 9. Probing the aggregation of Aβ peptides variants using Thioflavin T fluorescence. The black circles represent ThT fluorescence intensities for reduced Aβ (1-42), while the red circles represent ThT fluorescence intensities of Aβ (1-42) with oxidized Met 35. No aggregation was observed for Aβ (1-40) reduced or oxidized (green and blue circles).

4.4. Future Leads to Expand on Chapter 3

While Chapter 3 addresses several previously open questions on how Aβ (1-40) interacts with HSA, it also generated new questions that define the focus of future research in this field. For instance, one of the most significant contributions of Chapter 3 is the realization that Aβ (1-40) monomers are likely to be bound to HSA under physiological plasma conditions. However, the full implications of this finding are not yet fully appreciated and several questions on the Aβ (1-40) monomer: HSA complexes are still open:

(a) In Chapter 3, we provide evidence that Aβ (1-40) monomers bind HSA. This interaction is weak but specific and likely to occur in plasma. However, it is currently unknown how HSA binding to monomeric Aβ (1-40) affects Aβ (1-40) self-association. Experiments designed to address this question, will require solutions of monomeric Aβ (1-40) with or without high concetrations of HSA (> 0.1 mM). Formation of Aβ (1-40) oligomers can then be monitored through DLS and NMR, for instance. If the presence of HSA in high concentrations completely eliminates the formation of Aβ (1-40) oligomers, then it is likely that the binding of monomeric Aβ (1-40) by HSA is sufficient to inhibit Aβ (1-40) self-association. If the Aβ (1-40) monomer : HSA complexes are proven to be inhibitory with respect to Aβ (1-40) self-association, it will then be interesting to probe how they are affected by HSA modifications (*e.g.* glycation).

(b) What are the stoichiometries of the Aβ (1-40) monomer : HSA complexes and which HSA sites are involved in binding to monomeric Aβ (1-40) and with what specific affinities? NMR of labeled HSA domain constructs or of full length HSA bound to labeled ligands can be used to address this question. Competition with FAs is also likely to be informative in this respect.

(c) How can weak specific binding of Aβ (1-40) monomers to HSA be separated by viscosity and non-specific binding/crowding effects caused by HSA at high concentrations? To address this question Aβ peptides with reversed or randomized sequences could be used, in conjuction with relaxations experiments, such as ^{15}N T_2 (14) and/or ^{1}H STD/ORR measurements.

(d) Can the Aβ (1-40) monomer : HSA complexes be further supported by previous data on shorted Aβ peptides, such as Aβ (16-20) (as in Figure 1, page 243 of Dr. J. Milojevic's Ph.D. thesis)?

Other questions stemming from Chapter 3 pertain more broadly to the proposed inhibitory model:

(e) Is it possible to quantify the affinity of HSA for the DEST Aβ (1-40) oligomers using DEST monitored titration of concentrated DEST Aβ (1-40) samples with increasing amounts of HSA? This will be a central point in establishing the DEST method as a tool to monitor amyloid inhibition and not only formation.

(f) To what extent the interactions between HSA and the DEST Aβ (1-40) oligomers resemble those between the Aβ (1-40) monomers and the DEST Aβ (1-40) oligomers? An initial answer to this question is provided by the ΔΘ correlations shown in Chapter 3. However, further insight will be provided by mapping the ΔΘ profiles onto the 3D structures of Aβ (1-40) proto-fibrils currently available in the PDB. The resulting 3D ΔΘ maps may also indicate whether HSA is likely to select for one of the two edge of the protofibrils.

(g) Can the concentrated Aβ (1-40) low temperature solutions used in Chapter 3 be replaced by dilute Aβ (1-40) high temperature solutions? In other words, can the experiments of Chapter 3 be repeated on Aβ (1-40) oligomers induced not through increased concentrations but through heating, considering that the Aβ (1-40) self-association is driven also by hydrophobic effects? Preliminary results (Figure 10 and 11) indicate that this strategy might provide an alternative avenue to map Aβ (1-40) self-association by NMR, with the advantage of minimizing the use of Aβ (1-40) peptide and offering cross-validation opportunities.

(h) Last but not least, how general is the mechanism proposed in Chapter 3 for the HSA inhibition of Aβ (1-40) self-association. Do other plasma proteins with Aβ (1-40) self-association inhibitory functions, such as trasnferrin, bind Aβ (1-40) monomers? Can the model of Chapter 3 developed for Aβ (1-40) be extended to Aβ (1-42)?

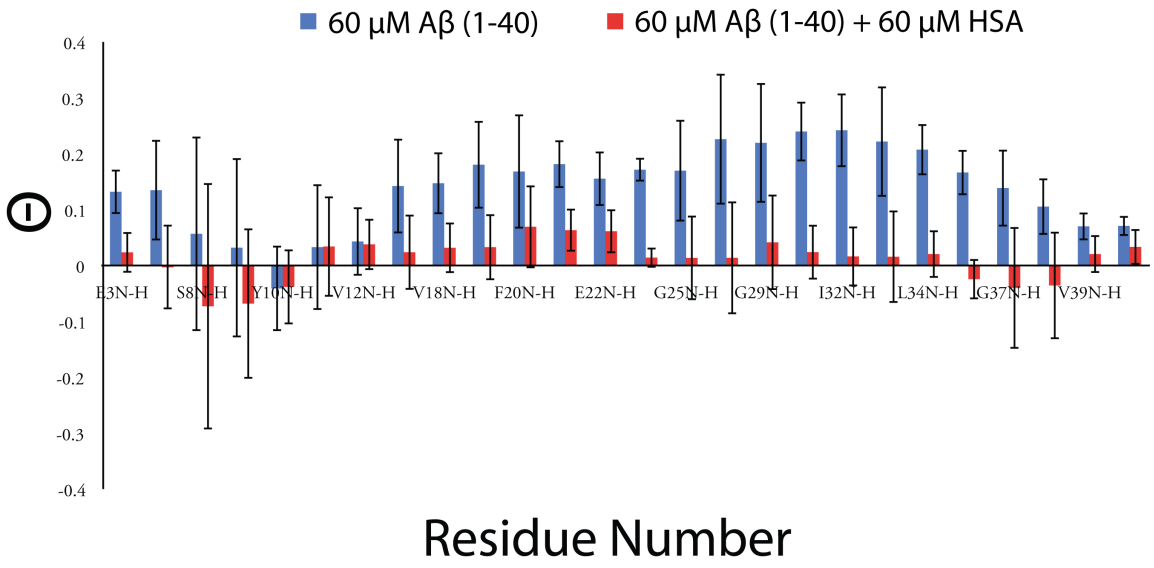

Figure 10. The DEST difference (Θ) for diluted Aβ (1-40) at 30 °C. Θ values at |4 KHz| for monomeric Aβ (1-40) samples in the absence (solid blue bars) and presence (solid red bars) of 60 μM HSA.

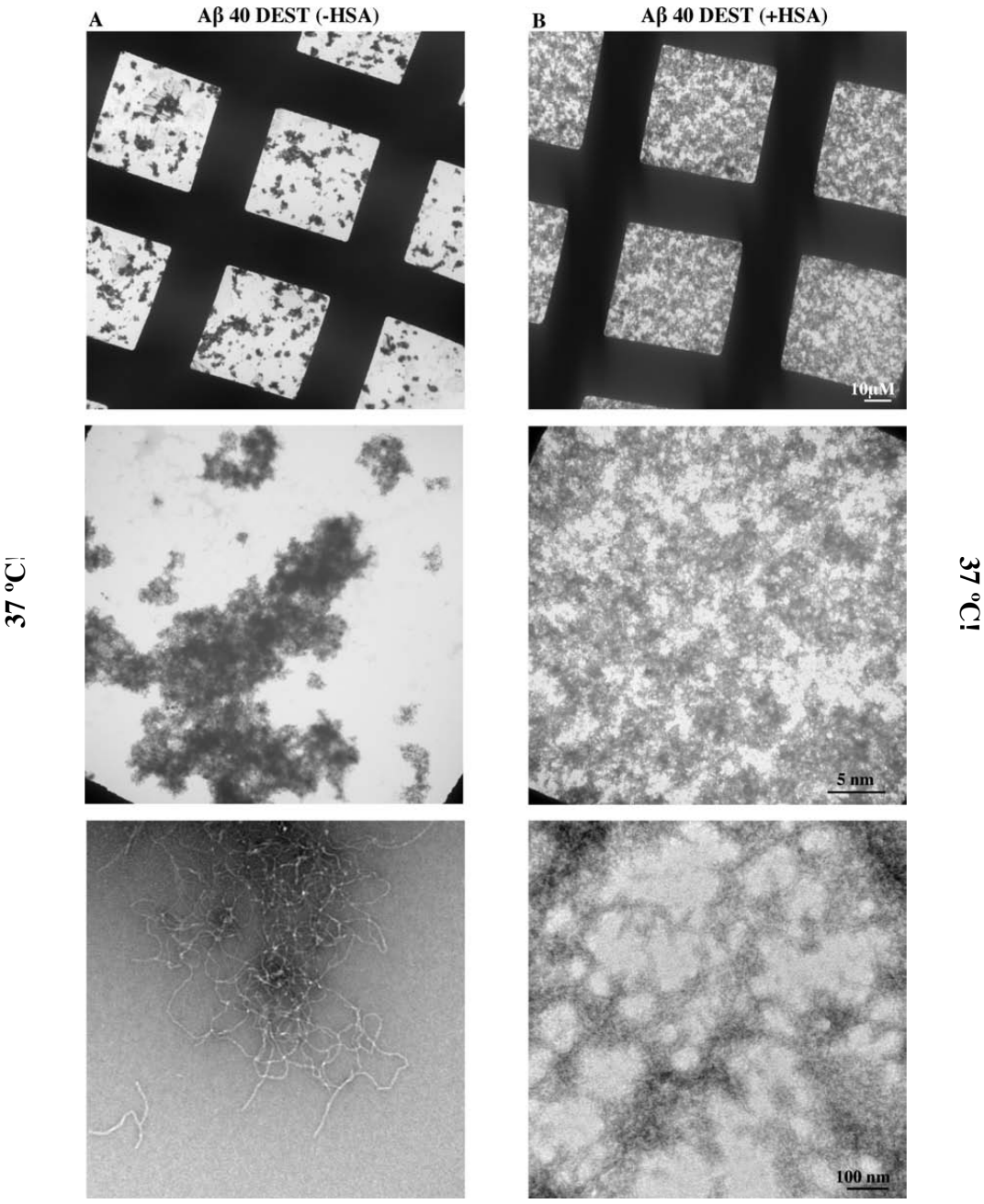

Figure 11. Electron microscopic CCD pictures of 300 μM Aβ (1-40) after performing negative stain using 1 % uranyl acetate. Images (top to bottom) were acquired at a magnification of 1000X, 4000X and 150,000X magnification respectively. A. 300 μM Aβ 40 under DEST conditions incubated at 10 ºC for 10 days with an additional incubation at 37 ºC for 24 hours. B. 300 μM Aβ 40 under DEST conditions kept at 10 ºC for a total time of 10 days with 50 μM HSA added on the 7th day of incubation. Finally, the sample was incubated at 37 ºC for 24 hours before imaging.

4.5. Materials and Methods Used to Generate Preliminary Data

Sample preparation. Aβ peptides used for generating the data presented in this chapter were prepared using the same protocol described in Chapter 2.

Fluorescence Spectroscopy. Tryptophan fluorescence spectra were acquired using a Tecan Safire fluorescence spectrometer and 96 well plates with 200 μL sample volumes and with the excitation and the emission slit width set to 2.5 nm. An excitation wavelength of 295 nm was used to excite the single tryptophan residue of HSA, Trp 214 (20, 21, 22). Aβ peptides were disaggregated using the protocol described earlier and(62) then mixed with HSA (with and without excess myristic acid) to prepare a solution containing 5 μM HSA, 100 μM Aβ (1-42) in 20 mM HEPES, pH 7.4. ThT fluorescence spectra were recorded using a Tecan Safire fluorescence spectrometer and half-area 96 well plates with 110 μL sample volumes. In this case excitation and emission wavelengths were set at 450 and 490 nm, respectively (23). All Aβ peptides variants were prepared at a 50 μM concentration according to the protocol described by Hou et al. (79). A 20 μL aliquot of 100 μM Thioflavin T in water was directly added to 90 μL of each peptide solution and fluorescence measurements were collected at room temperature for 40 hours.

References

1. Leggio, C., L. Galantini, P. V. Konarev, and N. V. Pavel. 2009. Urea-Induced Denaturation Process on Defatted Human Serum Albumin and in the Presence of Palmitic Acid. *J. Phys. Chem. B*. 113: 12590–12602.
2. Simard, J.R., P.A. Zunszain, C.-E. Ha, J.S. Yang, N. V Bhagavan, et al. 2005. Locating high-affinity fatty acid-binding sites on albumin by x-ray crystallography and NMR spectroscopy. *Proc. Natl. Acad. Sci. U. S. A*. 102: 17958–17963.
3. Milojevic, J., A. Raditsis, and G. Melacini. 2009. Human serum albumin inhibits Abeta fibrillization through a "monomer-competitor" mechanism. *Biophys. J*. 97: 2585–2594.
4. Bhattacharya, a a, T. Grüne, and S. Curry. 2000. Crystallographic analysis reveals common modes of binding of medium and long-chain fatty acids to human serum albumin. *J. Mol. Biol*. 303: 721–32.
5. Curry, S., H. Mandelkow, P. Brick, and N. Franks. 1998. Crystal structure of human serum albumin complexed with fatty acid reveals an asymmetric distribution of binding sites. *Nat. Struct. Biol*. 5: 827–835.
6. Oida, T. 1986. 1H-NMR study on the interactions of human serum albumin with free fatty acid. *J. Biochem*. 100: 1533–1542.
7. Simard, J.R., P.A. Zunszain, C.-E. Ha, J.S. Yang, N. V Bhagavan, et al. 2005. Locating high-affinity fatty acid-binding sites on albumin by x-ray crystallography and NMR spectroscopy. *Proc. Natl. Acad. Sci. U. S. A*. 102: 17958–17963.
8. Krenzel, E.S., Z. Chen, and J.A. Hamilton. 2013. Correspondence of fatty acid and drug binding sites on human serum albumin: A two-dimensional nuclear magnetic resonance study. *Biochemistry*. 52: 1559–1567.
9. Simard, J.R., P.A. Zunszain, J.A. Hamilton, and S. Curry. 2006. Location of High and Low Affinity Fatty Acid Binding Sites on Human Serum Albumin Revealed by NMR Drug-competition Analysis. *J. Mol. Biol*. 361: 336–351.
10. Simard, J.R., P. a Zunszain, J. a Hamilton, and S. Curry. 2006. Location of high and low affinity fatty acid binding sites on human serum albumin revealed by NMR drug-competition analysis. *J. Mol. Biol*. 361: 336–51.
11. Thornalley, P.J., A. Langborg, and H.S. Minhas. 1999. Formation of glyoxal, methylglyoxal and 3-deoxyglucosone in the glycation of proteins by glucose. *Biochem. J*. 344 Pt 1: 109–116.
12. Vogt, W. 1995. Oxidation of methionyl residues in proteins: Tools, targets, and reversal. *Free Radic. Biol. Med*. 18: 93–105.
13. Benseny-Cases, N., M. Cócera, and J. Cladera. 2007. Conversion of non-fibrillar beta-sheet oligomers into amyloid fibrils in Alzheimer's disease amyloid peptide aggregation. *Biochem. Biophys. Res. Commun*. 361: 916–921.
14. Li, C., and G.J. Pielak. 2009. Using NMR to distinguish viscosity effects from nonspecific protein binding under crowded conditions. *J. Am. Chem. Soc*. 131: 1368–1369.

15. Milojevic, J., V. Esposito, R. Das, and G. Melacini. 2007. Understanding the molecular basis for the inhibition of the Alzheimer's Abeta-peptide oligomerization by human serum albumin using saturation transfer difference and off-resonance relaxation NMR spectroscopy. *J. Am. Chem. Soc*. 129: 4282–4290.
16. Hou, L., I. Kang, R.E. Marchant, and M.G. Zagorski. 2002. Methionine 35 oxidation reduces fibril assembly of the amyloid abeta-(1-42) peptide of Alzheimer's disease. *J. Biol. Chem*. 277: 40173–6.